

UC Santa Barbara

UC Santa Barbara Electronic Theses and Dissertations

Title

NON-EDIBLE BIOMASS RESIDUE TO HIGH VALUE-ADDED CHEMICALS: A LIGNIN-DERIVED CATALYST DESIGN FOR PRODUCTION OF CHLORINE DIOXIDE & PREPARATION OF SUSTAINABLE POLAR APROTIC SOLVENTS FROM CELLULOSE

Permalink

<https://escholarship.org/uc/item/4zt3177p>

Author

Champ, Tayyebah Bakhshi

Publication Date

2020

Peer reviewed|Thesis/dissertation

UNIVERSITY OF CALIFORNIA

Santa Barbara

NON-EDIBLE BIOMASS RESIDUE TO HIGH VALUE-ADDED CHEMICALS: A
LIGNIN-DERIVED CATALYST DESIGN FOR PRODUCTION OF CHLORINE
DIOXIDE & PREPARATION OF SUSTAINABLE POLAR APROTIC SOLVENTS
FROM CELLULOSE

A dissertation submitted in partial satisfaction of the
requirements for the degree Doctor of Philosophy
in Chemistry

by

Tayyebah Bakhshi Champ

Committee in charge:

Professor Mahdi Abu-Omar, Chair

Professor Susannah Scott, Professor Peter C. Ford,

Professor Steven K. Buratto

December 2020

The dissertation of Tayyebah Bakhshi Champ is approved.

Mahdi Abu-Omar, Committee Chair

Susannah Scott

Peter C. Ford

Steven K. Buratto

December 2020

ACKNOWLEDGEMENTS

This work would not have been possible without the help and influence of many other people. I especially would like to thank my adviser Dr. Mahdi Abu-Omar who has a great positive influence in my life and helped me to grow into someone that I am dreaming of. I owe him all my knowledge on catalysis, kinetics, and thousands of little details about chemistry and materials around me. He has been an amazing mentor in my professional life. I am grateful and honored to work under his supervision and in his research lab.

I'd like to send my deepest gratitude to my committee members; Dr. Susannah Scott, Dr. Peter C. Ford, and Dr. Steven K. Buratto for all your supports, contribution, time, and efforts through past few years. Your ideas, input, and enthusiasm have assisted me in making improvements and growing into the person I am today.

The past and present Abu-Omar group members have been exceptionally helpful in assisting me throughout the years. Thank you all for the amazing dedication and effort towards the work whether it be sharing your scientific ideas, or maintaining the lab instruments, or sharing so many memories with each other. I am truly grateful, and I would like to express my sincere gratitude to every group member.

I need to also thank my parents, sisters and my husband for their constant love, support, and encouragement during my school years. Without them, I could not get through the hard times.

VITA OF TAYYEBEH BAKHSHI CHAMP

EDUCATION

Bachelor of science in chemistry, Birjand University, Iran 2002

Master of Science in Organic Chemistry, Ball State University, IN, Muncie 2014

Doctor of philosophy in inorganic chemistry, University of California, Santa Barbara 2020

PROFESSIONAL EMPLOYMENT

Teaching and Research Assistant, University of California, Santa Barbara CA 2016-2020

Teaching Assistant, Purdue University, West Lafayette IN 2014-2016

Teaching Assistant, Ball State University, Muncie IN 2012-2014

PUBLICATIONS

T. B. Champ, J. H. Jang, J. L. Lee, G. Wu, M. A. Reynolds, M. M. Abu-Omar, *Inorganic Chemistry*, revised and resubmitted 2020.

T. B. Champ, S. Liu, B. L. Wegenhart, T. Zhang, and M. M. Abu-Omar, under review.

S. F. Tayyari, T. Bakhshi, M. Ebrahimi, R. E. Sammelson, *Spectrochimica Acta Part A*, 73, 342 (2009).

S. F. Tayyari, T. Bakhshi, S. J. Mahdizadeh, S. Mehrani, R. E. Sammelson, *J. Mol. Struct.*, 938, 76 (2009).

REWARDS

UCSB Outstanding student in leadership during the 2018-2019 academic year

Individualized Professional Skills (IPS) Scholarship 2019

ABSTRACT

Non-Edible Biomass Residue to High Value-Added Chemicals: A Lignin-Derived Catalyst

Design for Production of Chlorine Dioxide & Preparation of Sustainable Polar Aprotic

Solvents From Cellulose

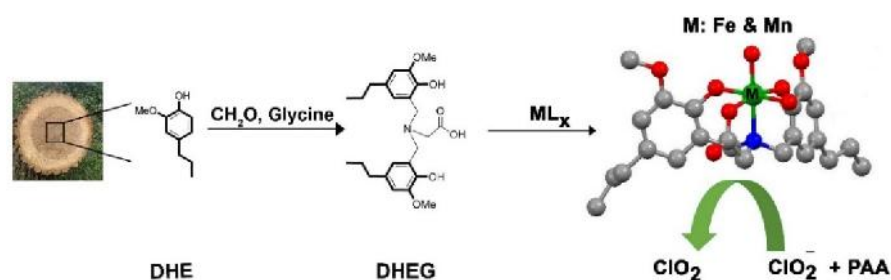
Tayyebah Bakhshi Champ

The global production of plant biomass waste is in the order of 140 Gt per year which offers a promising alternative to petroleum and a sustainable resource to produce fuels and chemicals. Inspired by innovative advancement in biomass valorization, two catalytic processes have been developed to produce chlorine dioxide and polar aprotic solvents from non-edible biomass residues.

The application of chlorine dioxide (ClO_2) in water treatment is growing because of its superior antimicrobial properties and lower tendency to generate harmful chlorinated organic by-products. Most of the previously investigated catalysts for the one electron oxidation of chlorite to ClO_2 are based on manganese or iron porphyrin complexes which suffer from expensive ligand and catalyst syntheses as well as the catalyst instability in oxidative environment. Chlorine dioxide chemistry and its catalytic production are explained in depth in chapter 1.

Second chapter describes a novel catalyst design based on molecules that can be derived from lignin for catalytic production of ClO_2 in water. A lignin-derived ligand bis(2-hydroxy-3-methoxy-5-propylbenzyl) glycine, (**DHEG**) was synthesized from 2-methoxy-4-propylphenol (dihydroeugenol (DHE)) and the amino acid glycine. Two mononuclear

iron and manganese complexes of **DHEG** were prepared, characterized, and employed for the oxidation of chlorite to chlorine dioxide in aqueous solution. Peroxyacetic acid (PAA) was used as a ‘green’ oxidant in the redox reactions for the catalyst activation generating high valent Fe and Mn(IV)-OH intermediates. EPR studies verified the formation of a high valent Mn^{IV} species. Both Fe and Mn activated complexes catalyzed chlorite oxidation with bimolecular rate constants of 32 and 144 M⁻¹ s⁻¹, respectively, at pH 4.0 and 25 °C. The Mn complex was found to be more efficient for chlorite oxidation with a turnover frequency of 17 h⁻¹ and remained active during subsequent additions of PAA. The rate of ClO₂ formation with PAA/Mn-DHEG was first-order in PAA and showed acidic pH dependence. A mechanism that accounts for all observations is presented.



Chapter 3 highlights the need of more environmentally benign polar aprotic solvents (PAS) from sustainable resources. Of particular interest for this work is the catalytic conversion of cellulose to short chain polyols and the coupling of these polyols with *N,N*-dimethylurea (DMU) to produce cyclic PAS. Detailed chemistry background for this transformation are presented within this chapter.

In the final chapter, a green and catalytic process is described for the synthesis of *N,N'*-dimethylimidazolidinone (**DMI**) and 1,3,4-trimethylimidazolidin-2-one (**TMI**) from

cellulose, the most abundant and non-edible component of biomass. The physical and chemical properties of **DMI** and **TMI** including high boiling point, remarkable chemical stability, and being more eco-friendly than DMF make them appealing for use in the pharmaceutical industry. Cellulose depolymerization and reaction of intermediate products with N,N-dimethylurea (DMU) to produce PAS have been investigated in a one-pot, two-step process at elevated temperature. Ru/C is an effective multifunctional catalyst for both C-C bond cleavage of cellulose and subsequent hydrogenation of the unsaturated products in the second step; the catalyst also promotes the condensation hydroxy ketone intermediates with DMU to create cyclic PAS concurrently. Such tandem reactions are challenging to achieve particularly when incompatible conditions are required for each step. Solvent selection is also challenging with the low solubility of cellulose in most common organic solvents. Herein, the overall 85% selectivity for PAS was achieved from the reactions of cellulose or sugar with DMU over Ru/C in DMI (the product) as a solvent. The optimized conditions for coupling of 1,2-propylene glycol with DMU was used in a mechanistic study for the production of PAS with both homogeneous and heterogenous Ru catalysts. Catalytic oxidation of 1,2-PG to hydroxy acetone is the key step to produce **TMI** with a higher yield obtained using electron-donating phosphine ligands on Ru.

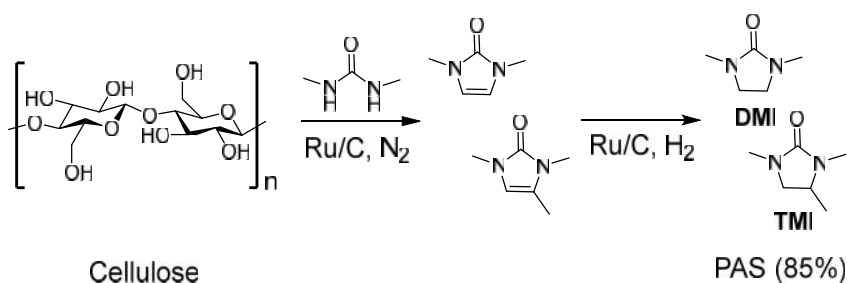


TABLE OF CONTENTS

ABSTRACT	v
LIST OF FIGURES	xi
LIST OF TABLES	xv
LIST OF SCHEMES	xvi
CHAPTER 1. CHLORINE DIOXIDE CHEMISTRY, APPLICATIONS, AND CATALYTIC PRODUCTION	1
1.1 Introduction	1
1.2 Chlorine dioxide: applications and industrial production	3
1.3 Catalytic oxidation of chlorite into chlorine dioxide.	5
1.4 High-spin Mn-oxo complexes	11
1.5 Molecular orbital theory of terminal metal-oxo complexes	14
1.6 Chlorine dioxide decomposition	16
1.7 Environmental concerns: accumulation and toxicity	18
1.8 Summary	19
1.9 References	21
CHAPTER 2. LIGNIN DERIVED NON-HEME IRON AND MANGANESE COMPLEXES FOR THE PRODUCTION OF CHLORINE DIOXIDE	27
2.1 Introduction	27
2.2 Experimental	29
2.2.1 Materials	29
2.2.2 Instrumentation	30
2.3 Purification of sodium chlorite	31

2.4	Ligand Synthesis	32
2.5	Synthesis of Fe and Mn Complexes	33
2.6	Elemental analysis	35
2.7	X-ray Structure of 2, Fe-DHEG	35
2.8	General procedure for drawing Job plot by UV–vis method:	37
2.9	Oxidation State of 2, Fe-DHEG	39
2.10	Oxidation State of 3, Mn-DHEG	40
2.11	Catalytic oxidation of Chlorite (ClO_2^-) to chlorine dioxide (ClO_2)	43
2.11.1	Fe-DHEG and Formation of ClO_2	43
2.11.2	Mn-DHEG and Formation of ClO_2	44
2.12	Catalyst activation	46
2.12.1	Oxidation of Fe-DHEG by PAA	46
2.12.2	Oxidation of Mn-DHEG by PAA	47
2.13	Electron Paramagnetic Resonance (EPR)	49
2.14	The Effect of pH on the yield of chlorine dioxide by Mn-DHEG/PAA	50
2.15	Kinetic analysis for catalytic oxidation of chlorite	53
2.15.1	Catalysis by Mn-DHEG	53
2.15.2	Catalysis by Fe-DHEG	55
2.16	Catalytic decomposition of chlorine dioxide	58
2.16.1	ClO_2 decay by catalyst 3, Mn-DHEG	58
2.16.2	ClO_2 decay by catalyst 2, Fe-DHEG	62
2.17	Iodometric method to determine the concentration of chlorite and chlorate ions	63
2.18	Results and discussion	66
2.19	Conclusion	72
2.20	References	73
CHAPTER 3. PREPARATION OF SUSTAINABLE POLAR APROTIC SOLVENTS FROM BIOMASS		77
3.1	Introduction	77
3.2	Cellulose conversion to polyols	79

3.3	Retro-aldol condensation of cellulose	82
3.4	Cellulose solubility	84
3.4.1	Non-aqueous cellulose solvent	84
3.5	Synthesis of polar aprotic solvents (PAS)	86
3.5.1	Coupling of diols with dimethylurea	86
3.5.2	Coupling of furfural derivatives with amines	87
3.6	Conclusions	88
3.7	References	89
 CHAPTER 4. ONE-POT TWO-STEP CATALYTIC REACTION OF CELLULOSE AND N,N-DIMETHYLUREA OVER RU/C		94
4.1	Introduction	94
4.2	Experimental section	98
4.2.1	Material	98
4.2.2	General procedure	98
4.2.3	Product Characterization for Compounds TMI and TMHI	99
4.2.4	Instrumentation and Analysis	100
4.2.5	HPLC analysis	100
4.2.6	NMR Analysis	101
4.3	Results	102
4.3.1	PAS from cellulose	102
4.3.2	Conversion of glucans directly to PAS	108
4.3.3	Coupling of 1,2-PG with DMU and solvent effects	111
4.3.4	Electronic effect of Ruthenium on the reaction of 1,2-PG and DMU	115
4.4	Discussion	116
4.5	Conclusions	119
4.6	References	120

LIST OF FIGURES

Figure 1.1 Iron protoporphyrin IX, the active site of Cytochrome P450 and Compound I in Cytochrome P450	7
Figure 1.2 Manganese porphyrins and porphyrazine investigated as catalysts.	11
Figure 2.1: ESI-MS spectra of Fe-DHEG and Mn-DHEG complexes.....	34
Figure 2.2 X-ray crystal structure of 2 Fe-DHEG	36
Figure 2.3 (a) UV-vis absorption titration spectra of $\text{Mn}(\text{CH}_3\text{COO})_3 \cdot 2\text{H}_2\text{O}$ and DHEG and triethylamine in methanol. (b) Benesi-Hildebrand plot of DHEG with Mn^{3+} at pH 9.8.	38
Figure 2.4 Job's plot diagram of a DHEG –Mn complex determined at 490 nm.....	39
Figure 2.5 (a) UV-vis of various concentration of 2 Fe-DHEG in methanol; (b) Extinction coefficient () of the absorption bands is calculated.....	39
Figure 2.6 EPR spectrum of 2 Fe-DHEG in DMF/THF at 10 K and Mossbauer Spectra of 2 Fe-DHEG.....	40
Figure 2.7 UV-vis Spectra of DHEG ligand, Mn-DHEG in MeOH and extinction coefficient () of the absorption bands is calculated.....	42
Figure 2.8 EPR spectrum of 3 , Mn-DHEG in DMF/THF at 10 K.	43
Figure 2.9 UV-vis spectral changes of the chlorite oxidation with 2 Fe-DHEG.....	44
Figure 2.10 (a) Absorption spectral changes of $[\text{ClO}_2^-]$ upon addition of Mn-DHEG and PAA at pH 5.0 (b) The effect of using other oxidants such as H_2O_2 or APS on oxidation of chlorite and uncatalyzed reaction with PAA.	45

Figure 2.11 (a) UV-Vis spectral changes for the reaction of Fe-DHEG with PAA, (b) Time-resolved of absorbance at 540 nm due to formation of Mn ^{IV} complex, the reaction of Mn with various concentration of PAA (c) Plot of pseudo-first order rate constant (k_{obs}) of the decay of Fe ^{III} (OOR) versus initial [PAA].	46
Figure 2.12 (a) Formation of Mn ^{IV} species supported by UV-vis spectroscopy when Mn-DHEG is reacted with PAA. (b) Time-resolved absorbance at 490 nm, the reaction of Mn with various concentration of PAA (c) Plot of pseudo-first order rate constant (k_{obs}) of the decay of Mn ^{III} versus [PAA].	47
Figure 2.13 (b) Time-resolved of absorbance at 330 nm due to formation of Mn ^{IV} complex, (c) Plot of pseudo-first order rate constant (k_{obs}) of the decay of Mn ^{III} (OOR) versus initial [PAA].	48
Figure 2.14 Activation of 3 Mn-DHEG with H ₂ O ₂ , H ₂ O ₂ and acetic acid, and PAA	49
Figure 2.15 EPR spectrum of the resulting complex from reaction of 3 with PAA.	50
Figure 2.16 The effect of pH on the formation of ClO ₂	51
Figure 2.17 Time dependent concentration of chlorine dioxide at 360 nm at pH 5.0	51
Figure 2.18 Time dependent concentration of chlorine dioxide at 360 nm at pH 4.0	52
Figure 2.19 Time dependent concentration of chlorine dioxide at pH 4.0 catalyzed by Mn-DHEG and the plots of k_{obs} vs [PAA], and [Mn-DHEG] respectively.	55
Figure 2.20 Time dependent concentration of chlorine dioxide at pH 4.0 catalyzed by Fe-DHEG and the plots of k_{obs} vs [PAA], [Fe-DHEG], and [NaClO ₂]	57

Figure 2.21 Activation of 3 Mn-DHEG with ClO ₂ at pH 4.0.....	59
Figure 2.22 The effect of multiple addition of PAA on ClO ₂ production	60
Figure 2.23 Time profile of chlorite oxidation with Mn-DHEG and PAA at pH 5.0	61
Figure 2.24 Time profile of chlorine dioxide decomposition with Mn-DHEG and various concentration of PAA at pH 5.0 and plot of pseudo-first order rate constant (k_{obs}) of the ClO ₂ decay versus [PAA] at pH 4.0 and pH 5.0.....	62
Figure 2.25 Time profile of chlorine dioxide decomposition with Fe-DHEG and various concentration of PAA at pH 4.0 and plot of pseudo-first order rate constant (k_{obs}) of the ClO ₂ decay versus [PAA] at pH 4.0	63
Figure 3.1 Industrially Important Polar Aprotic Solvents (PAS)	78
Figure 3.2 Ru(PNN) complex and dearomatization by base.	88
Figure 3.3 Dehydrogenative coupling of THFA with secondary amine to synthesize aprotic amides with Ru(PNN) catalyst.	88
Figure 4.1. Industrially Important Polar Aprotic Solvents (PAS)	95
Figure 4.2. Cellulose conversion to PAS and polyols, the experimental schematic and mass balance	104
Figure 4.3. Analysis of PAS and polyol fractions from the catalytic conversion of cellulose in various solvents	107
Figure 4.4. Analysis of PAS and polyol products obtained from the catalytic conversion of fructose (Fru) and glucose (Glu) in various solvents.....	110

Figure 4.5 Plot of TMHI yields vs. Hammett constants of various para substituents on the phenyl phosphine ligands. 116

LIST OF TABLES

Table 2.1 Elemental analysis of the DHEG ligand and the corresponding Fe/Mn complexes.	35
Table 2.2 Results for the catalytic conversion of chlorite to chlorine dioxide in 50.0 mM acetate buffer at pH = 5.0	52
Table 2.3: Results for the catalytic conversion of chlorite to chlorine dioxide in 50.0 mM acetate buffer at pH = 4.0	52
Table 2.4 Iodometric method to determine the concentration of chlorite and chlorate ions for the catalytic decomposition of ClO ₂ by Mn-DHEG 3 at pH 5.0.....	65
Table 2.5 Rate constants for reactions of Fe-DHEG 2 and Mn-DHEG 3	71
Table 4.1 The effect of catalyst loading on the cellulose conversion and PAS selectivities	105
Table 4.2 Coupling of 1,2-PG and DMU	112
Table 4.3 Results of reactions with varying ratios of 1,2-PG and DMU.....	114
Table 4.4 Results of coupling reactions of 1,2-PG and DMU at various temperature	114
Table 4.5 Results of <i>in situ</i> formation of Ru catalysts with varying phosphine ligands ...	115

LIST OF SCHEMES

Scheme 1.1 Industrial methods for producing chlorine dioxide from sodium chlorate.	4
Scheme 1.2 Mechanism of oxygen activation and O-atom transfer to substrate in Cytochrome P450	9
Scheme 1.3 Qualitative orbital splitting diagrams for oxo-metal complexes with (A) tetragonal and (B) trigonal symmetries. (C) Structure of the oxomanganese (III) precursor	14
Scheme 1.4 Qualitative crystal field splitting for octahedral metal-oxo complexes.	15
Scheme 1.5 Proposed mechanisms for the decomposition of chlorine dioxide.	18
Scheme 2.1. Synthesis of ligand 1 and its Fe and Mn complexes 2 and 3 . $ML_3 \cdot YH_2O$ represents $FeCl_3 \cdot 6H_2O$ or $Mn(CH_3COO)_3 \cdot 2H_2O$	29
Scheme 2.2 Equilibrium reaction of PAA with hydrogen peroxide	48
Scheme 2.3: Consecutive first-order reactions of the chlorite oxidation and the ClO_2 decay.	61
Scheme 2.4 proposed mechanism for chlorite oxidation catalyzed by 3 Mn-DHEG in the presence of PAA and decomposition of chlorine dioxide.	71
Scheme 3.1 . Biomass conversion to chemicals useful for solvent synthesis.....	79
Scheme 3.2 Catalytic conversion of cellulose into polyols	80
Scheme 3.3 Reaction pathways for the production of glycolaldehyde and dihydroxyacetone from glucose decomposition in supercritical water	83

Scheme 3.4 Synthesis of PAS from coupling of diols with DMU	87
Scheme 4.1 Catalytic conversion of cellulose into polar aprotic solvent (PAS) via tandem catalysis.....	96
Scheme 4.2 Plausible mechanism for the production of unsaturated product TMHI.....	118

CHAPTER 1

CHAPTER 1. CHLORINE DIOXIDE CHEMISTRY, APPLICATIONS, AND CATALYTIC PRODUCTION

1.1 Introduction

Modern chemistry plays a crucial role in the improvement of quality of life around the world. However, these advances frequently came with an increase in contamination of the environment by toxic substances. Nowadays steps are being taken to reform the industrial processes to protect the environment mainly due to the rapid environmental degradation and massive extinction of species over last decades. In this context, catalysis has and will continue to impact the discovery and development of environmentally attractive technologies and products. Over last century, catalysis used in several industrial processes such as polymer production, oil refinery, ammonia synthesis and ... that would hardly possible without active and selective catalysts. In other technologies, the stoichiometric reactions often applied which is inevitably associated with waste formation.^{1,2}

Water disinfection process, mainly chlorination, has been established by decades to eliminate the pathogens that are responsible for waterborne diseases from water supplies. Pathogens are generally considered a higher health risk than chemicals.³⁻⁵ Chlorination has been so successful that freedom from epidemics of waterborne diseases is now virtually taken for granted. Chlorine gas and sodium hypochlorite are the two major chemicals used for water disinfection. Poor biocidal activities of these compounds have been well documented which consequently result in bacterial resistance. Microbial resistance adds nearly \$1,400 to the bill for treating a bacterial infection and costs the nation more than \$2

CHAPTER 1

billion annually, according to a study in *Health Affairs*. It is also documented that halogenated organic byproducts formed during the water treatment are linked to cancer and endocrine disruption.⁶ Of the disinfection by-products, there are over 400 potential chemical species.⁷ Chlorate and chlorite ions are also formed during the slow decomposition of sodium hypochlorite solutions; reaching the concentration of these chemicals above the EPA standards in our water system. The growing concern about the release of these materials into the environment is well understood.⁸ The negative health effects of water disinfection chemicals and the lack of its efficacy against certain pathogens have promoted the reexamination of available disinfection methodology to determine alternative agents or procedures. For these reasons, chlorine dioxide, ozone, and hydrogen peroxide are considered the alternatives where their production must be improved. Chlorine dioxide, ClO_2 has largely replaced chlorine in the pulp and paper bleaching⁸ which allows the higher strength/quality bleached pulp and generates much less amounts of chlorinated organics. Global chlorine dioxide market reports forecast its major growth in water and wastewater treatment by 2028.

The primary commercial use of chlorine dioxide is as an oxidizing agent for pulp bleaching and water disinfection/treatment.⁹ Chlorine dioxide is quite toxic and thus requires great care when handling. Chlorine dioxide is preferred over chlorine gas (Cl_2) for water treatment as it exhibits superior antimicrobial activity and generates trace amount of harmful chlorinated by-products.⁷ One major drawback; however, is the instability of ClO_2 at high pressure, a fact that effectively prohibits its transport as a gas. Hence, on-site production of ClO_2 is a prerequisite to any practical application.

CHAPTER 1

The current industrial production of ClO_2 uses stoichiometric reagents which is inevitably associated with formation of waste and halogenated byproducts.¹ The majority of these industrial methods apply highly corrosive and acidic conditions, which raise health, environmental, and safety concerns. Clearly, developing a simpler and greener process to produce ClO_2 will have a significant positive impact on the environment and human health. To this context, catalytic generation of chlorine dioxide is considered an alternative path for the development of environmentally attractive disinfection process for water treatment. In this study, we describe a simpler catalyst design with the use of an earth-abundant metal and readily available ligand that offers a convenient route to ClO_2 production under reasonably mild and noncorrosive conditions. This system also remediates ClO_2 at lower rate than ClO_2 production which is of interest from an environmental standpoint.

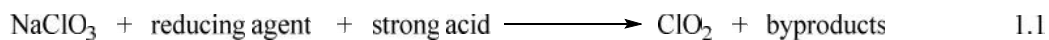
1.2 Chlorine dioxide: applications and industrial production

The chlorine dioxide radical is a yellowish-green gas with an odd number of electrons making it a paramagnetic radical. ClO_2 is considered a powerful one electron oxidant ($E^\circ = 0.936 \text{ V}$).¹⁰ It is highly soluble in water, 8 g/mL at 20 °C, that remains a gas in solution.¹¹ Chlorine dioxide condenses to form an unstable liquid. Both the gas and liquid are sensitive to temperature, pressure, and light. At concentrations above 10% in air, chlorine dioxide may be explosive.⁹ As a result, the preparation and distribution of chlorine dioxide in bulk have not been deemed practical. It has been generated and used on site.

CHAPTER 1

The primary commercial use of chlorine dioxide is as an oxidizing agent for pulp bleaching and water disinfection/treatment.⁹ Chlorine dioxide is quite toxic and thus requires great care when handling. Chlorine dioxide is preferred over chlorine gas (Cl₂) for water treatment as it exhibits superior antimicrobial activity and generates trace amount of harmful chlorinated by-products.⁷ Microorganisms cannot build up any resistance against Chlorine dioxide because it reacts directly with amino acids and RNA in the cell causing several cellular processes to be interrupted. Chlorine dioxide is one of disinfectants that are effective against Giardia Lambia and Cryptosporidium parasites which are found in drinking water.

Industrially, there are several methods for the production of chlorine dioxide (Scheme 1.1). Chlorine oxyanions (ClO_n⁻, n = 1- 4) are the prevalent source of ClO₂ in every method. The reduction of sodium chlorate is the more efficient process and is generally used when large volumes and high concentrations of chlorine dioxide are needed.



Scheme 1.1 Industrial methods for producing chlorine dioxide from sodium chlorate.

From these reactions, several by-products are formed: chlorine gas, sodium sulfate, oxygen and water. The benefit of using sulfuric acid as the strong acid over hydrochloric acid is the trace amount chlorine gas as the byproduct generated. Furthermore, at higher concentration of sulfuric acid, sodium sesquisulfate (Na₃H(SO₄)₂) can be isolated as a

CHAPTER 1

precipitate and converted into sodium sulfate and sulfuric acid.¹¹ The recovered sulfuric acid is then returned to the chlorine dioxide reactor making sulfuric acid a very cost-effective reagent for chlorine dioxide production.

As the reaction chemistry is much faster when using hydrogen peroxide, hydrogen peroxide can be used to replace sulfur dioxide, and chloride. Changing to hydrogen peroxide brings a number of advantages: higher capacity for the existing reactor, less dangerous reducing agent, and purer chlorine dioxide.¹¹

The majority of chlorine dioxide is stoichiometrically produced using these reactants for cost effectiveness and reliability reasons. Consequently, high concentration of chlorate and extremely acidic conditions; sulfuric acid (pH ~ 1), are required to maintain the production of chlorine dioxide at certain rate. The one-electron electrochemical oxidation (Eq. 1.14) of chlorite offers an alternative route to ClO₂ but requires a substantial energy input and regular maintenance of equipment. Therefore, a catalytic process is of interest from an environmental standpoint and merits exploration which will be discussed in the remaining of this chapter.

1.3 Catalytic oxidation of chlorite into chlorine dioxide.

Although chlorite oxidation to chlorine dioxide seems simply electron transfer away from chlorite; mechanistically, this process contains the oxidation of the metal center and proton transfer. Enzymes such as chlorite dismutase (ClD), horseradish peroxidase (HRP), and chloroperoxidase (CPO) are known to catalyze the conversion of chlorite.¹²⁻¹⁶ Chlorite dismutase converts chlorite ion efficiently to dioxygen gas and Cl⁻ ion with hypochlorous

CHAPTER 1

acid (HOCl) as proposed reaction intermediate. Unlike Cl₂, horseradish peroxidase yields only chlorine dioxide and chloride.¹⁵

The cytochromes P450 are a family of iron-containing enzymes that catalyze the transfer of an oxygen atom from O₂ to organic substrates, producing water as a by-product.¹⁷

Thousands of P450 enzymes are known and have been found in a range of organisms including bacteria, fungi, plants, insects, and mammals.¹⁷ Although the various members of the P450 family share some structural similarities, by far the most important conserved feature in P450 is a cysteine-ligated heme (iron protoporphyrin IX, Figure 1.1).^{18, 19} This heme prosthetic group is the active site of oxygen activation and O-atom transfer by P450. P450s are remarkable because they catalyze the monooxygenation of a variety of substrates using O₂ as an oxidant. It is important, however, to note that when one oxygen atom from O₂ is passed to a substrate, the remaining oxygen atom is reduced to water by two protons and two electrons. The two electrons needed in order to carry out this reduction are provided to P450 by a system of electron transport proteins and ultimately come from common NAD(P)H reducing equivalents.¹⁸ In most cases, this electron transport system consists of a flavoprotein (plus an iron-sulfur protein for mitochondrial and bacterial P450s) that shuttles electrons from NAD(P)H to P450.²⁰ However, self-sufficient P450 enzymes are known (such as P450-BM3 from *Bacillus mageterium*) which contain both the heme active site as well as an electron-shuttling flavin system in^{20, 21} the same subunit.

CHAPTER 1

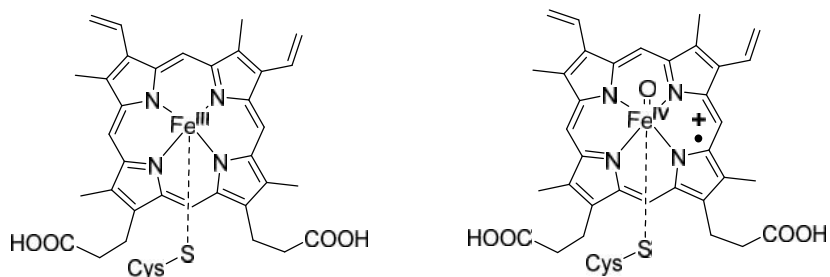


Figure 1.1 Left) Iron protoporphyrin IX, the active site of Cytochrome P450; Right) Compound I in Cytochrome P450

The catalytic mechanism of oxygen activation and substrate oxidation by Cytochrome P450 was an area of much active debate for many years.²² However, it has been confirmed by Rittle and Green that the reactive, hydroxylating intermediate in P450 catalysis is an oxoiron(IV) porphyrin cation radical²³ (Compound I, Figure 1.1). This interesting species is not unique to P450 but can be found as an active intermediate in other heme enzymes including CPO²⁴ and HRP²⁵.

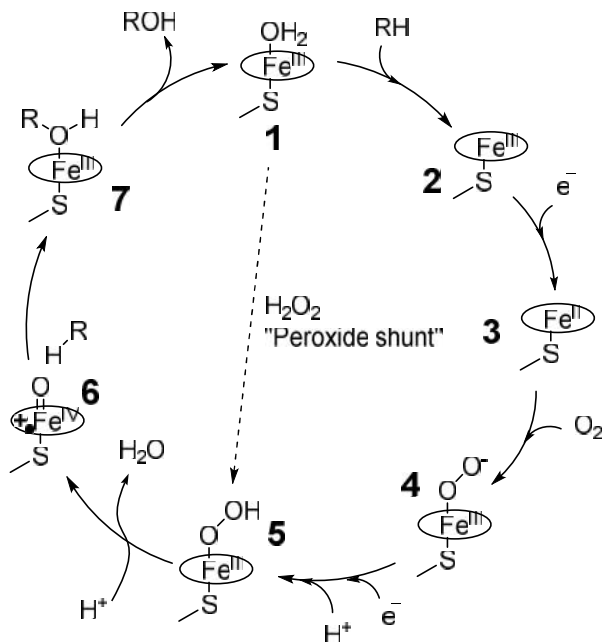
The mechanism where P450 activates O₂ to generate Compound I is given in Scheme 1.2.¹⁹ The hexa-coordinate aqua iron (III), **1**, was found as being a low-spin, d⁵ doublet.^{19, 25} Binding of a substrate displaces the aqua ligand resulting in high spin iron III complex and rising the reduction potential of the heme iron by as much as +300 mV.¹⁷ The O₂/ferrous heme complex (**4**) can be written as a pair of redox tautomers (O₂-Fe^{II} or O₂-Fe^{III}). This complex is diamagnetic and EPR-silent, although Mössbauer spectroscopy and the weakened O-O stretching frequency suggest that the iron (III) complex more properly describes the intermediate.^{26, 27} The oxyheme complex is then further reduced by a second electron to afford a peroxyiron(III) complex. In addition to being an intermediate on the pathway of oxygen activation to generate Compound I, this peroxyiron(III) species has

CHAPTER 1

also been implicated as a nucleophilic oxidant that is active in some P450s.²⁸ Protonation of the peroxy(III) intermediate affords a hydroperoxyiron(III) species (**5**) that was for a long time the last observable and isolable intermediate in the P450 mechanism.⁶ This species can also be generated from activation of hydrogen peroxide by the ferric enzyme via the peroxide shunt pathway (Scheme 1.2). Heterolytic O-O bond cleavage of this hydroperoxyiron(III) is understood to proceed via the “push-pull” mechanism, proposed by Dawson, *et al.*¹⁸

Heterolytic cleavage of the hydroperoxy O-O bond affords an oxoiron species formally at the oxidation state of Fe^V^{23-25, 29, 30}. Numerous studies have shown that this oxoiron species is more properly an oxoiron(IV) antiferromagnetically coupled to a porphyrin cation radical (**6**, Compound I^{20, 31-34}). Compound I has been long known and observed in CPO²⁴ and HRP²⁵ and recently isolated and characterized in P450.²³

CHAPTER 1



Scheme 1.2 Mechanism of oxygen activation and O-atom transfer to substrate in Cytochrome P450.¹⁹

The history of synthetic manganese porphyrins as biomimetic catalysts has evolved almost simultaneously along with analogous iron porphyrins. Manganese porphyrins have performed better than iron porphyrins as catalysts, particularly being less sensitive to bleaching during turnover. Synthetic manganese porphyrin (MnTPP) could catalyze a variety of hydrocarbon oxidations, including epoxidation, hydroxylation, and chlorination.^{35, 36} The existence of oxomanganese (IV and V) porphyrins was confirmed and proven that the oxo-Mn^V will be more stable with better electron withdrawing substituents. The rate of this reaction was found to be highly dependent on pH, resulting in the speculation that protons were required to activate a stable oxomanganese species.^{37,}

CHAPTER 1

Synthetic iron and manganese porphyrin analogues of Cytochrome P450 have been shown to catalyze dismutation of chlorite to give O₂ and Cl⁻ ion. Under physiological pH and aqueous conditions, some of these porphyrin analogues produce water-soluble ClO₂ gas from ClO₂⁻. Preparations of water-soluble Fe and Mn porphyrins were accomplished using cationic porphyrins (Figure 1.2). Clearly, the charge and electronic characters of the porphyrin ligand have a dramatic effect on the reactivity of these Compound I analogues. Highly electron-deficient water-soluble manganese and iron porphyrin analogues catalyze the oxidation of chlorite generating ClO₂ rapidly and efficiently with high turnover frequency under physiological conditions.³⁹⁻⁴³

Abu Omar and co-workers has reported on the dismutation of chlorite under physiological pH using water-soluble ferric porphyrins.⁴²⁻⁴⁴ In these model systems, the reaction proceeds for the most part to the disproportionation products, chloride and chlorate, in 1:2 stoichiometry. One exception was the fluorinated [Fe^{III}(TF4TMAP)]⁺ complex (1.2), which afforded moderate O₂ yields. More recently, a computational study on the [Fe^{III}(TF4TMAP)]⁺ complex supports the formation of Fe^{IV}(O) and chlorine monoxide intermediates via homolytic bond cleavage.⁴²⁻⁴⁴

Unlike the fluorinated ferric porphyrin, the manganese analogue favors the formation of ClO₂ as opposed O₂. The conversion of chlorite to chlorine dioxide in good yields catalyzed by [Fe^{III}(TF4TMAP)]⁺ under physiological pH at room temperature (Figure 1.2) has been reported in the literature.^{39, 40} Groves and co-workers have also independently shown that [Mn^{III}(TDMImP)]⁺ among other manganese porphyrin catalysts also convert chlorite to chlorine dioxide. Initial turnover frequencies at 25 °C for 2 mM

CHAPTER 1

ClO_2^- and catalyst $[\text{Mn}^{\text{III}}(\text{TDMImP})]^+$ ($10 \mu\text{M}$) were 1.00 , 1.03 , and 0.47 s^{-1} at pH 4.7 , 5.7 , and 6.8 respectively (Figure 1.2).⁴⁵ Chlorite can oxidize the transition metals as both a 1 and 2-electron oxidant. The oxidation state of the Mn(III)-porphyrin remained unchanged during turnover which was rationalized by the fast regeneration of Mn(III) compared to any changes in the oxidation state of Mn at the initial steps. Therefore the oxidation of Mn(III) by chlorite must be the rate-determining steps of overall catalytic cycle. Extremely high activity (32 TO/s) was reported for Mn (III) porphyrazine, $[\text{Mn}^{\text{III}}(\text{TM}_2\text{PyP})]^+$.⁴¹ The use of non-heme ligands as opposed to heme ligands, $[\text{Mn}^{\text{II}}(\text{N4Py})]^{2+}$ and $[\text{Mn}^{\text{II}}(\text{Bn-TPEN})]^{2+}$, has also been shown to catalyze the conversion of chlorite to ClO_2 .³⁹

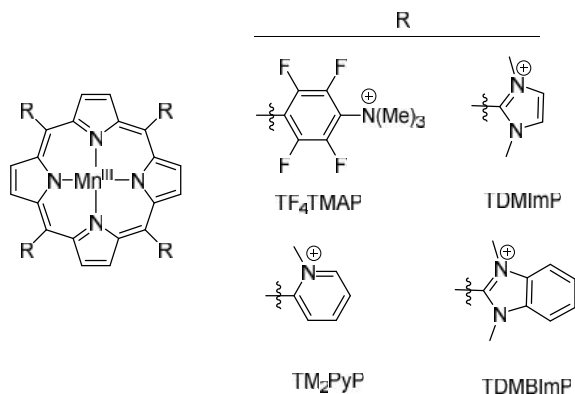


Figure 1.2 Manganese porphyrins and porphyrazine investigated as catalysts.

1.4 High-spin Mn–oxo complexes

Many first-row d-block elements, V, Mn, Fe, Co, Ni, Cu and Zn, except Ti and Cr were used in biology.⁴⁶ As we move across the 3d row, the ionization energies (IEs) increase on the metal as each electron removed. The highest accessible oxidation states as well as the number of accessible oxidation states increase up to Mn then decrease to Zn where only the $2+$ state is observed.^{46, 47} Nature choose Mn for oxidation of water into dioxygen

CHAPTER 1

producing 21% of our atmosphere. Oxidation of water via S-cycle is a four-electron process where electrons and protons must be removed and transferred away rapidly and efficiently. Various oxidation states must exist that permit rapid binding of substrates, and the whole structure must be sufficiently robust to survive tens of thousands of turnovers. In addition to a various oxidation states of Mn, more than the other 3d metals, the reduction potentials of all the higher states, from Mn(III) upwards, hydroxo- or oxo-species are in the range of the O-transformation reactions. Dioxygen production occurs at the active site of the enzyme photosystem II (PSII), referred to as the oxygen-evolving complex (OEC), which contains a unique Mn_4CaO cluster.^{48, 49} This embedded tetra manganese-calcium cluster in PSII catalyzes water oxidation to O_2 with a high turnover number (10^6) and a maximal turnover frequency (TOF) of 500 s^{-1} .^{50, 51} There is agreement that formation of the O–O bond occurs in the higher oxidized state of manganese. Quantum chemical studies have provided insight into this process with two various mechanisms.⁵⁰⁻⁵³ Most computational reports suggest a high valent Mn center with a terminal oxido ligand (Mn–oxo), which is a Mn^{IV} -oxyl radical (Mn–O•) rather than the isoelectronic Mn^{V} -oxo species.⁵⁰⁻⁵³

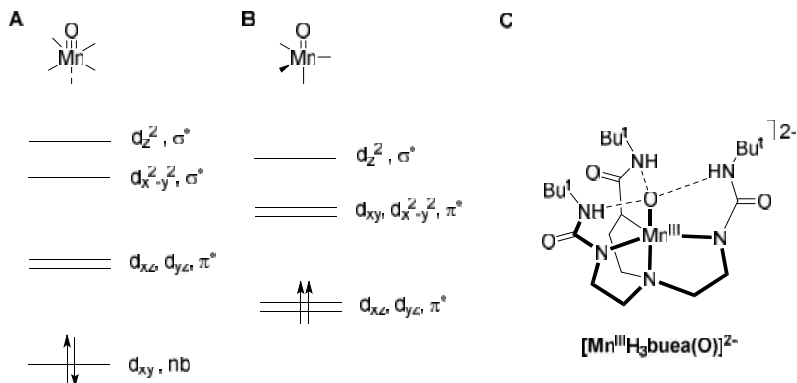
Complexes containing ancillary porphyrin,^{54, 55} corrole,⁵⁶ corrolazine⁵⁶ or salen ligand,⁵⁷ have been previously investigated to develop synthetic systems with Mn–oxo species and to investigate spectroscopically whether they support either a Mn^{V} -oxo state or a Mn^{IV} -oxyl state.⁵⁸⁻⁶¹ These catalytic systems were producing species that are tetragonal d^2 low-spin with $S=0$ spin ground states (scheme 1.3). Hence, they will be diamagnetic resulting in a triple bond between the metal center and the terminal oxo ligand, $\text{Mn}\equiv\text{O}$.^{62, 63} The

CHAPTER 1

strength of multiple metal-oxygen bonding is indicated by short M-O distances and high M-O stretching frequencies (900- 1000 cm^{-1}).⁶³ In some cases, these oxo complexes cannot be protonated even in concentrated acid solution. Results from oxygen-17 labeling studies showed that the Mn-oxo unit becomes more electrophilic as the manganese center is oxidized, which would enhance its reactivity toward a nucleophile.

Mayer and Thorn were the first to suggest that metal-oxo complexes that adopt a trigonal structure will form two degenerate orbitals accommodating two electrons for d^2 metal-oxo complexes and producing $S=1$ spin ground state.^{64, 65} The metal-oxo interactions in such complexes are weaker than those with tetragonal symmetry, making the former a more reactive species. Results from a few reports on high spin Mn^{V} -oxo complexes ($S=1$) are indicative of paramagnetic properties with trigonal geometry.^{14, 35, 44} Paramagnetic Mn^{V} -oxo porphyrin³⁵ and Mn^{V} -imido corrole⁴⁴ species have been observed for hydrocarbon oxidation and hydrogen atom transfer without studying details on the geometry of these complexes. A series of $[\text{Mn}^{\text{n}}\text{H}_3\text{buea}(\text{O})]^{\text{m}}$ ($n = 3+$ to $5+$; $m = 2-$ to 0) complexes have been designed to impose local trigonal geometry within the complex by Borovik and his co-workers to investigate the electron distribution within the Mn-oxo unit and the spin density on the oxido ligand. It is established that the density on oxyl radical is less than what is expected and a high-spin Mn^{V} -oxo center should be considered a viable candidate for the high valent site in the formation of the O-O bond.^{14, 61}

CHAPTER 1



Scheme 1.3 (A, B) Qualitative orbital splitting diagrams for oxo-metal complexes with (A) tetragonal and (B) trigonal symmetries. (C) Structure of the oxomanganese (III) precursor.

1.5 Molecular orbital theory of terminal metal-oxo complexes

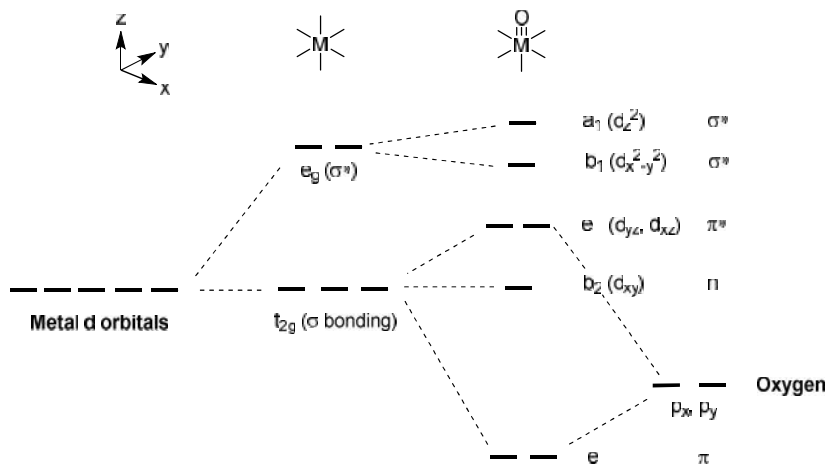
A number of ligands including oxo (O^{2-}) not only forms σ bonds to a metal center but also have additional lone pairs that can be involved in bonding. The additional lone pairs are of π symmetry, so these ligands are termed π donors. π bonding will be important when the ligand lone pairs both overlap well and have a good energy match with the metal orbitals of π symmetry (d orbitals). Productive π interactions that stabilize the metal-ligand bond, requires that the metal d orbital(s) be empty. If the metal d orbitals are filled, however; it will result in destabilizing antibonding interactions.

In a molecular orbital picture, overlap of two orbitals generates both bonding and antibonding orbitals, our focus being σ and π^* orbitals. The determination of a simple bond order assumes that the destabilization of π^* is equal to the stabilization of σ . But even at the simplest level of molecular orbital theory the antibonding interaction is greater than the bonding: for the overlap of two identical orbitals, σ is stabilized by an energy $-(1 + S)$ while π^* is destabilized by $+(1 - S)$ where S is the overlap integral.^{63, 66}

CHAPTER 1

The theory reinforces our qualitative understanding that the overlap of two filled orbitals is an unfavorable interaction. There are no examples of stable terminal oxo complexes in the cobalt, nickel, or copper triads. The oxo ligand in the stable oxides and oxo complexes of the late transition metals always bridges two or more metal centers. This is because in most late-metal terminal oxo complexes metal-oxygen antibonding orbitals would have to be occupied.

The molecular orbital description of octahedral mono-oxo complexes (Scheme 1.4) is well established from spectroscopic, theoretical, and chemical studies.⁶³ The ligand field splitting resembles the octahedral "two above three" pattern except that two of the t_{2g} orbitals (d_{xz} , d_{xy}) are involved in bonding with the oxo; they are the antibonding components of the M-O bond. Note that the two bonds are degenerate in C_{4v} symmetry and therefore the M-O bond should be described as a triple bond. The splitting between the nonbonding d_{xy} and the d_{xz} , d_{xy} is large enough that all known d^2 mono-oxo complexes are diamagnetic, with the electrons paired in the d_{xy} orbital.¹⁴



Scheme 1.4 Qualitative crystal field splitting for octahedral metal-oxo complexes.

CHAPTER 1

In this picture up to two d electrons can be accommodated without population of e_g levels. This explains why the vast majority of terminal oxo complexes have d^0 , d^1 , or d^2 configurations.

Reactive d^4 iron-oxo analogues to cytochrome P450 have been shown low stretching frequencies [$\nu(\text{Fe-O}) = 800\text{-}850\text{ cm}^{-1}$] and long Fe-O distances.⁶⁷ Low metal-oxo stretching frequencies are also observed for excited states of metal oxo complexes in which e_g orbitals are populated. The d^4 iron-oxo complexes are stable only when very bulky ancillary ligands (e.g. tetramesitylporphyrin) are used to prevent dimerization to μ -oxo species. The conversion of terminal oxo ligands to bridging groups is a common way to decrease antibonding. The p -symmetry lone pair(s) on a bridging oxygen are less available for bonding and metal-oxygen overlap is less at the longer distances found for μ -oxo species.

1.6 Chlorine dioxide decomposition

The decay of the ClO_2 in various condition has been investigated previously by several research groups (Scheme 1.5). Kinetic evidence shows three concurrent pathways exhibiting a first order dependence in $[\text{OH}^-]$ but variable order in $[\text{ClO}_2]$. Pathway 1 is the disproportionation reaction and first order in chlorite anion concentration. The $(\text{HOCl}(\text{O})\text{O})^-$ intermediate proposed in pathway 1 is the adduct of OH^- with Cl atom of ClO_2 where is observed similarly in reaction of ClO_2 with hydrogen peroxide (HO_2^-),⁶⁸ and thiosulfate ($\text{S}_2\text{O}_3^{2-}$)⁶⁹. Computational studies of this adduct $(\text{HOCl}(\text{O})\text{O})^-$ revealed that a significant amount of negative charge from OH^- is transferred to ClO_2 .⁷⁰ The kinetics and

CHAPTER 1

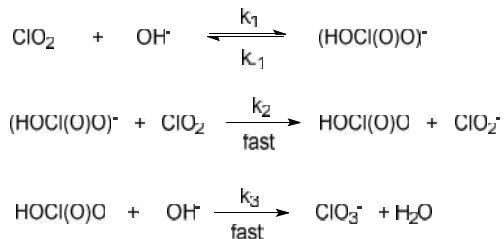
the ab initio calculation support that nucleophile, in this case OH^- , and ClO_2 must come together in the transition state assisting the electron-transfer process from the outer sphere.

The proposed intermediate in pathway 2 (OCIOOH^-) is the adduct of OH^- with the oxygen atom of ClO_2 .⁷¹ Computational studies are indicative of this intermediate as the most favorable intermediate where OCl is weakly bound to an OOH fragment. A rapid electron transfer with a second ClO_2 will produce ClO_2^- and OCIOOH making the latter species undergo reaction with OH^- favorably to generate HOClO and HOO^- . The reaction of ClO_2 and HOO^- is known to give ClO_2^- and O_2 .⁷¹ The second-order reaction rate constant for the ClO_2 decay by hydrogen peroxide (HO_2^-) is calculated to be $1.3 \times 10^5 \text{ M}^{-1}\text{s}^{-1}$ and the low lying plateau value at pH lower than 6 is indicative of the unreactive nature of non-dissociated H_2O_2 ($k < 0.1 \text{ M}^{-1}\text{s}^{-1}$).⁷¹ Pathway 2 is first order in chlorine dioxide but forms chlorite anion as the only chlorine containing product.

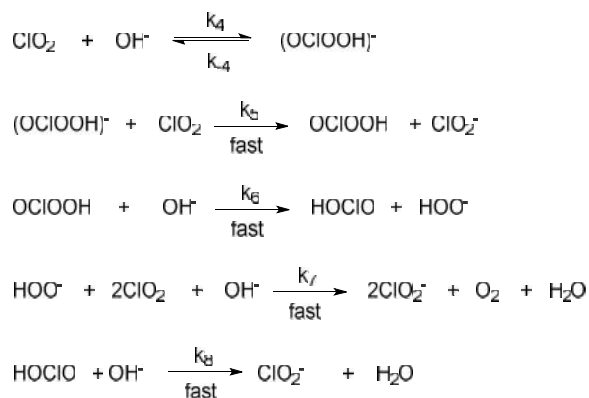
Pathway 3 is considered second order in chlorine dioxide and generates equal amounts of ClO_2^- and ClO_3^- . A Cl_2O_4 intermediate is proposed in this path which was proposed by Halperin and Taube.⁷² Similar intermediate Br_2O_4 was proposed for BrO_2^- .⁷³ At high concentrations of ClO_2 , pathway 3 causes the overall ClO_3^- yield to approach the overall yield of ClO_2^- attack on an oxygen atom of ClO_2 that leads to peroxide intermediates and yields ClO_2^- . Considering all the chlorinated products formed, pathway 3 is not sufficient enough and combination of two pathways should be present to produce all in the decomposition of ClO_2 . Pathway 2 is attributed to OH^- and O_2 as products.

CHAPTER 1

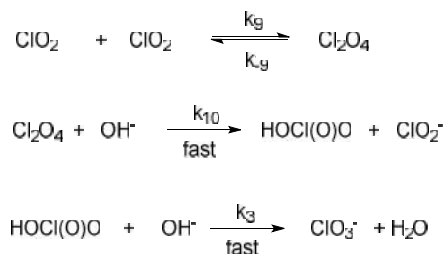
Pathway 1. First-order in $[\text{ClO}_2]$; products: $[\text{ClO}_2^-] = [\text{ClO}_2^-]$.



Pathway 2. First-order in $[\text{ClO}_2]$; products: $[\text{ClO}_2^-]$ and O_2 .



Pathway 3. First-order in $[\text{ClO}_2]$; products: $[\text{ClO}_2^-] = [\text{ClO}_2^-]$.



Scheme 1.5 Proposed Mechanisms for the Decomposition of Chlorine Dioxide.

1.7 Environmental concerns: accumulation and toxicity

The oxyanion of chlorine (ClO_x^- , $x = 1-4$) have found numerous industrial applications as bleaching agents, explosives, herbicides, and disinfectant. The wide range of applications and high solubility in water has led to severe contamination of water sources by these toxic

CHAPTER 1

anthropogenic pollutants. Despite thermodynamic properties of these oxyanion as strong oxidizing reagents, slow kinetics generally limits their reactivity. Perchlorates, the most unstable class of these oxyanions, require a decomposition temperature as high as 150 °C for ammonium perchlorate or 492 °C for sodium perchlorate.⁷⁴ The lack of reactivity results from high strength of chlorine-oxygen bonds, and the requirement that reduction proceed by removal of an oxygen atom, rather than by direct interaction of a reducing agent with a chlorine atom.^{74, 75} This capacity as a strong oxidant and the limited reactivity nature allow these oxyanions to persist in the environment and they are hard to treat by chemical reduction, while catalytically and biologically mediated reactions can effectively degrade them. Due to highly solubility and stability nature of these oxyanions; they mobilize through the water-soil system and accumulate in the water supplies or even in edible plant species of high human consumption which has attracted recent attention. The ingestion of food products containing these oxyanions represents a potential health risk to people due to their adverse effects on thyroid, hormone, and neuronal development, mainly in infants and fetuses.

1.8 Summary

This introduction has described the latest hygienic concerns of the 21st century and an innovative way to resolve these via chemical catalysis. Chlorine Dioxide is a superior biocide that serves as the best alternative to chlorination in multiple industries such as water/wastewater treatment, hospitals, food, and agriculture industries. We have seen also how biomimetic model compounds based on iron and manganese porphyrins have not only

CHAPTER 1

assisted in understanding P450 reactivity but have also provided new insights that are of much use for the future of biomimetic and practical catalysis.

The previously investigated catalysts for one electron oxidation of chlorite to ClO_2 are based on the manganese or iron porphyrin complexes.⁴⁰⁻⁴² In these systems, the chlorite dismutation initiates through the electron transfer (ET) followed by oxygen atom transfer to afford high valent manganese and iron-oxo. Both oxidation states (IV and V) of these oxo complexes will oxidize chlorite directly to ClO_2 .⁴⁰⁻⁴² Although the full conversion of chlorite to ClO_2 was achieved under physiological pH using water soluble Fe or Mn porphyrins, they suffer from a few drawbacks such as the instability of the catalysts in oxidative environment, and poor atom economy in the synthesis of these catalysts. Interest in developing a simpler catalyst design, enhancing the stability of the catalyst in oxidative environment, and obtaining materials from renewable resources inspired us to design a class of catalysts derived from the lignin precursors. Lignin has an outstanding characteristic of being highly resistant/recalcitrant towards both chemical and biological degradation, resistant to oxidative transformation in particular.⁷⁶ In next chapter, we will describe a simpler catalyst design with the use of an earth-abundant metal and readily available ligand that offers a convenient route to ClO_2 production under mild and noncorrosive conditions. This system clearly reaffirms the production of high valent Mn and Fe-oxo intermediate. ClO_2 remediation occurs at lower rate than ClO_2 production which is of interest from an environmental standpoint.

1.9 References

1. Delidovich, I.; Palkovits, R., Catalytic versus stoichiometric reagents as a key concept for Green Chemistry. *Green Chemistry* **2016**, *18* (3), 590-593. DOI: 10.1039/c5gc90070k
2. Sheldon, R. A., Fundamentals of green chemistry: efficiency in reaction design. *Chem. Soc. Rev.* **2012**, *41* (4), 1437-51. DOI: 10.1039/c1cs15219j
3. Zhang, X.; Chen, Z.; Shen, J.; Zhao, S.; Kang, J.; Chu, W.; Zhou, Y.; Wang, B., Formation and interdependence of disinfection byproducts during chlorination of natural organic matter in a conventional drinking water treatment plant. *Chemosphere* **2020**, *242*, 125227. DOI: 10.1016/j.chemosphere.2019.125227
4. Hrudey, S. E., Chlorination disinfection by-products, public health risk tradeoffs and me. *Water Res.* **2009**, *43* (8), 2057-92. DOI: 10.1016/j.watres.2009.02.011
5. Wu, Z.; Fang, J.; Xiang, Y.; Shang, C.; Li, X.; Meng, F.; Yang, X., Roles of reactive chlorine species in trimethoprim degradation in the UV/chlorine process: Kinetics and transformation pathways. *Water Res.* **2016**, *104*, 272-282. DOI: 10.1016/j.watres.2016.08.011
6. Kirchhoff, M. M., Promoting green engineering through green chemistry. *Environ. Sci. Technol.* **2003**, *37* (23), 5349-53. DOI: 10.1021/es0346072
7. Ashbolt, N. J., Risk analysis of drinking water microbial contamination versus disinfection by-products (DBPs). *Toxicology* **2004**, *198* (1-3), 255-62. DOI: 10.1016/j.tox.2004.01.034
8. Kringstad, K. P.; Lindstrom, K., Spent liquors from pulp bleaching. *Environ. Sci. Technol.* **1984**, *18* (8), 236A-48A. DOI: 10.1021/es00126a714
9. Ogata, N.; Shibata, T., Protective effect of low-concentration chlorine dioxide gas against influenza A virus infection. *J Gen Virol* **2008**, *89* (Pt 1), 60-7. DOI: 10.1099/vir.0.83393-0
10. Ison, A.; Odeh, I. N.; Margerum, D. W., Kinetics and mechanisms of chlorine dioxide and chlorite oxidations of cysteine and glutathione. *Inorg. Chem.* **2006**, *45* (21), 8768-75. DOI: 10.1021/ic0609554
11. Vogt, H.; Balej, J.; Bennett, J. E.; Wintzer, P.; Sheikh, S. A.; Gallone, P.; Vasudevan, S.; Pelin, K., Chlorine Oxides and Chlorine Oxygen Acids. In *Ullmann's Encyclopedia of Industrial Chemistry*, Wiley-VCH: 2010; Vol. 8, p 623.
12. van Ginkel, C. G.; Rikken, G. B.; Kroon, A. G.; Kengen, S. W., Purification and characterization of chlorite dismutase: a novel oxygen-generating enzyme. *Arch. Microbiol.* **1996**, *166* (5), 321-6. DOI: 10.1007/s002030050390
13. Streit, B. R.; DuBois, J. L., Chemical and steady-state kinetic analyses of a heterologously expressed heme dependent chlorite dismutase. *Biochemistry* **2008**, *47* (19), 5271-80. DOI: 10.1021/bi800163x
14. Taguchi, T.; Gupta, R.; Lassalle-Kaiser, B.; Boyce, D. W.; Yachandra, V. K.; Tolman, W. B.; Yano, J.; Hendrich, M. P.; Borovik, A. S., Preparation and properties of a monomeric high-spin Mn(V)-oxo complex. *J. Am. Chem. Soc.* **2012**, *134* (4), 1996-9. DOI: 10.1021/ja210957u

CHAPTER 1

15. Jakopitsch, C.; Spalteholz, H.; Furtmuller, P. G.; Arnhold, J.; Obinger, C., Mechanism of reaction of horseradish peroxidase with chlorite and chlorine dioxide. *J. Inorg. Biochem.* **2008**, *102* (2), 293-302. DOI: 10.1016/j.jinorgbio.2007.09.002
16. Dereven'kov, I. A.; Shpagilev, N. I.; Valkai, L.; Salnikov, D. S.; Horvath, A. K.; Makarov, S. V., Reactions of aquacobalamin and cob(II)alamin with chlorite and chlorine dioxide. *J. Biol. Inorg. Chem.* **2017**, *22* (4), 453-459. DOI: 10.1007/s00775-016-1417-0
17. Ortiz de Montellano, P. R., Hydrocarbon hydroxylation by cytochrome P450 enzymes. *Chem. Rev.* **2010**, *110* (2), 932-48. DOI: 10.1021/cr9002193
18. Sono, M.; Roach, M. P.; Coulter, E. D.; Dawson, J. H., Heme-Containing Oxygenases. *Chem. Rev.* **1996**, *96* (7), 2841-2888. DOI: 10.1021/cr9500500
19. Denisov, I. G.; Makris, T. M.; Sligar, S. G.; Schlichting, I., Structure and chemistry of cytochrome P450. *Chem. Rev.* **2005**, *105* (6), 2253-77. DOI: 10.1021/cr0307143
20. Fulco, A. J., P450BM-3 and other inducible bacterial P450 cytochromes: biochemistry and regulation. *Annu Rev Pharmacol Toxicol* **1991**, *31* (1), 177-203. DOI: 10.1146/annurev.pa.31.040191.001141
21. White, K. A.; Marletta, M. A., Nitric oxide synthase is a cytochrome P-450 type hemoprotein. *Biochemistry* **1992**, *31* (29), 6627-31. DOI: 10.1021/bi00144a001
22. Su, J.; Groves, J. T., Mechanisms of peroxyne interactions with heme proteins. *Inorg. Chem.* **2010**, *49* (14), 6317-29. DOI: 10.1021/ic902157z
23. Rittle, J.; Green, M. T., Cytochrome P450 compound I: capture, characterization, and C-H bond activation kinetics. *Science* **2010**, *330* (6006), 933-7. DOI: 10.1126/science.1193478
24. Palcic, M. M.; Rutter, R.; Araiso, T.; Hager, L. P.; Dunford, H. B., Spectrum of chloroperoxidase compound I. *Biochem. Biophys. Res. Commun.* **1980**, *94* (4), 1123-1127. DOI: 10.1016/0006-291x(80)90535-5
25. Palaniappan, V.; Turner, J., Resonance Raman spectroscopy of horseradish peroxidase derivatives and intermediates with excitation in the near ultraviolet. *J. Biol. Chem.* **1989**, *264* (27), 16046-53. DOI: 264/27/16046.full
26. Masuya, F.; Tsubaki, M.; Makino, R.; Hori, H., EPR studies on the photoproducts of ferric cytochrome P450cam (CYP101) nitrosyl complexes: effects of camphor and its analogues on ligand-bound structures. *J. Biochem.* **1994**, *116* (5), 1146-52. DOI: 10.1093/oxfordjournals.jbchem.a124641
27. Fukuto, J. M.; Collins, M. D., Interactive endogenous small molecule (gaseous) signaling: implications for teratogenesis. *Curr Pharm Des* **2007**, *13* (29), 2952-78. DOI: 10.2174/138161207782110525
28. Meunier, B.; de Visser, S. P.; Shaik, S., Mechanism of oxidation reactions catalyzed by cytochrome p450 enzymes. *Chem. Rev.* **2004**, *104* (9), 3947-80. DOI: 10.1021/cr020443g
29. Egawa, T.; Proshlyakov, D. A.; Miki, H.; Makino, R.; Ogura, T.; Kitagawa, T.; Ishimura, Y., Effects of a thiolate axial ligand on the pi-->pi* electronic states of oxoferryl porphyrins: a study of the optical and resonance Raman spectra of compounds I and II of chloroperoxidase. *J. Biol. Inorg. Chem.* **2001**, *6* (1), 46-54. DOI: 10.1007/s007750000181

CHAPTER 1

30. Stone, K. L.; Behan, R. K.; Green, M. T., X-ray absorption spectroscopy of chloroperoxidase compound I: Insight into the reactive intermediate of P450 chemistry. *Proc Natl Acad Sci U S A* **2005**, *102* (46), 16563-5. DOI: 10.1073/pnas.0507069102
31. Staunton, J.; Wilkinson, B., Biosynthesis of Erythromycin and Rapamycin. *Chem. Rev.* **1997**, *97* (7), 2611-2630. DOI: 10.1021/cr9600316
32. Zilly, F. E.; Acevedo, J. P.; Augustyniak, W.; Deege, A.; Hausig, U. W.; Reetz, M. T., Tuning a p450 enzyme for methane oxidation. *Angew. Chem. Int. Ed. Engl.* **2011**, *50* (12), 2720-4. DOI: 10.1002/anie.201006587
33. Hermans, I.; Spier, E. S.; Neuenschwander, U.; Turrà, N.; Baiker, A., Selective Oxidation Catalysis: Opportunities and Challenges. *Top. Catal.* **2009**, *52* (9), 1162-1174. DOI: 10.1007/s11244-009-9268-3
34. Costas, M., Selective C–H oxidation catalyzed by metalloporphyrins. *Coord. Chem. Rev.* **2011**, *255* (23-24), 2912-2932. DOI: 10.1016/j.ccr.2011.06.026
35. Groves, J. T.; Kruper, W. J.; Haushalter, R. C., Hydrocarbon oxidations with oxometalloporphyrins. Isolation and reactions of a (porphinato)manganese(V) complex. *J. Am. Chem. Soc.* **1980**, *102* (20), 6375-6377. DOI: 10.1021/ja00540a050
36. Hill, C. L.; Schardt, B. C., Alkane activation and functionalization under mild conditions by a homogeneous manganese(III)porphyrin-iodosylbenzene oxidizing system. *J. Am. Chem. Soc.* **1980**, *102* (20), 6374-6375. DOI: 10.1021/ja00540a049
37. Jin, N.; Bourassa, J. L.; Tizio, S. C.; Groves, J. T., Rapid, Reversible Oxygen Atom Transfer between an Oxomanganese(V) Porphyrin and Bromide: A Haloperoxidase Mimic with Enzymatic Rates. *Angew. Chem.* **2000**, *112* (21), 4007-4009. DOI: 10.1002/1521-3757(20001103)112:21<4007::Aid-ange4007>3.0.Co;2-6
38. Lahaye, D.; Groves, J. T., Modeling the haloperoxidases: reversible oxygen atom transfer between bromide ion and an oxo-Mn(V) porphyrin. *J. Inorg. Biochem.* **2007**, *101* (11-12), 1786-97. DOI: 10.1016/j.jinorgbio.2007.07.017
39. Hicks, S. D.; Kim, D.; Xiong, S.; Medvedev, G. A.; Caruthers, J.; Hong, S.; Nam, W.; Abu-Omar, M. M., Non-heme manganese catalysts for on-demand production of chlorine dioxide in water and under mild conditions. *J. Am. Chem. Soc.* **2014**, *136* (9), 3680-6. DOI: 10.1021/ja5001642
40. Hicks, S. D.; Petersen, J. L.; Bougher, C. J.; Abu-Omar, M. M., Chlorite dismutation to chlorine dioxide catalyzed by a water-soluble manganese porphyrin. *Angew. Chem. Int. Ed. Engl.* **2011**, *50* (3), 699-702. DOI: 10.1002/anie.201005128
41. Umile, T. P.; Wang, D.; Groves, J. T., Dissection of the mechanism of manganese porphyrin-catalyzed chlorine dioxide generation. *Inorg. Chem.* **2011**, *50* (20), 10353-62. DOI: 10.1021/ic201430v
42. Zdilla, M. J.; Lee, A. Q.; Abu-Omar, M. M., Bioinspired dismutation of chlorite to dioxygen and chloride catalyzed by a water-soluble iron porphyrin. *Angew. Chem. Int. Ed. Engl.* **2008**, *47* (40), 7697-700. DOI: 10.1002/anie.200801521
43. Zdilla, M. J.; Lee, A. Q.; Abu-Omar, M. M., Concerted Dismutation of Chlorite Ion: Water-Soluble Iron-Porphyrins As First Generation Model Complexes for Chlorite Dismutase. *Inorg. Chem.* **2009**, *48* (5), 2260-2268. DOI: 10.1021/ic801681n
44. Zdilla, M. J.; Dexheimer, J. L.; Abu-Omar, M. M., Hydrogen atom transfer reactions of imido manganese(V) corrole: one reaction with two mechanistic pathways. *J. Am. Chem. Soc.* **2007**, *129* (37), 11505-11. DOI: 10.1021/ja073027s

CHAPTER 1

45. Umile, T. P.; Groves, J. T., Catalytic generation of chlorine dioxide from chlorite using a water-soluble manganese porphyrin. *Angew. Chem. Int. Ed. Engl.* **2011**, *50* (3), 695-8. DOI: 10.1002/anie.201004482
46. Armstrong, F. A., *Philos Trans R Soc Lond B Biol Sci* **2008**, *363* (1494), 1263-70; discussion 1270. DOI: 10.1098/rstb.2007.2223
47. Atkins, P. W., Overton, T. L., Rourke, J. P., Weller, M. T. & Armstrong, F. A. , 2006 Shriver & Atkins: inorganic chemistry, 4th edn. Oxford, UK: Oxford University Press.
48. Yano, J.; Kern, J.; Sauer, K.; Latimer, M. J.; Pushkar, Y.; Biesiadka, J.; Loll, B.; Saenger, W.; Messinger, J.; Zouni, A.; Yachandra, V. K., Where water is oxidized to dioxygen: structure of the photosynthetic Mn₄Ca cluster. *Science* **2006**, *314* (5800), 821-5. DOI: 10.1126/science.1128186
49. Britt, R. D.; Campbell, K. A.; Peloquin, J. M.; Gilchrist, M. L.; Aznar, C. P.; Dicus, M. M.; Robblee, J.; Messinger, J., Recent pulsed EPR studies of the photosystem II oxygen-evolving complex: implications as to water oxidation mechanisms. *Biochim. Biophys. Acta* **2004**, *1655* (1-3), 158-71. DOI: 10.1016/j.bbabi.2003.11.009
50. Cox, N.; Retegan, M.; Neese, F.; Pantazis, D. A.; Boussac, A.; Lubitz, W., Photosynthesis. Electronic structure of the oxygen-evolving complex in photosystem II prior to O-O bond formation. *Science* **2014**, *345* (6198), 804-8. DOI: 10.1126/science.1254910
51. Cox, N.; Pantazis, D. A.; Neese, F.; Lubitz, W., Biological water oxidation. *Acc. Chem. Res.* **2013**, *46* (7), 1588-96. DOI: 10.1021/ar3003249
52. Siegbahn, P. E., Structures and energetics for O₂ formation in photosystem II. *Acc. Chem. Res.* **2009**, *42* (12), 1871-80. DOI: 10.1021/ar900117k
53. Ames, W.; Pantazis, D. A.; Krewald, V.; Cox, N.; Messinger, J.; Lubitz, W.; Neese, F., Theoretical evaluation of structural models of the S₂ state in the oxygen evolving complex of Photosystem II: protonation states and magnetic interactions. *J. Am. Chem. Soc.* **2011**, *133* (49), 19743-57. DOI: 10.1021/ja2041805
54. Jin, N.; Groves, J. T., Unusual Kinetic Stability of a Ground-State Singlet Oxomanganese(V) Porphyrin. Evidence for a Spin State Crossing Effect. *J. Am. Chem. Soc.* **1999**, *121* (12), 2923-2924. DOI: 10.1021/ja984429q
55. Song, W. J.; Seo, M. S.; George, S. D.; Ohta, T.; Song, R.; Kang, M. J.; Tosha, T.; Kitagawa, T.; Solomon, E. I.; Nam, W., Synthesis, characterization, and reactivities of manganese(V)-oxo porphyrin complexes. *J. Am. Chem. Soc.* **2007**, *129* (5), 1268-77. DOI: 10.1021/ja066460v
56. Gross, Z.; Golubkov, G.; Simkhovich, L., *Angew. Chem.* **2000**, *39* (22), 4045-4047. DOI: 10.1002/1521-3773(20001117)39:22<4045::Aid-anie4045>3.0.Co;2-p
57. Jacobsen, E. N.; Zhang, W.; Muci, A. R.; Ecker, J. R.; Deng, L., *J. Am. Chem. Soc.* **1991**, *113* (18), 7063-7064. DOI: 10.1021/ja00018a068
58. Collins, T. J.; Powell, R. D.; Sleboznick, C.; Uffelman, E. S., *J. Am. Chem. Soc.* **1990**, *112* (2), 899-901. DOI: 10.1021/ja00158a077
59. Lansky, D. E.; Mandimutsira, B.; Ramdhanie, B.; Clausen, M.; Penner-Hahn, J.; Zvyagin, S. A.; Telser, J.; Krzystek, J.; Zhan, R.; Ou, Z.; Kadish, K. M.; Zakharov, L.; Rheingold, A. L.; Goldberg, D. P., *Inorg. Chem.* **2005**, *44* (13), 4485-98. DOI: 10.1021/ic0503636

CHAPTER 1

60. Groves, J. T.; Stern, M. K., *J. Am. Chem. Soc.* **1988**, *110* (26), 8628-8638. DOI: 10.1021/ja00234a009
61. Gupta, R.; Taguchi, T.; Lassalle-Kaiser, B.; Bominaar, E. L.; Yano, J.; Hendrich, M. P.; Borovik, A. S., High-spin Mn-oxo complexes and their relevance to the oxygen-evolving complex within photosystem II. *Proc Natl Acad Sci U S A* **2015**, *112* (17), 5319-24. DOI: 10.1073/pnas.1422800112
62. Winkler, J. R.; Gray, H. B., Electronic Structures of Oxo-Metal Ions. In *Molecular Electronic Structures of Transition Metal Complexes I*, Mingos, D. M. P.; Day, P.; Dahl, J. P., Eds. Springer Berlin Heidelberg: Berlin, Heidelberg, 2012, 10.1007/430_2011_55pp 17-28.
63. Mayer, J. M., *Comments Inorg. Chem.* **1988**, *8* (4), 125-135. DOI: 10.1080/02603598808035790
64. Mayer, J. M.; Thorn, D. L.; Tulip, T. H., Synthesis, reactions, and electronic structure of low-valent rhenium-oxo compounds. Crystal and molecular structure of $\text{Re}(\text{O})\text{I}(\text{MeC.tplbond.CMe})_2$. *J. Am. Chem. Soc.* **1985**, *107* (25), 7454-7462. DOI: 10.1021/ja00311a039
65. Hess, A.; Hörz, M. R.; Liable-Sands, L. M.; Lindner, D. C.; Rheingold, A. L.; Theopold, K. H., Insertion of O_2 into a Chromium-Phenyl Bond: Mechanism of Formation of the Paramagnetic d_2 Oxo Complex $[\text{TptBu}, \text{MeCrIV}(\text{O})\text{OPh}]$. *Angew. Chem. Int. Ed.* **1999**, *38* (1-2), 166-168. DOI: 10.1002/(sici)1521-3773(19990115)38:1/2<166::Aid-anie166>3.0.Co;2-e
66. Orchin, M.; Jaffe, H. H., *The Importance of Antibonding Orbitals* (Houghton Mifflin, New York, 1967).
67. McMurray, T. J.; Groves, J. T., *Cytochrome P450_ Structure Mechanism and Biochemistry*, 3rd Edition ed.; (Plenum Press, New York, 2004).
68. Ni, Y.; Wang, X., Mechanism and kinetics of chlorine dioxide reaction with hydrogen peroxide under acidic conditions. *The Canadian Journal of Chemical Engineering* **1997**, *75* (1), 31-36. DOI: 10.1002/cjce.5450750107
69. Horváth, A. K.; Nagypál, I., Kinetics and Mechanism of the Reaction between Thiosulfate and Chlorine Dioxide. *The Journal of Physical Chemistry A* **1998**, *102* (37), 7267-7272. DOI: 10.1021/jp981714n
70. Wang, L.; Nicoson, J. S.; Huff Hartz, K. E.; Francisco, J. S.; Margerum, D. W., Bromite ion catalysis of the disproportionation of chlorine dioxide with nucleophile assistance of electron-transfer reactions between $\text{ClO}(2)$ and $\text{BrO}(2)$ in basic solution. *Inorg. Chem.* **2002**, *41* (1), 108-13. DOI: 10.1021/ic010849w
71. Hoigné, J.; Bader, H., Kinetics of reactions of chlorine dioxide (OClO) in water—I. Rate constants for inorganic and organic compounds. *Water Res.* **1994**, *28* (1), 45-55. DOI: 10.1016/0043-1354(94)90118-x
72. Halperin, J.; Levine, W., Incidence of maternal mortality related to anesthesia. *Curr Res Anesth Analg* **1952**, *31* (5), 301-8. DOI: 10.1021/ja01122a026
73. Buxton, G. V. D., F. R. S., The radiolysis of aqueous solutions of oxybromine compounds; the spectra and reactions of BrO and BrO_2 . *Proceedings of the Royal Society of London. Series A. Mathematical and Physical Sciences* **1997**, *304* (1479), 427-439. DOI: 10.1098/rspa.1968.0095

CHAPTER 1

74. Srinivasan, A.; Viraraghavan, T., Perchlorate: health effects and technologies for its removal from water resources. *Int J Environ Res Public Health* **2009**, *6* (4), 1418-42. DOI: 10.3390/ijerph6041418
75. Sellers, K. A., W.; Clough, S.; Hoyt, M.; Pugh, B.; Robb, J.; Weeks, K. , *Perchlorate: Environmental Problems and Solutions*. CRC Press: Boca Raton, FL, USA: 2006; p. 177.
76. Ruiz-Duenas, F. J.; Martinez, A. T., Microbial degradation of lignin: how a bulky recalcitrant polymer is efficiently recycled in nature and how we can take advantage of this. *Microb Biotechnol* **2009**, *2* (2), 164-77. DOI: 10.1111/j.1751-7915.2008.00078.x

CHAPTER 2. LIGNIN DERIVED NON-HEME IRON AND MANGANESE
COMPLEXES FOR THE PRODUCTION OF CHLORINE DIOXIDE

2.1 Introduction

The application of chlorine dioxide (ClO_2) in water treatment is growing because of its superior antimicrobial properties and lower tendency to generate harmful chlorinated organic by-products.¹⁻⁵ Chlorine dioxide is a radical species that represents the oxidation number +4 for the central chlorine atom. It exists as a monomer but is explosive as a compressed gas. As a result, it must be manufactured at the point of use. However, ClO_2 is readily soluble in water, does not hydrolyze, and is quite stable in neutral or acidic solutions. In its reactions with contaminants, ClO_2 electron-transfer reactions have been compared to those of singlet oxygen.^{6,7} Because bromide is not oxidized by chlorine dioxide, water treatment with chlorine dioxide, unlike ozone or chlorine, avoids formation of bromoform.⁸

Most of the previously investigated catalysts for the one electron oxidation of chlorite to ClO_2 are based on manganese or iron porphyrin complexes.^{4,5,9,10} In these systems, the chlorite dismutation initiates through oxidation of Mn (II or III) or Fe (III) by chlorite ions to afford high valent Mn and Fe (IV or V) and hypochlorite ions. Both oxidation states IV and V oxidize chlorite directly to ClO_2 .^{4,5,9,10} Although the full conversion of chlorite to ClO_2 was achieved in water using water soluble Fe or Mn porphyrins, these systems suffer from expensive ligand and catalyst syntheses. Interest in developing a simpler catalyst design, enhancing the stability of the catalyst in an oxidative

CHAPTER 2

environment, and obtaining materials from renewable resources inspired us to design a class of catalysts based on molecules that can be derived from lignin.

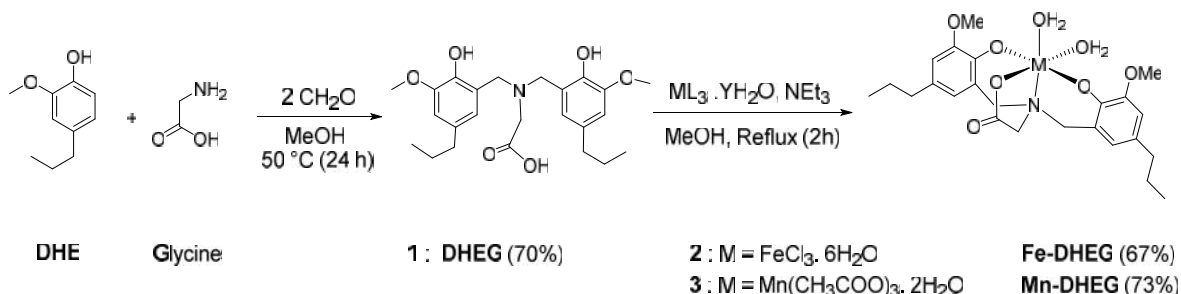
Lignin has an outstanding characteristic of being highly resistant towards both chemical and biological degradation, and resistant to oxidative transformation in particular.¹¹

Catalytic depolymerization of lignin results in monomeric product distribution where 2-methoxy-4-propylphenol (dihydroeugenol, **DHE**, **1**) was reported as one of the main products of lignin valorization.^{12, 13} In this paper, we describe a simple catalyst design based on a readily available ligand that offers a convenient route to ClO₂ production in water. This system proceeds through high valent Mn and Fe (IV and V) intermediates with rates of ClO₂ production that are higher than its subsequent degradation, which makes these catalysts of interest for environmental applications.

Mannich condensation reaction of **DHE** with formaldehyde and amino acids (glycine in this study) affords a class of ligands similar to the salan type ligands known to be versatile and resistant to oxidative damage¹⁴⁻¹⁶ (Scheme 1). This class of ligands is readily synthesized, can be easily modified, and they are suitable for binding iron and manganese with a large formation constant.¹⁷⁻¹⁹ Here we provide the synthesis and characterization of two lignin derived non-heme Fe-DHEG **2** [Fe^{III}(DHEG-3H)(H₂O)₂] and Mn-DHEG **3** [Mn^{III}(DHEG-3H)(H₂O)₂] complexes and their catalytic generation of chlorine dioxide from the oxyanion chlorite under mild conditions. In contrast to porphyrin complexes, peroxyacetic acid (PAA) is required to initiate catalysis and generates the putative high-valent Mn and Fe complexes. This step is the rate determining step. The reaction proceeds efficiently reaching completion within 15

CHAPTER 2

minutes in the presence of 2 mol% catalyst loading at 25 °C. Kinetics of ClO₂ further reaction with **3**/PAA is studied and its mechanism illuminated.



Scheme 2.1. Synthesis of ligand **1** and its Fe and Mn complexes **2** and **3**. ML₃ · YH₂O represents FeCl₃ · 6H₂O or Mn(CH₃COO)₃ · 2H₂O. Isolated yields are reported in parentheses.

2.2 Experimental

2.2.1 Materials

2-Methoxy-4-propylphenol (dihydroeugenol, **DHE**), glycine, iron(III)chloride hexahydrate (FeCl₃ · 6H₂O), manganese (III) acetate dihydrate (Mn(CH₃COO)₃ · 2H₂O), triethylamine, hydrogen peroxide (30 wt % in water), peracetic acid solution (32 wt % in dilute acetic acid), potassium iodide, sodium thiosulfate, and thyodene were purchased from Sigma-Aldrich. Formaldehyde (37 wt.% solution in water, methanol-stabilized) was obtained from Spectrum Chemicals. Sodium chlorite (NaClO₂, 80%) was purchased from Acros Organics Chemicals.

Reactions were mainly carried out under air unless otherwise indicated where using standard Schlenk techniques with an atmosphere of either purified nitrogen or argon. Solvents were purchased from Scientific Fisher and were used without further purification. Commercial chemicals were used as received without further purification

CHAPTER 2

except sodium chlorite. Deionized (DI) water was obtained from a Millipore Milli-Q Academic TC water purification system. Acetate buffers (50.0 mM) were prepared by dissolving sodium acetate (2.47 g) in 1-liter deionized water and adding acetic acid to the desired pH. Phosphate buffers (50.0 mM) were prepared by dissolving mono sodium phosphate (27.6 g) and dibasic sodium phosphate (53.7 g) into 1-liter water separately. A mixture of 195 mL of monobasic and 305 mL of dibasic sodium phosphate was prepared in 1-liter volumetric flask and filled with DI water up to the mark line reaching the desired pH.

2.2.2 Instrumentation

^1H -NMR and ^{13}C -NMR spectra were recorded on a Varian 400 MHz spectrometer at 298 K and referenced against residual solvent signal. ESI mass spectra were obtained using a Finnigan LTQ Linear Ion Trap Mass spectrometer in positive ion mode. UV-vis and kinetic measurements were carried out at 25.0 ± 0.1 °C in a quartz cuvette (3.5 mL total volume, path length = 1.00 cm) fitted with a septum. Rate constants for chlorite oxidation by PAA in the presence of a catalytic **2** or **3** were determined by monitoring the appearance of the absorption bands at 360 nm due to the formation of chlorine dioxide. Typically, chlorite concentration was in excess and much larger than that of PAA. Yields of ClO_2 were calculated based on the extinction coefficient of ClO_2 at 360 nm and based on a stoichiometry of 2:1 for ClO_2^- : PAA.

Fast reactions (less than one minute) were performed on a KinetAsystTM SF-61SX2 Stopped Flow spectrometer using traditional UV-vis and rapid mixing techniques. Solutions of catalyst were prepared in acetate buffer (pH 4.0) /methanol mixed 1:1 ratio

CHAPTER 2

by volume. PAA solution was prepared in acetate buffer at pH 4.0. All reactions and rate calculation are based on final concentrations resulting from 1:1 mixing mode of the two reactants solutions. The catalyst signals were monitored by the decay of absorption bands at 330 and 490 nm. Analysis was an average of 5 experiments and fitting employed the KinetAsyst software package.

X-ray Data Collection, Structure Solution and Refinement; the crystal was mounted on a cryo-loop and transferred to a Bruker Kappa APEX II diffractometer. The APEX2 program was used to determine the unit cell parameters and data collection (30 sec / frame, 0.5 deg. /frame Omega scan). The data were collected at 100k with Oxford cryo-system. The raw frame data were processed using SAINT program. The absorption correction was applied using program SADABS. Subsequent calculations were carried out using SHELXTL program. The structure was solved by direct methods and refined on F^2 by full-matrix least-squares techniques.

2.3 Purification of sodium chlorite

Sodium chlorite was purified by dissolving 10.0 g (111 mmol) of sodium chlorite in minimal water (~20.0 mL) resulting in a homogeneous solution of faint yellow color. Approximately 0.10 g (0.48 mmol) of barium chloride (BaCl_2) was then added to the solution and stirred to give a white precipitate, $\text{Ba}(\text{ClO}_3)_2$. The precipitate was removed by filtration. The resulting solution was then subjected to heat and reduced pressure resulting in a white solid. The resulting solid was then dissolved in a minimal amount of water (~20 mL) and ethanol (200 proof, ~ 8 mL) was added dropwise until a white precipitate was observed. If ethanol is added in very large excess (>500 mL), sodium

CHAPTER 2

chloride will also precipitate. The resulting precipitate was isolated by vacuum filtration and dried under vacuum for 2 hours resulting in 4 g of white solid. The purity (99.4%) was confirmed by UV-vis spectroscopy. Chlorite has an absorbance at 260 nm, $\epsilon = 154 \text{ M}^{-1} \text{ cm}^{-1}$.

2.4 Ligand Synthesis

The ligand **1** (**DHEG**, bis(2-hydroxy-3-methoxy-5-propylbenzyl) glycine) was synthesized using previously reported literature.²⁰ DHE (6.6 g, 40 mmol) was added into a mixture of glycine (1.5 g, 20 mmol) and 37 % aqueous formaldehyde (3.3 g, 40 mmol) at ambient temperature. Overall, 60 mL methanol/water (2:1 ratio) were used in this reaction. The mixture was stirred at reflux for 24 hours. A white solid precipitated upon removing 50% of methanol by a rotary evaporator and collected by vacuum filtration. Further purification was achieved by dissolving the white solid in minimal amount of methanol (~10 mL) at 60 °C and adding hot water until a precipitate was observed. The resulting solution was left in a refrigerator (5 °C) overnight, filtered the white precipitate, and then dried under vacuum. Yield: 6.1 g, 14 mmol (70 %, white solid), ¹H-NMR (CDCl₃-400 MHz): (ppm) 6.42 (s, Ar-H, 2H), 6.27 (s, Ar-H, 2H), 3.52 (s, O-CH₃, 6H), 3.43 (s, CH₂, 4H), 3.00 (s, CH₂, 2H), 2.38 (t, CH₂, 4H, J=8 Hz), 1.52 (m, CH₂, 4H), 0.89 (t, CH₃, 6H, J=8 Hz). ¹³C-NMR (CDCl₃-125 MHz): (ppm) 177.2, 147.6, 143.7, 133.0, 122.0, 121.7, 111.3, 56.5, 56.3, 55.5, 37.8, 25.0, 14.1. ESI-MS (positive mode, MeOH solution): m/z calcd for C₂₄H₃₃NO₆ Na 454.23, found 454.2 [M+Na]⁺; elemental analysis calculated for C₂₄H₃₂NO₆Na.2H₂O: C 58.88, H 7.41, N 2.86; Found: C 58.2, H 6.9, N 3.0.

CHAPTER 2

Single crystals of the sodium salt of **DHEG** ligand was obtained either from acetone or dichloromethane by slow evaporation at ambient temperature, indicative of bonds forming between formaldehyde -CH₂ and the ortho position on the phenol ring.

2.5 Synthesis of Fe and Mn Complexes

Fe-DHEG, 2: Triethylamine (Et₃N, 1 mL, 0.73 g, 7.2 mmol) was added into a solution of **1 DHEG** (0.50 g, 1.16 mmol) in 10 mL methanol in air, stirred at room temperature for an hour deprotonating the hydroxyl groups on the ligand **1**. Upon addition of the solution of FeCl₃·6H₂O (0.31 g, 1.16 mmol) in 10 mL methanol to the ligand / Et₃N mixture, the color of the solution turned purple. The reaction mixture was refluxed in air overnight. After the reaction cooled to room temperature, the solvent was removed by rotary evaporator. Upon addition of 10 mL acetone/Et₂O (1:1 v/v) to this mixture, a white precipitate, triethylammonium chloride, was formed which then filtered from a solution and washed with Et₂O. The Fe complex was obtained from the filtrate after removing the solvent using rotary evaporator. Single crystal was obtained in acetone/water (1:1 ratio). Yield: 0.376 g, 0.78 mmol (67%, purple solid), elemental analysis calculated for C₂₄H₃₀FeNO₆·H₂O: C 57.4, H 6.4, N 2.79; Found: C 57.7, H 6.9, N 2.6; ESI-MS (positive mode, MeOH solution): m/z calcd for C₂₄H₃₀FeNO₆ 484.35, found 539.1 [M+ Na + CH₃OH]⁺; UV/Vis [MeOH]: λ_{\max} , nm (, M⁻¹ cm⁻¹): 286 (8920), 320 (5310), 540 (2470). X-band, perpendicular-mode EPR (MeOH, 90 K) g = 8.4, 4.3. Mössbauer (MeOH, 77 K) $\delta = 0.32$ mm/s; $E_Q = 0.44$ mm/s. Evans' method (CD₃OD, 298 K, 400 MHz), $\mu_{\text{eff}} = 5.7 \mu_B$.

CHAPTER 2

Mn-DHEG, 3: A solution of $\text{Mn}(\text{CH}_3\text{COO})_3 \cdot 2\text{H}_2\text{O}$ (0.31 g, 1.16 mmol) in 10 mL methanol was added to a mixture of DHEG (0.50 g, 1.16 mmol), Et_3N (1 mL, 0.73 g, 7.2 mmol), and methanol (15 mL) under ambient atmosphere, immediately resulting in a red-brown solution. The solution was refluxed in air for 6 h. Subsequently, the solvent was removed under vacuum. Following the same work up procedure as Fe complex, the desired Mn-complex was obtained from the filtrate after removing the solvent under vacuum. Yield: 0.092 g, 0.19 mmol (73%, brown solid), elemental analysis calculated for $\text{C}_{24}\text{H}_{30}\text{MnNO}_6 \cdot 2\text{H}_2\text{O}$: C 55.49, H 6.60, N 2.70; Found: C 55.5, H 6.4, N 3.1; ESI-MS (positive mode, MeOH solution): m/z calcd for $\text{C}_{24}\text{H}_{30}\text{MnNO}_6$ 483.44, found 506.2 $[\text{M}+\text{Na}]^+$, and 538.2 $[\text{M}+\text{Na}+\text{CH}_3\text{OH}]^+$; UV/Vis [MeOH]: λ_{max} , nm (, $\text{M}^{-1} \text{cm}^{-1}$): 248 (15218), 280 (8331), 370 (3613), 490 (2789). Evans' method (CD_3OD , 298 K, 400 MHz), $\mu_{\text{eff}} = 4.2 \mu_{\text{B}}$.

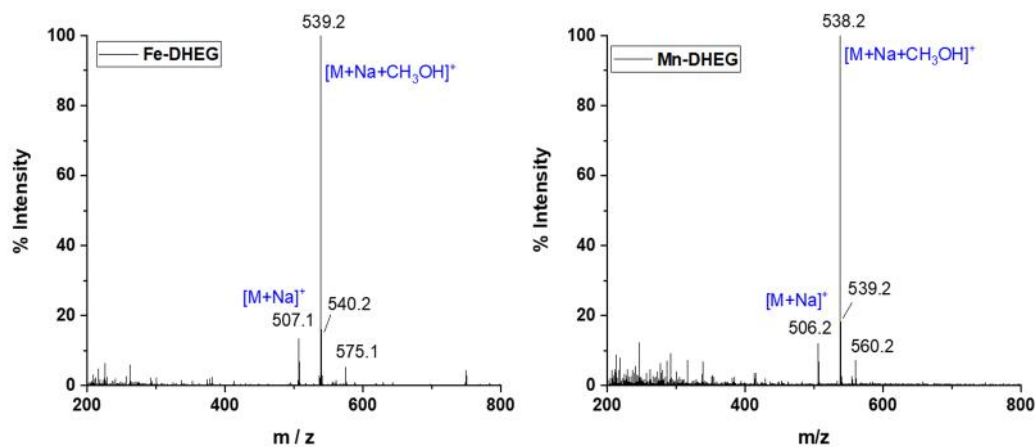


Figure 2.1: ESI-MS spectra of Fe-DHEG and Mn-DHEG complexes, both are consistent of the mononuclear compounds and the absence of chlorine coordination.

ESI-MS spectra of the complexes do not show any halogen pattern indicating that no chlorine is retained as a ligand or an anion in the resulting complexes (Figure 2.1). Only

CHAPTER 2

two major peaks appeared on the ESI-MS (positive mode, in methanol) spectra which were assigned to $M+Na+CH_3OH$ (the base peak) and $M + Na$ where M represents the molar mass of the corresponding mononuclear Fe or Mn complex.

These complexes are well soluble in MeOH, acetonitrile, THF, DCM, less soluble in $CHCl_3$ and acetone, and insoluble in less polar solvents such as Et_2O and hexane.

2.6 Elemental analysis

Elemental analysis of the complexes (**2-3**) fits with two molecules of water coordinated to the metal center (Table 2.1). Higher ratio of C/N was obtained which can be attributed to the presence of small triethyl amine coordination.

Table 2.1 Elemental analysis of the DHEG ligand and the corresponding Fe/Mn complexes.

Weight %	C	H	N	C/N ratio	
Experimental	DHEG	58.22	6.859	2.926	19.90
Theoretical	Na Salt, 2H ₂ O	58.88	7.41	2.86	20.58
Experimental	Fe-DHEG	55.74	6.91	2.548	21.88
Theoretical	Fe-DHEG, 2H ₂ O	55.39	6.59	2.69	20.59
Experimental	Mn-DHEG	55.53	6.399	3.079	18.04
Theoretical	Mn-DHEG, 2H ₂ O	55.49	6.60	2.70	20.55

2.7 X-ray Structure of **2**, Fe-DHEG

Single crystal of **2** was obtained in acetone/water (1:1 ratio) by slow evaporation at ambient temperature. An ORTEP diagram of **2** is shown in Figure 2.2. The X-ray crystal

CHAPTER 2

structure of **2** indicates mononuclear Fe^{III}-DHEG complex where Fe is coordinated by three O anions of OH groups on the ligand **1**, one N atom as well as two solvent (water) molecules of crystallization to complete the octahedral geometry. This structure agrees well with the elemental analysis data and mass spectrum. Clearly, the conformation of n-propyl substituent on the phenol ring is captured in two various crystalline packings. Carbon atoms of n-propyl group can rotate in various angles which might create problems with respect to growing a single crystal suitable for X-ray.

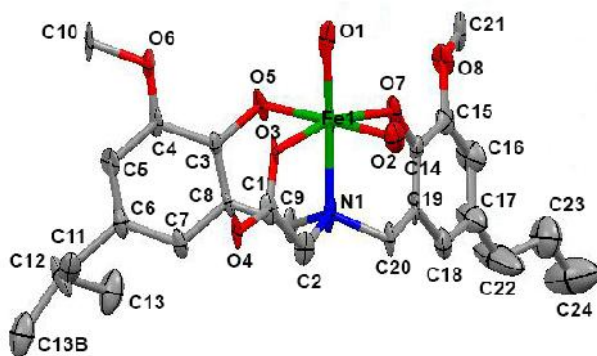


Figure 2.2 X-ray crystal structure of **2** Fe-DHEG (hydrogens are omitted for clarity).

Attempts to get the molecular structure of **3** Mn-DHEG by X-ray diffraction analysis were unsuccessful even though crystalline solids were obtained several times. Crystal structure of similar complexes indicate a wide diversity of conformations due to the flexibility of the tetradentate ligand. In this study, the n-propyl group on the ligands may also increase the number of degrees of freedom and the number of possible crystal packing variations.

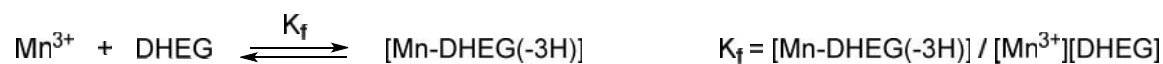
The association constant of **3** is also determined using Benesi-Hildebrand equation (Figure 2.3). Even though, ESI mass spectroscopy and the elemental analysis verified

CHAPTER 2

the mononuclearity of **3**, the titration experiment fits nicely a 1:1 (metal:ligand) binding model as suggested by the Job's plot diagram (Figure 2.4).

2.8 General procedure for drawing Job plot by UV-vis method:

Stock solution of $\text{Mn}(\text{CH}_3\text{COO})_3 \cdot 2\text{H}_2\text{O}$ (20ml, 3.0×10^{-4} M) and DHEG (20ml, 3.0×10^{-4} M) were prepared in methanol. Triethylamine (NEt_3 , 0.36 g, 1.4×10^{-2} M) were added to the solution of DHEG before the solvent reaches to the line marked on the volumetric flask. PH of the solution was 9.8 and stayed constant during the titration. Various volume of the $\text{Mn}(\text{CH}_3\text{COO})_3 \cdot 2\text{H}_2\text{O}$ solution were titrated into DHEG solution. The UV-vis absorbance in each case were measured after 0.5 hour stirring at room temperature. Benesi-Hildebrand equation was used to determine the binding constant value of Mn^{3+} with DHEG.²¹⁻²³



$$\frac{1}{A - A_0} = \frac{1}{K_f(A_m - A_0)[\text{Mn}^{3+}]} + \frac{1}{A_m - A_0}$$

Where A is the absorbance of Mn-DHEG complex during the titration, A_0 is the absorbance at the beginning (before addition Mn^{3+} into the DHEG solution). A_{max} is the maximum absorbance in this titration. K_f is the association constant (M^{-1}) and $[\text{Mn}^{3+}]$ represents the concentration of Mn^{3+} added. K_f values can be determined from the slope of the plot, $1/(A-A_0)$ vs $1/[\text{Mn}^{3+}]$.

CHAPTER 2

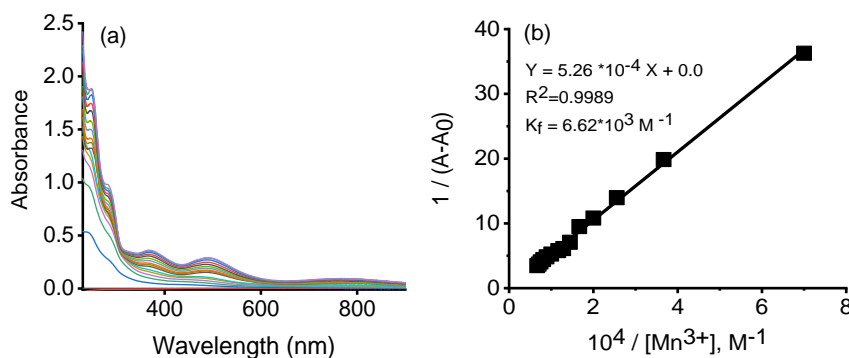


Figure 2.3 (a) UV-vis absorption titration spectra of $Mn(CH_3COO)_3 \cdot 2H_2O$ (20ml, $3.0 \times 10^{-4} M$) and DHEG (20ml, $3.0 \times 10^{-4} M$) and triethylamine (NEt_3 , 0.36 g, $1.4 \times 10^{-2} M$) in methanol. (b) Benesi-Hildebrand plot of DHEG with Mn^{3+} at pH 9.8.

The association constant of **3** was also determined using the Benesi-Hildebrand equation (Figure 2.3) and found to be $6.62 \times 10^3 M^{-1}$ in water at pH 9.8 and $25^\circ C$.²¹⁻²³ Although, ESI mass spectroscopy and elemental analysis verified the mononuclearity of **3**, the method of continuous variation was performed to determine the stoichiometry of ligand to metal binding in complex **3**. The titration results fit well for a 1:1 DHEG/Mn (χ_L is the mole ratio of DHEG/Mn) binding model as suggested by Job's plot (Figure 2.4). Thus, we conclude that complex **3** is a mononuclear Mn(III) complex in solution.

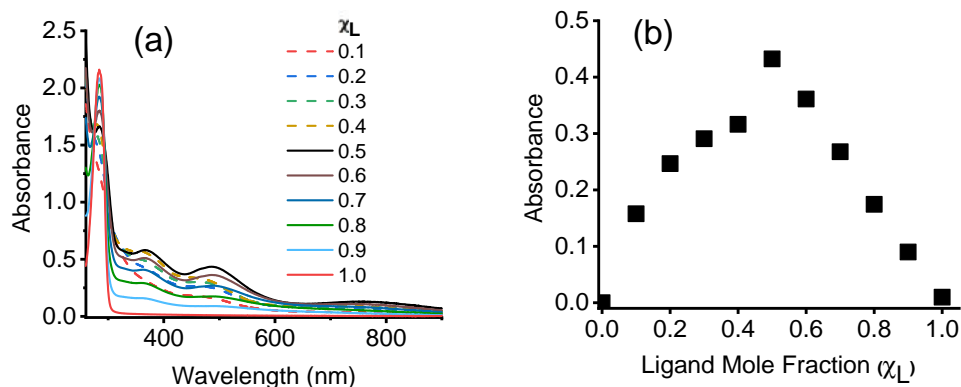


Figure 2.4 (a) UV-vis absorption spectra of [DHEG] (3.0×10^{-4} M) in the presence of Mn^{3+} (b) Job's plot diagram of a DHEG–Mn complex determined at 490 nm and pH 9.8 (χ_L is the mole fraction of DHEG / Mn).

2.9 Oxidation State of 2, Fe-DHEG

The electronic absorption spectra of complex **2** has been recorded in methanol solution (Figure 2.5). The UV-vis spectra of **Fe-DHEG** contains three main absorption bands at 286 nm ($8920 \text{ cm}^{-1} \text{ M}^{-1}$), 320 nm ($5310 \text{ cm}^{-1} \text{ M}^{-1}$), and 540 nm ($2470 \text{ cm}^{-1} \text{ M}^{-1}$).

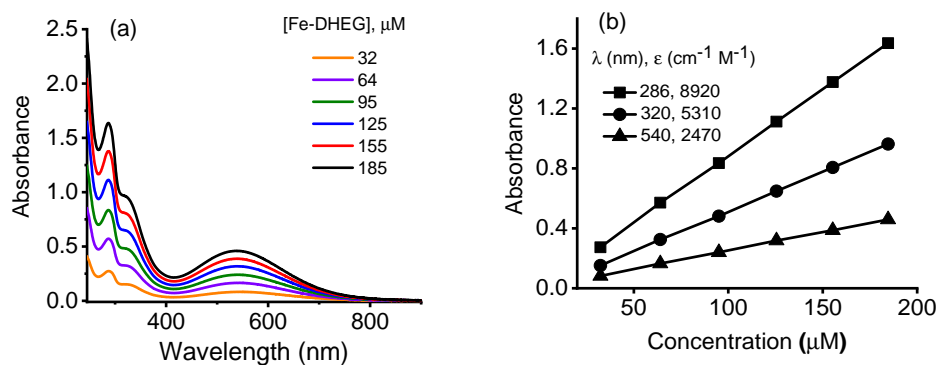


Figure 2.5 (a) UV-vis of various concentration of **2** in methanol; (b) Extinction coefficient (ϵ) of the absorption bands is calculated.

CHAPTER 2

EPR of complex **2** in perpendicular mode at 10 K showed peaks with g values at 8.1, 5.4 and 4.3 that are consistent with a rhombic mononuclear high spin Fe (III) ($S=5/2$) (Figure 2.6). This oxidation state (+3) for **2** was further supported by the magnetic susceptibility determined in CD_3OD solution (Evan's method) at ambient temperature which gave $\mu_{\text{eff}} = 5.7 \mu_{\text{B}}$ (associated with 5 unpaired electrons). The Mossbauer spectrum of **2** (Figure 2.6) showed a well resolved doublet with the isomer shift $\text{IS} = 0.32 \text{ mm/s}$ and quadrupole splitting $\text{QS} = 0.44 \text{ mm/s}$ indicative of the high spin (HS) Fe^{3+} ($S=5/2$).

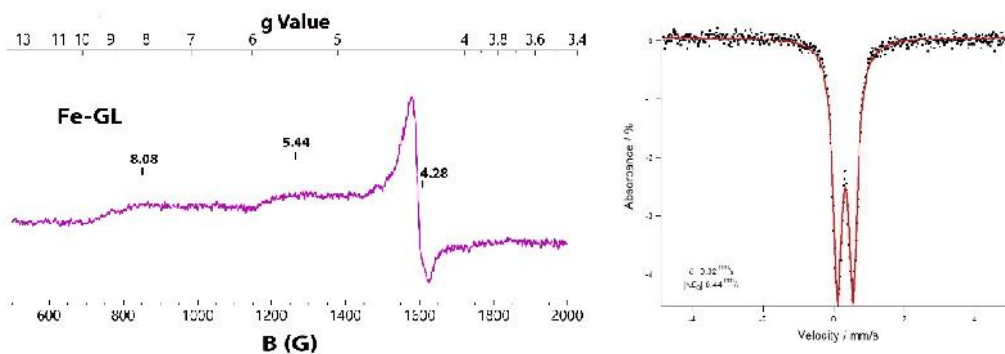


Figure 2.6 (left) EPR spectrum of **2** Fe-DHEG in DMF/THF at 10 K; (right) Mossbauer Spectra of **2** Fe-DHEG

2.10 Oxidation State of **3**, Mn-DHEG

The electronic absorption spectra of red-green manganese complexes have been recorded in methanol solution confirming the oxidation state of +3 for Mn compound **3** (Figure 2.7). Mn (III) ($3d^4$, $S = 2$) is considered one of the transition-metal ion that commonly forms octahedral high-spin (HS) complexes.²⁴ The ground state of the high-spin $3d^4$ ion is 5D which splits into 5E_g and $^5T_{2g}$ components in an octahedral field.²⁵ An

CHAPTER 2

unpaired electron in the d_{z^2} HOMO orbital of a high spin d^4 octahedral transition metal compound exhibits elongation (z-out) Jahn-Teller distortion (JTD).²⁶⁻²⁸ If this distortion is static in nature and sufficiently large, one might expect to see up to four “visible” bands arising from transitions to the three components of ${}^5T_{2g}$ (splits in ${}^5B_{2g}$ and 5E_g) and the other component of 5E_g (splits in ${}^5B_{1g}$ and ${}^5A_{1g}$) in low symmetry. These four bands were observed on the absorption spectra of Mn-DHEG at 280, 370, 490, and 800nm, where the three former bands overlapped with charge transfer (CT) transitions. The band at 800 nm is only observed for the Mn(III) HS complexes.²⁶ The most intense absorption was centered at 250 nm ($15218 \text{ cm}^{-1} \text{ M}^{-1}$) indicative of ${}^5E_g \rightarrow {}^5A_{1g}$ transitions in the phenolates. The shoulder at 280 nm ($8331 \text{ cm}^{-1} \text{ M}^{-1}$) is due to overlapping of spin forbidden d-d transition with ligand absorption. Similarly to what was observed for manganese complexes of tetradentate diphenolate-amino ligands,^{27, 29} analysis of transitions shows that the band centered at 370 nm ($3613 \text{ cm}^{-1} \text{ M}^{-1}$) and 490 nm ($2789 \text{ cm}^{-1} \text{ M}^{-1}$) with a wide excitation range was tentatively assigned these as metal-to-ligand charge-transfer (MLCT) from Mn-O orbitals to Mn-DHEG π^* molecular orbitals. MLCTs are very broad in character, hence it is attributed to mask any weak band due to d-d transition centered on the Mn(III) metal.

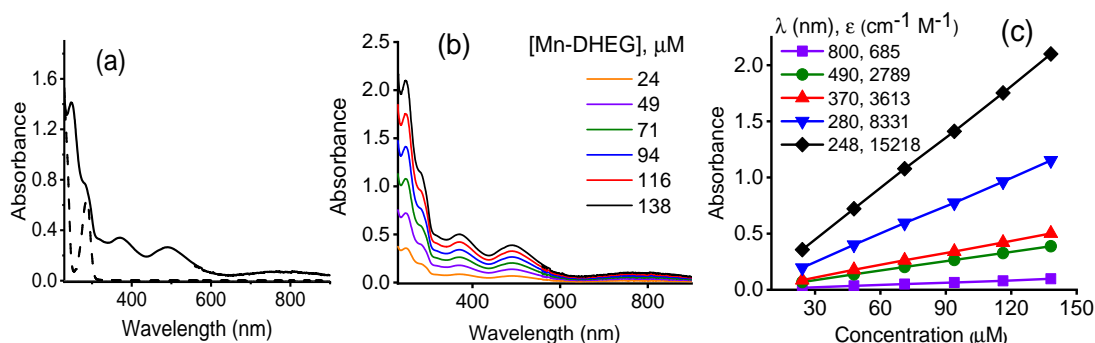


Figure 2.7 (a) UV-vis Spectra of DHEG ligand (67 μM, dashed line), Mn-DHEG (94 μM, solid line) in MeOH; (b) UV-vis of various concentration of **3** Mn-DHEG in methanol; (c) Extinction coefficient (ε) of the absorption bands is calculated.

Jahn-Teller distortion is not expected in $3d^3$, and $3d^5$ HS electron configurations in transition metals because of the high symmetry of E_g orbitals (E_g orbitals are not occupied in d^3 or evenly occupied in d^5).³⁰ Thus neither Mn(II) or Mn(IV) high spin complexes, nor Fe(III) would be expected to experience JTD. Martina and co-worker have reported a series of Mn(II) ligands with two types of donor atoms, mainly NHC and phenolate donors.³⁰ In each case, only two bands were observed, one near 250 nm, and the other between 300-500 nm. Similarly, Fe-DHEG (HS, $3d^5$) display two peaks at 285 nm ($6,745 \text{ M}^{-1} \text{ cm}^{-1}$) and 520 nm ($\text{M}^{-1} \text{ cm}^{-1}$) with intensities indicative of charge-transfer transitions.

Magnetic susceptibilities were determined using the Evans NMR method at ambient temperature in CD_3OD and resulted in the expected values of high-spin Mn(III) (4 unpaired electrons for **3**, $\mu_{\text{eff}} = 4.2 \mu_B$).

EPR spectra of **3**, Mn complex was obtained at 77 K and 10 K, in perpendicular (\perp) and parallel (\parallel) modes (Figure 2.8). The features are much more resolved at 10 °K than at 77

CHAPTER 2

°K but both are in agreement with each other. Mn-DHEG, in ||-mode at 10 K, has features at $g = 4.9, 3.1, 2.1$ in addition to a characteristic EPR peak at $g=10$ in ||-mode consistent with a high spin mononuclear Mn(III) center ($S=2$). It agrees well with the magnetic susceptibilities determined by Evan's method. The large hyperfine constant of 525 MHz for a Mn(III) center, indicating the unpaired electrons are localized on the Mn.

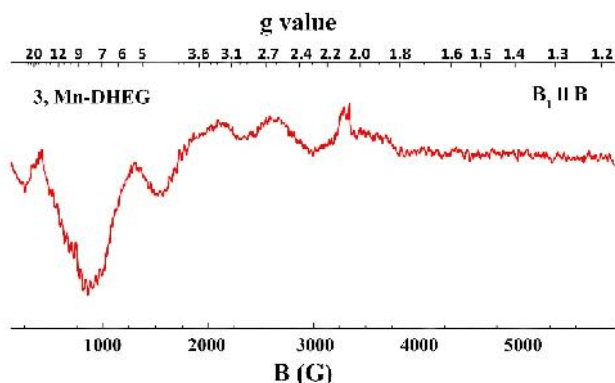


Figure 2.8 EPR spectrum of 3, Mn-DHEG in DMF/THF at 10 °K.

2.11 Catalytic oxidation of Chlorite (ClO_2^-) to chlorine dioxide (ClO_2)

2.11.1 Fe-DHEG and Formation of ClO_2

Catalytic oxidation of chlorite to chlorine dioxide ClO_2 by non-heme iron/manganese complexes, **2** and **3** has been studied at ambient temperature at pH 5.0. Figure 2.9 shows the typical spectral change observed in the presence of catalyst **2**. The UV-visible spectrum of the Fe-DHEG in the presence of chlorite anion shows a small blue shift from 540 to 520 nm and does not change further over 40 minutes (Figure 2.9, blue spectrum), demonstrating the resistance of catalyst **2** to chlorite solution. This is in sharp contrast to what has been observed previously with Fe/Mn porphyrins where chlorite

CHAPTER 2

oxidizes the catalyst to higher oxidation states (IV or V). These catalysts revealed high stability of the oxidation state of +3 on the metal. Addition of 1.3 mM PAA to a mixture of chlorite (6.2 mM) and catalytic amount of Fe-DHEG (0.04 mM) in acetate buffer (pH 5.0) results in spectral changes as shown in Figure 2.9. Chlorite is consumed as seen at 260 nm ($\epsilon = 154 \text{ M}^{-1} \text{ cm}^{-1}$), formation of chlorine dioxide is observed at 360 nm ($\epsilon = 1200 \text{ M}^{-1} \text{ cm}^{-1}$), and the Fe-DHEG characteristic absorption band at 520 nm is vanished. These results suggest that the oxidation of **2** to Fe (IV or V) is the rate determining step in the catalytic reaction. A stronger oxidant such as PAA will facilitate this step which is further studied by stopped flow spectroscopy.

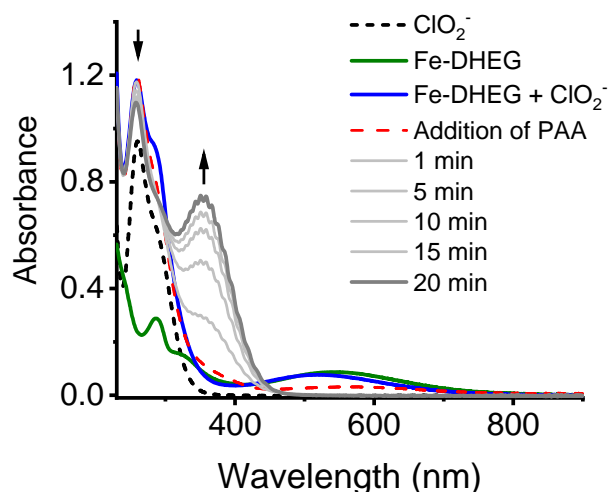


Figure 2.9 UV-vis spectral changes of the chlorite oxidation with **2** Fe-DHEG at pH 5.0. Conditions: $[\text{ClO}_2^-]$ (6.2 mM, dashed black), initial catalyst $[\text{Fe-DHEG}]$ (0.04 mM, green), mixture of chlorite and Fe-DHEG (blue, stays the same over 40 minutes), after addition of PAA (1.3 mM, dashed red), change in concentration of ClO_2 versus time after addition of PAA.

2.11.2 Mn-DHEG and Formation of ClO_2

Catalytic oxidation of chlorite ClO_2^- to chlorine dioxide ClO_2 by non-heme manganese complex **3** (Mn-DHEG) has been studied using peracetic acid, PAA; as a secondary

CHAPTER 2

oxidant at 25.0 °C at pH 4.0 and 5.0 Figure 2.10 shows the typical spectral change observed in the presence of the catalyst. The absorbance increase at 360 nm is primarily attributed to chlorine dioxide formation. Around 260 nm region, the net effect of the disappearance of chlorite ion and the formation of ClO_2 is observed. Good yields of ClO_2 (80%) were observed in less than 10 minutes in the presence of 30 μM Mn-DHEG and various ratio of peroxyacetic acid at pH 4.0. The yields of ClO_2 drops to 55% at pH 5.0.

Oxidation of chlorite was not obtained using other oxidants such as hydrogen peroxide (H_2O_2) and ammonium persulfate (APS), as shown in Figure 2.10. Uncatalyzed reaction was performed with no manganese present in the solution at pH 4.0 and 5.0. The rate of oxidation is insignificant compared to the corresponding catalyzed reaction indicating that negligible amount is attributed to the uncatalyzed reaction (Figure 2.10).

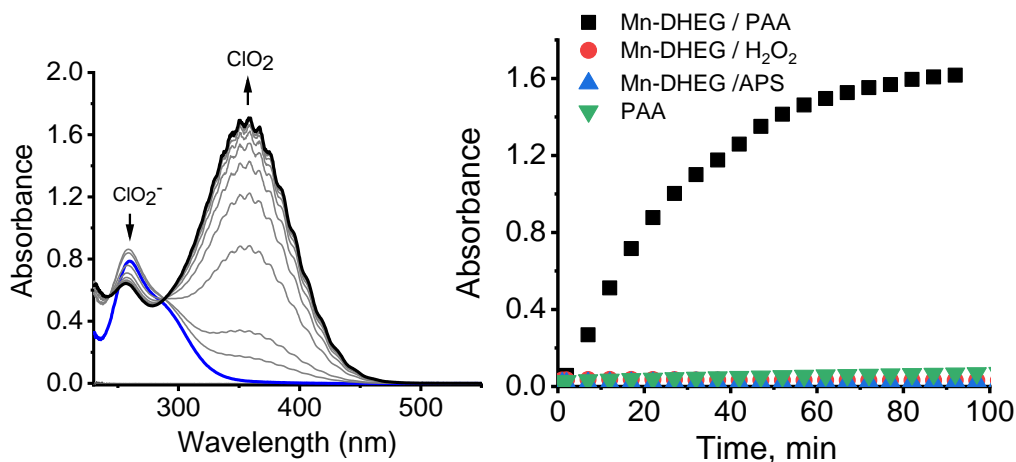


Figure 2.10 Left) Absorption spectral changes of $[\text{ClO}_2^-]$ (5.1 mM, blue line) upon addition of Mn-DHEG (30.0 μM) and PAA (1.27 mM) (gray and red lines) at pH 5.0 b) The effect of using other oxidants such as H_2O_2 , (2.5 mM) or APS (2.7 mM) on one electron oxidation of chlorite and uncatalyzed reaction with PAA (2.5 mM); Right) The effect of using other oxidants such as hydrogen peroxide (H_2O_2 , 2.5 mM) or ammonium persulfate (APS, 2.7 mM) on one electron oxidation of chlorite; and the uncatalyzed reaction of chlorite with PAA (2.5 mM).

2.12 Catalyst activation

2.12.1 Oxidation of Fe-DHEG by PAA

The time profiles of the reaction of **2** with PAA were obtained by a stopped flow spectrometer. Upon addition of PAA, **2** is fully consumed giving rise to higher oxidation states of the iron complex as evident by UV-Vis (Figure 2.11a). UV-vis spectra of the activated catalysts exhibit a band at 330 nm and two isosbestic points (407 and 344 nm) during this reaction. The presence of the isosbestic points indicates that only two species contributing to the UV-vis absorbance without any intermediates involved in the reaction.

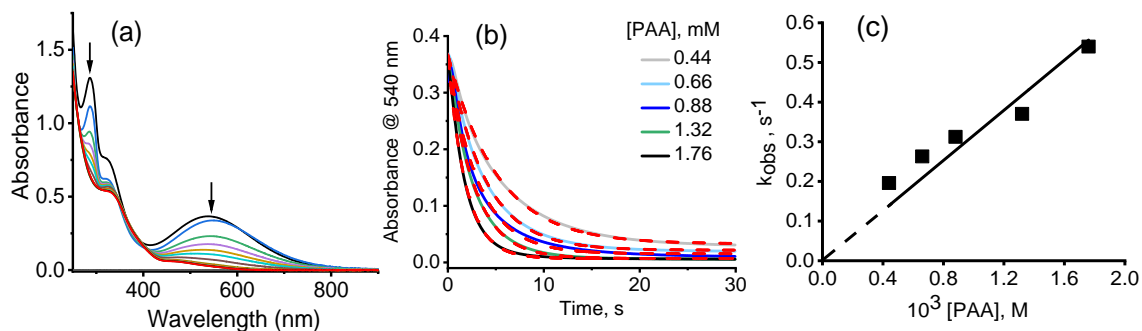


Figure 2.11 (a) UV-Vis spectral changes for the reaction of **2** with PAA, Fe-DHEG (0.14 mM, black line), added PAA (0.22 mM). (b) Time-resolved of absorbance at 540 nm due to formation of Mn^{IV} complex, the reaction of 0.14 mM of Mn with various concentration of PAA (solid lines), first order kinetic modeling fits (dotted lines). (c) Plot of pseudo-first order rate constant (k_{obs}) of the decay of Fe^{III}(OOR) versus initial [PAA]. The observed second-order rate constant (k_{obs}) is $(306 \pm 20) \text{ M}^{-1}\text{s}^{-1}$.

The time profile of the activation of **2** obeys the first-order kinetics and allows us to fit it into a modeled exponential curve to obtain the observed pseudo-first order rate constant (k_{obs}) (Figure 2.11b). The observed second order rate constant (k_{obs}) calculated from the

CHAPTER 2

slope of k_{obs} vs $[\text{PAA}]$ is $306 \pm 20 \text{ M}^{-1}\text{s}^{-1}$. During the catalyst activation, at the first stage, heterolytic peroxide bond cleavage will result in formation of $[\text{Fe(IV)=O}]$ species.³¹

2.12.2 Oxidation of Mn-DHEG by PAA

The time profiles of the reaction of **3** with PAA were acquired by a stopped flow spectrometer. Upon addition of PAA, **3** is fully consumed giving rise to higher oxidation states of the manganese complex as evident by UV-Vis and EPR spectroscopy (Figure 2.12a). UV-vis spectra of the activated catalysts exhibit a band at 330 nm that can be assigned to Mn(IV) species as reported in previous literatures.^{32, 33} The sixteen-line hyperfine pattern of EPR spectrum is clearly indicative of manganese (IV) which is in agreement with previously reported of these type of Mn(IV) species.^{31, 34}

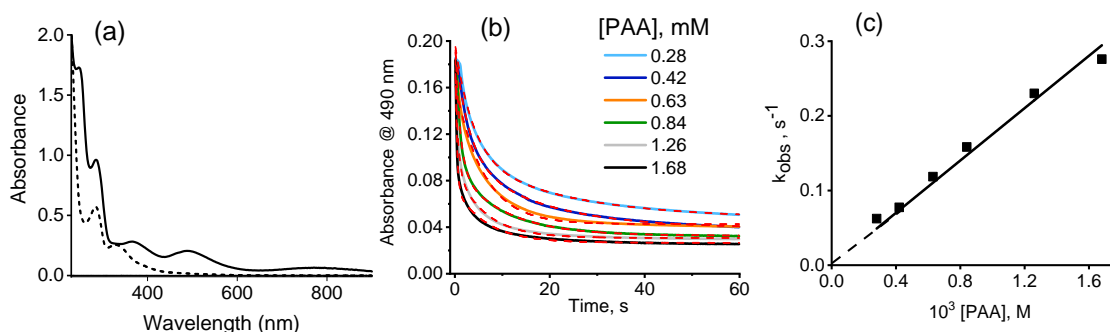


Figure 2.12 (a) Formation of Mn^{IV} species supported by UV-vis spectroscopy when Mn-DHEG is reacted with PAA. Mn-DHEG (0.14 mM, black line), added PAA (0.84 mM, dashed line), (b) Time-resolved absorbance at 490 nm, the reaction of 0.14 mM of Mn with various concentration of PAA (solid lines), first-order kinetic fits (dashed lines). (c) Plot of pseudo-first order rate constant (k_{obs}) of the decay of Mn^{III} versus $[\text{PAA}]$. The second-order rate constant ($k_{3, \text{PAA}}$) is $(175 \pm 8) \text{ M}^{-1}\text{s}^{-1}$.

The time profile of the formation of Mn(IV) obeys the first-order kinetics at lower concentration of PAA ($< 8 [\text{Mn}]$) allows us to fit it into a modeled exponential curve to

CHAPTER 2

obtain the observed pseudo-first order rate constant (k_{obs}) (Figure 2.12b). The observed second order rate constant (k_{obs}) calculated from the slope of k_{obs} vs [PAA] is $175 \pm 8 \text{ M}^{-1}\text{s}^{-1}$. This agrees with kinetic study at 330 nm under steady-state conditions with $k_{3, \text{PAA}} = 151 \pm 6 \text{ M}^{-1}\text{s}^{-1}$ (Figure 2.13). During the reaction of **3** (pre-catalyst) with PAA, catalyst activation, an acylperoxo $[\text{Mn}^{\text{III}}\text{-(OOR)}]$ intermediate is likely formed, followed by conversion to Mn(IV)-OH .³¹

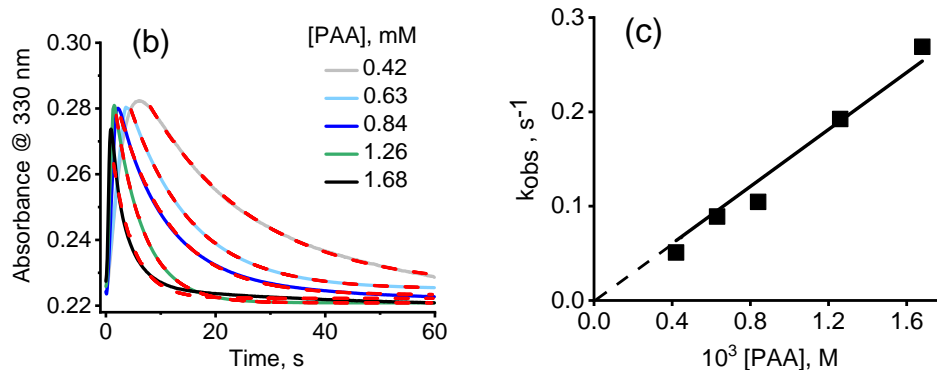


Figure 2.13 (b) Time-resolved of absorbance at 330 nm due to formation of Mn^{IV} complex, the reaction of 0.14 mM of Mn with various concentration of PAA (solid lines), first order kinetic modeling fits (dashed lines). (c) Plot of pseudo-first order rate constant (k_{obs}) of the decay of $\text{Mn}^{\text{III}}(\text{OOR})$ versus initial [PAA]. The observed second-rate constant (k_{obs}) is $(151 \pm 6) \text{ M}^{-1}\text{s}^{-1}$

The chemistry after application of PAA is more complex because it is added as a mixture of PAAH, CH_3COOH , H_2O_2 (Scheme 2.2). UV-vis spectra of the catalysts remained unchanged in the presence of H_2O_2 (Figure 2.14), nor chlorite oxidation taken place using a mixture of **3** Mn-DHEG and H_2O_2 . At lower concentration of PAA, it takes longer than 60 seconds for **3** to get fully activated.



Scheme 2.2 Equilibrium reaction of PAA with hydrogen peroxide

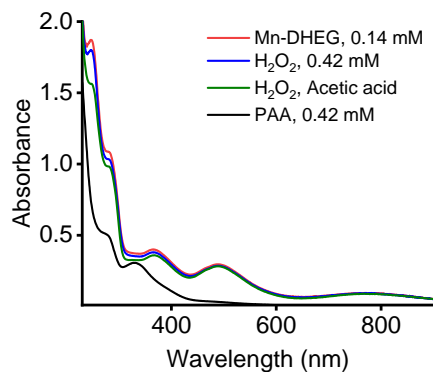


Figure 2.14 Activation of Mn-DHEG with H_2O_2 , H_2O_2 and acetic acid, and PAA

2.13 Electron Paramagnetic Resonance (EPR)

EPR spectroscopy was used to identify the change in oxidation state of the manganese catalyst. The spectra from the frozen Mn-DHEG (10 mM) and PAA (20 mM) in methanol shows a six-line hyperfine pattern at $g = 2$ with a broad resonance at $g = 4$ consistent with a high spin $S = 3/2$ mononuclear Mn(IV) center (Figure 2.15). This is a typical EPR spectrum for a d^3 Mn(IV) ion with relatively small axial zero field splitting parameter (D).^{31, 34-36} When D is small ($2D \ll h\nu$), a strong signal at $g \sim 2$ and a weaker one at $g \sim 4$ is predicted. The EPR spectrum of higher concentration of PAA is identical with that obtained at lower concentration of PAA.

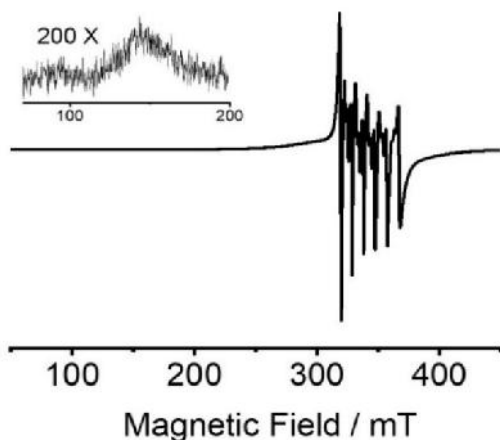


Figure 2.15 EPR spectrum of the resulting complex from reaction of **3** with PAA. Conditions: Mn-DHEG (10 mM) is reacted with PAA (20 mM) in methanol. The EPR spectrum is taken 20 minutes after the addition of PAA in perpendicular mode at 90 K.

2.14 The Effect of pH on the yield of chlorine dioxide by Mn-DHEG/PAA

The kinetics of the catalytic oxidation of ClO_2^- was studied following the formation of chlorine dioxide (ClO_2) at 360 nm because of the minimal contribution of the catalyst absorption in this region and its low extinction coefficients. Kinetics of ClO_2 formation at pH 5.0 or higher showed an induction period prior to ClO_2 formation (Figure 2.16 and 2.17). While time profiles at 360 nm fit a single exponential equation to a first approximation, the time profiles exhibit features of more complex kinetics (see Figure 2.17 and 2.18). The yield of ClO_2 at pH 5.0 was lower than expected by the stoichiometry of equation 1. Although, PAA is fully consumed over 30 minutes, the yield of the reaction depends upon pH of the reaction, around 50-60 % at pH 5.0 (Table 2.2) and 80% at pH 4.0 (Table 2.3). The sensitivity of chlorine dioxide yield indicates product inhibition or further decomposition of chlorine dioxide at higher concentration of PAA. To explain these phenomena, the reaction of chlorine dioxide with PAA in the

CHAPTER 2

presence of catalysts was studied. Decomposition of ClO_2 was observed which will be discussed later in this chapter.

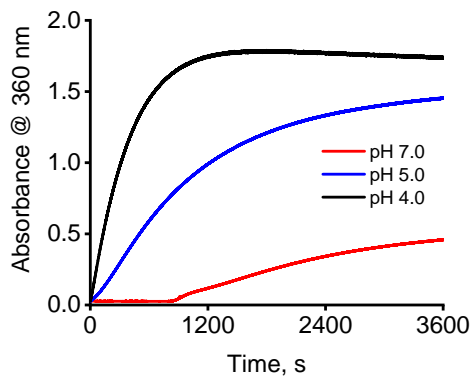


Figure 2.16 The effect of pH on the formation of ClO_2 . Time profile of absorbance at 360 nm due to formation of ClO_2 in the one-electron oxidation of NaClO_2 (6.5 mM) by addition Mn-DHEG (30 μM) and PAA (1.27 mM) at various pH.

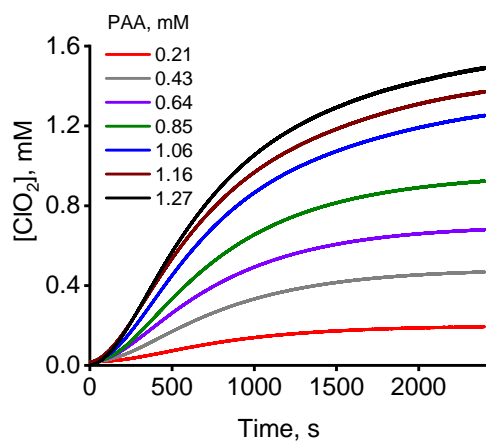


Figure 2.17 Time dependent concentration of chlorine dioxide at 360 nm, pH 5.0, and 25 $^{\circ}\text{C}$, [Mn-DHEG] (30 μM), $[\text{ClO}_2^-]$ (19.5 mM), and various concentration of PAA.

CHAPTER 2

Table 2.2 Results for the catalytic conversion of chlorite to chlorine dioxide in 50.0 mM acetate buffer at pH = 5.0. ^a

[PAA], mM	[ClO ₂], mM	Yield%
0.2	0.19	48
0.43	0.47	54
0.62	0.68	55
0.85	0.92	54
1.06	1.3	59
1.16	1.4	59
1.27	1.5	59

^a Chlorine dioxide concentrations were obtained from the experiments on Figure 2.16. Yields are calculated by using the final concentration of chlorine dioxide divided by twice the concentration of PAA.

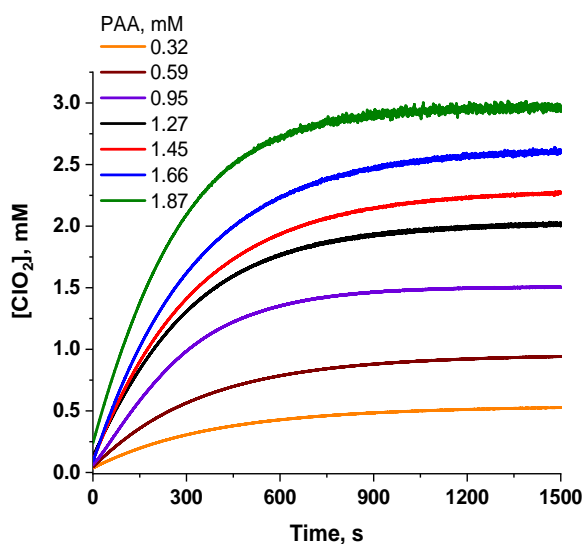


Figure 2.18 Time dependent concentration of chlorine dioxide at 360 nm, pH 4.0, and 25 °C, [Mn-DHEG] (30 μM), [ClO₂⁻] (19.5 mM), and various concentration of PAA.

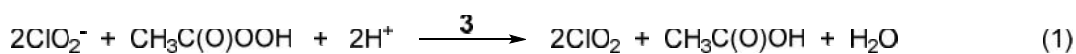
Table 2.3: Results for the catalytic conversion of chlorite to chlorine dioxide in 50.0 mM acetate buffer (pH = 4.0). ^a

[PAA], mM	[ClO ₂], mM	Yield%
0.32	0.53	82
0.59	0.94	80
0.95	1.50	79
1.27	2.02	80
1.45	2.28	78
1.66	2.60	78
1.87	2.93	78

^a Chlorine dioxide concentrations were quantified by using UV-vis spectroscopy at 360 nm and obtained from experiments on Figure 2.18.

CHAPTER 2

The presence of an induction period in the kinetic profiles at pH 5.0 indicates that the catalyst is not fully activated at the onset of the reaction. Giving more time for the catalyst activation enhanced the reaction yield up to 60% at pH 5.0. Furthermore, the catalyst activation is assisted by the higher acid concentration where the disappearance of the induction period was observed at pH 4.0. Under these experimental conditions ($\text{pH} > 4$), chlorite was present almost exclusively in the unprotonated form (pK_a (chlorous acid, HClO_2) = 2 at 25 °C).³⁷ The UV-vis spectra of chlorite stay the same over the reaction period of time as an evidence of chlorite being unprotonated. The yield dependence on pH must originate from a catalytic phenomenon. The stoichiometry of the reaction is 1:2 PAA: ClO_2^- as shown in equation 1.



2.15 Kinetic analysis for catalytic oxidation of chlorite

2.15.1 Catalysis by Mn-DHEG

The kinetics for ClO_2 formation by **3**, Mn-DHEG were investigated in 50.0 mM acetate buffer at pH 5.0 and 4.0. When a solution of chlorite (19.5 mM) was monitored in the presence of **3**, an induction period was observed before the first order appearance of chlorine dioxide at pH 5.0 (Figure 2.16). The kinetics of ClO_2 formation catalyzed by complex **3** at pH 4.0 did not exhibit an induction period. The induction period is approximately 100 – 200 s depending upon the pH of the solution as well as the initial concentration of PAA. Under limiting PAA and excess ClO_2^- (chlorite = 19.5 mM) the time profiles followed first order kinetics (Figure 2.19a). The experimentally determined

CHAPTER 2

rate law showed first-order in [PAA] (Figure 2.19a & c), zero-order in [ClO₂⁻] (Figure 2.19b), and first-order in catalyst **3** (Figure 2.19d). The rate law is shown in equation 2. Control experiments in the absence of catalyst **3** afford minimal chlorine dioxide (Figure 2.10). The second-order rate constant k_3 was determined to be $144 \pm 2 \text{ M}^{-1} \text{ s}^{-1}$. This value is in excellent agreement with the rate constant ($175 \pm 8 \text{ M}^{-1} \text{ s}^{-1}$) determined for the reaction of Mn-DHEG (**3**) with PAA by stopped-flow measurements (vide supra). This confirms that under steady-state catalysis the oxidation of **3** by PAA is the rate determining step.



In the pH range 3.7-4.3, k_{obs} of the catalytic reaction does not increase linearly with increase in acid concentration. The observed rate constant value increased by only 20% whereas [H⁺] is doubled. The pH dependence of the catalyst activation, reaction of **3** with PAA, was investigated in the pH range 3.7 to 5.0 by stopped-flow spectrometry. The reaction kinetics (k_3) did not show dependence on proton concentration. As a result, the pH influences subsequent reactions of the product ClO₂ rather than the reaction of **3** with PAA.

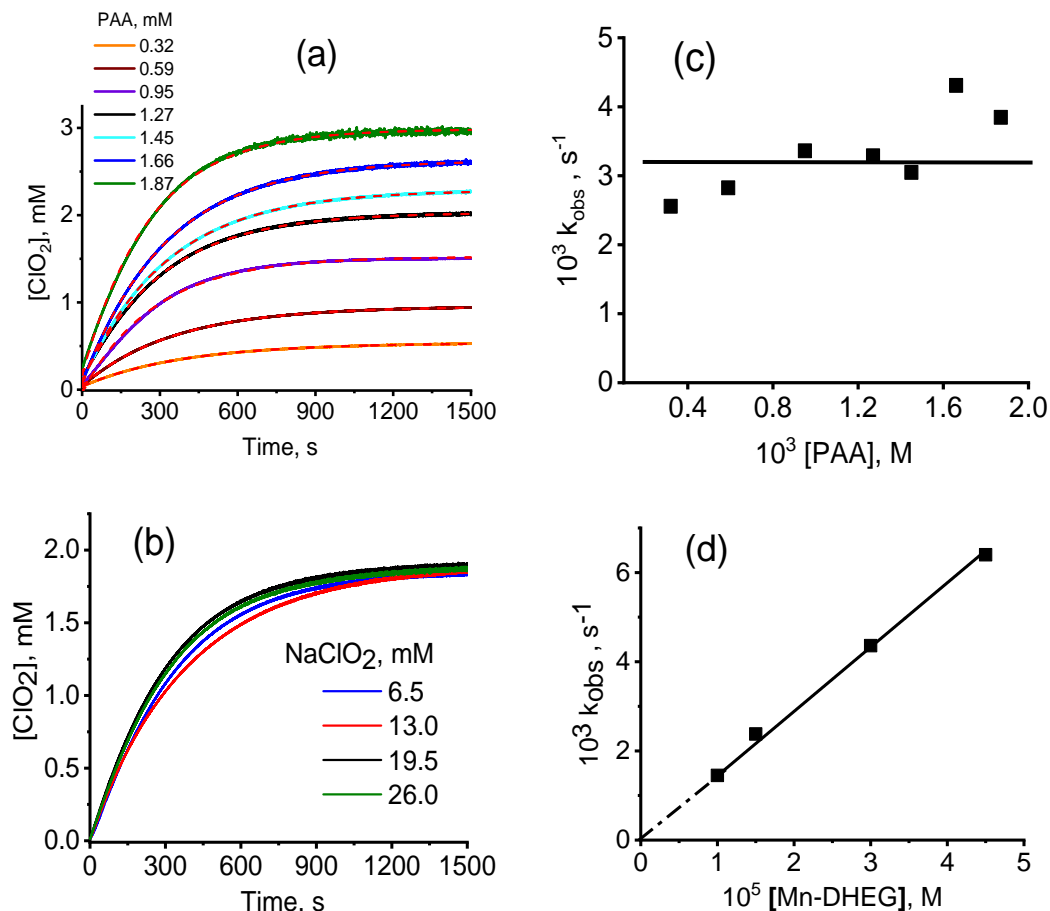


Figure 2.19 Time dependent concentration of chlorine dioxide at pH 4.0 and 25 °C (a) [Mn-DHEG] (30 μM), $[\text{ClO}_2^-]$ (19.5 mM), and various concentration of PAA; (b) [Mn-DHEG] (30 μM), [PAA] (1.27 mM), and various concentration of chlorite (ClO_2^-); (c) and (d) plot of k_{obs} vs [PAA], and [Mn-DHEG] respectively.

2.15.2 Catalysis by Fe-DHEG

In similar investigations, the kinetics for the catalytic formation of ClO_2 by **2** (Fe-DHEG) have been studied under steady-state conditions in 50.0 mM acetate buffer at pH 4.0 leading to a second-order rate equation as that observed for the manganese complex **3** (Figure 2.20). The second-order rate constant k_2 was determined to be $32 \pm 3 \text{ M}^{-1}\text{s}^{-1}$

CHAPTER 2

(Figure 2.20c & d). The steady-state rate constant for the iron system is significantly lower than the observed rate constant for the reaction of **2** with PAA ($k_{2,PAA} = 306 \pm 20 \text{ M}^{-1} \text{ s}^{-1}$) determined by stopped flow (see Figure 2.11). One plausible explanation is that further reactions of ClO_2 in the presence of catalyst **2** become significant and interfere in the kinetic study under steady-state conditions lowering the observed k value and yield of ClO_2 . The observed yield of ClO_2 for catalyst **2** is 40%, which is lower than that of **3**, even though the reaction rate for **2** with PAA is higher. This agrees with what has been previously reported on the water-soluble iron¹⁰ and manganese⁹ porphyrin systems.

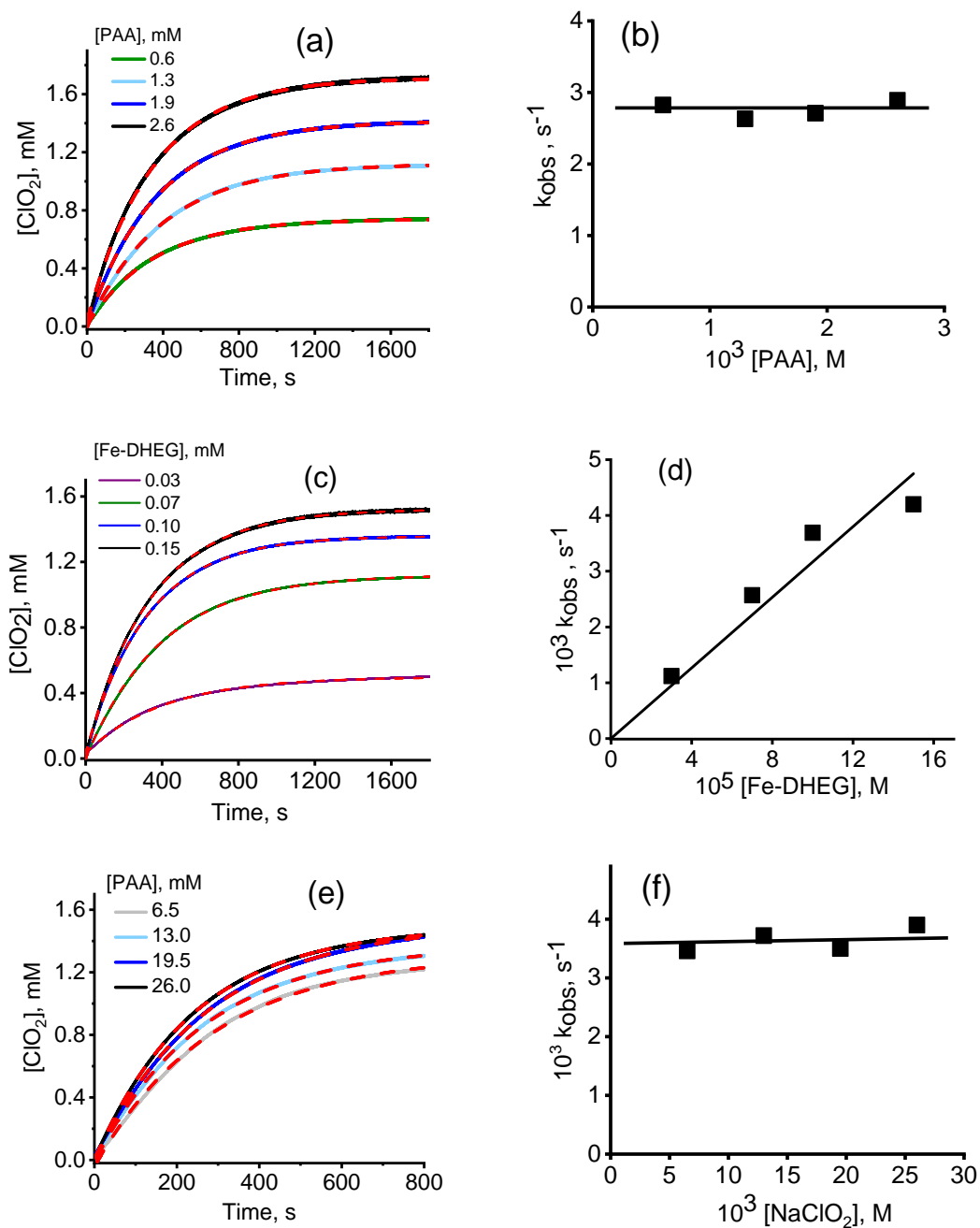


Figure 2.20 Time dependent concentration of chlorine dioxide at pH 4.0 and 25 °C. (a) [Fe-DHEG] (70 μM), $[\text{ClO}_2^-]$ (19.5 mM), and various concentration of PAA; (c) $[\text{ClO}_2^-]$ (19.5 mM), [PAA] (1.27 mM), and various concentration of Mn-DHEG; (e) [Fe-DHEG] (70 μM), [PAA] (1.27 mM), and various concentration of chlorite; (b), (d), (f) plot of k_{obs} vs [PAA], [Fe-DHEG], and $[\text{NaClO}_2]$ respectively for the one-electron oxidation of chlorite.

2.16 Catalytic decomposition of chlorine dioxide

2.16.1 ClO₂ decay by catalyst **3**, Mn-DHEG

In an attempt to probe whether the product affects the reaction, chlorine dioxide was collected in 50.0 mM acetate buffer (pH 4.0) as described previously in Ref. 38 and the reactivity of the catalyst **3**, Mn-DHEG with chlorine dioxide was examined. Aqueous solutions of ClO₂ were prepared by mixing NaClO₂ (6.5 g) and K₂S₂O₈ (10.5 g) in sulfuric acid solution (0.2 mL H₂SO₄ into 20 mL DI water) and bubbling the gas into a solution with the desired pH.³⁸ The first set of experiment was conducted to determine if chlorine dioxide would be able to activate the catalyst in the absence of PAA. This was achieved by reacting Mn-DHEG (0.036 mM) with ClO₂ (2.0 mM) in the presence of sodium chlorite (19.5 mM) at pH 4.0 shown in Figure 2.21, black line. No change in absorbance indicates that ClO₂ cannot activate the catalyst to initiate the catalytic reaction. The same result was obtained giving a longer activation time (0.5 hour) for the mixture of ClO₂ and Mn-DHEG and then introduce the chlorite solution into the mixture. Addition of PAA to this solution with black line results in the ClO₂ decay (Figure 2.21, blue line). It is worth mentioning that the catalyst **3** is required for the decomposition of ClO₂ with PAA. In the absence of the catalyst **3**, the ClO₂ decay was not observed at pH 4.0.

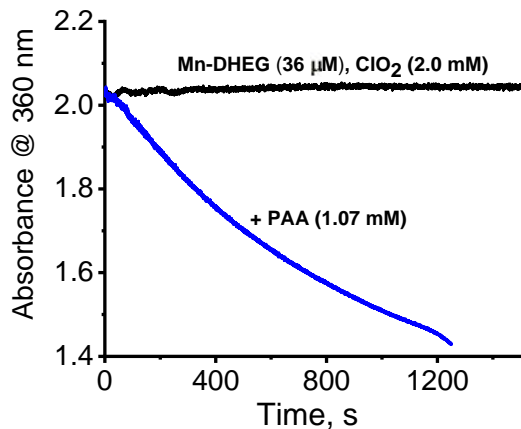


Figure 2.21 . Black line) Activation of **3** Mn-DHEG (0.036 mM) with ClO_2 (2.0 mM) at pH 4.0. Chlorite oxidation was not occurred; blue line) change in concentration of ClO_2 versus time after PAA (1.07 mM) added to the solution at 1500 s, the end of the black line.

The second set of the experiments was conducted to confirm these data in the presence of chlorite upon multiple addition of PAA and the catalyst **3** at pH 5.0 (Figure 2.22).

Upon completion of the reaction (black line), Mn-DHEG (0.036 mM) was injected into the UV-vis cuvette with excess amount of chlorite. No change in absorbance is observed verifying that ClO_2 could not activate the catalyst (blue line) for further oxidation of chlorite. Multiple addition of PAA (the second and third addition) was examined after 1500 second and the completion of the reaction (at the end of the black line) shown as the green and the orange line in Figure 2.22. The result from the second addition of PAA verified the ClO_2 decomposition which is consistent with previous data obtained at pH 4.0. Therefore, the presence of Mn (IV) or Mn (V) is required to initiate the ClO_2 decomposition. The catalyst is deactivated at the end of this process (at the end of green line) as no change in absorbance was observed on the orange line.

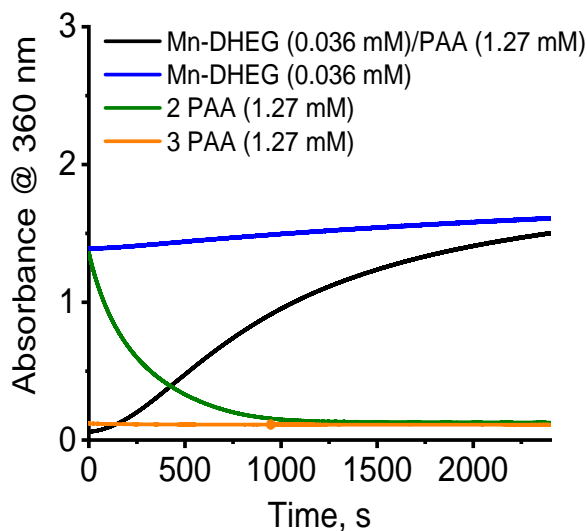
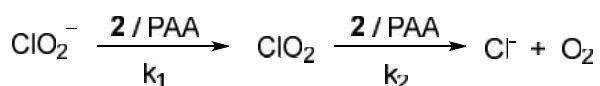


Figure 2.22 Multiple addition of PAA; Black line) Time profile of chlorite (19.5 mM) oxidation with Mn-DHEG (0.036 mM) and PAA (1.27 mM) at pH 5.0; Blue line) addition of Mn-DHEG (0.036 mM) at 1500 s to the reaction mixture at the end of the black line; Green line) Second addition of PAA (1.27 mM) at 1500 s to the black line mixture; Orange line) addition of PAA (1.27 mM) after 1500 s to the green line mixture.

The similar results were obtained at lower concentration of chlorite anion (6.5 mM) at pH 5.0. The reaction of ClO_2 with **3** in the presence of PAA was investigated at pH 5.0. This was achieved by reacting Mn-DHEG (36 μM) with ClO_2 (2.0 mM) in the presence and absence of sodium chlorite (19.5 mM) and PAA at pH 4.0 (Figure 2.23). ClO_2 decayed over hundreds of seconds reaching a concentration $[\text{ClO}_2] = 1.2 \text{ mM}$ in 20 min. Similar behavior was observed at pH 5.0 (Figures 2.22 and 2.23). Both catalyst **3** and PAA are required for decomposition of the ClO_2 product. It is notable that the kinetics of the ClO_2 reaction is significantly faster at pH 5.0 than 4.0. ClO_2 is entirely gone in 20 min (Figure 2.23) and furthermore, by the end of this reaction the catalyst is no longer active for generating ClO_2 from chlorite. These results are consistent with a competing reaction of the active catalyst from **3**/PAA that consumes ClO_2 . This reaction is pH sensitive and degrades the catalyst.

CHAPTER 2

Second addition of Mn-DHEG (0.036) and PAA (1.27 mM); where the overall concentration of PAA is doubled, represents a kinetics resemblance to the consecutive first-order reactions (Figure 19, red line). Chlorine dioxide, the product of the first reaction, is consumed on the subsequent steps.



Scheme 2.3: Consecutive first-order reactions of the chlorite oxidation and the ClO_2 decay.

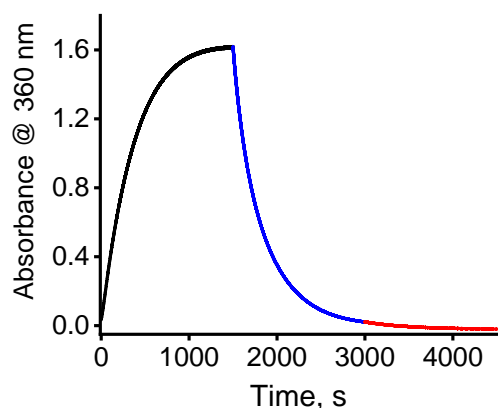


Figure 2.23 (Black line) Time profile of chlorite (6.5 mM) oxidation with Mn-DHEG (0.036 mM) and PAA (1.27 mM) at pH 5.0; (blue line) addition of PAA (1.27 mM) at 1500 s to the black line mixture; (red line) addition of PAA (1.27 mM) at the end of blue line at 3000 s.

To account for the observed decay of ClO_2 (Figure 2.24), the kinetics for the decomposition of ClO_2 with **3**/PAA was investigated in 50.0 mM acetate buffer at pH 4.0 and 5.0. The ClO_2 absorbance at 360 nm disappeared faster at pH 5.0 than pH 4.0 upon addition of a mixture of PAA and Mn-DHEG. The time profiles for ClO_2 decay followed first-order in the limiting reagent, ClO_2 (Figure 2.24a & b), first-order in catalyst [**3**], first-order in [PAA] (Figure 2.24c), and inverse dependence on $[\text{H}_3\text{O}^+]$ (Figure 2.24c). High excess in concentration of PAA at pH 4.0 was necessary to achieve comparable reaction times as a result of its slower ClO_2 decomposition compared to pH

5.0. Based on the experimental rate-law in equation 3, the rate constant for ClO_2 decay with catalyst **3** is $k_{d,\text{ClO}_2} = 0.56 \text{ M}^{-1} \text{ s}^{-1}$. This value is significantly smaller than $k_3 = 144 \text{ M}^{-1} \text{ s}^{-1}$ for ClO_2 formation at pH 4.0 from chlorite (Figure 7).

$$-d[\text{ClO}_2]/dt = \frac{k_{3,\text{ClO}_2} [\mathbf{3}][\text{ClO}_2][\text{PAA}]}{[\text{H}^+]} \quad (3)$$

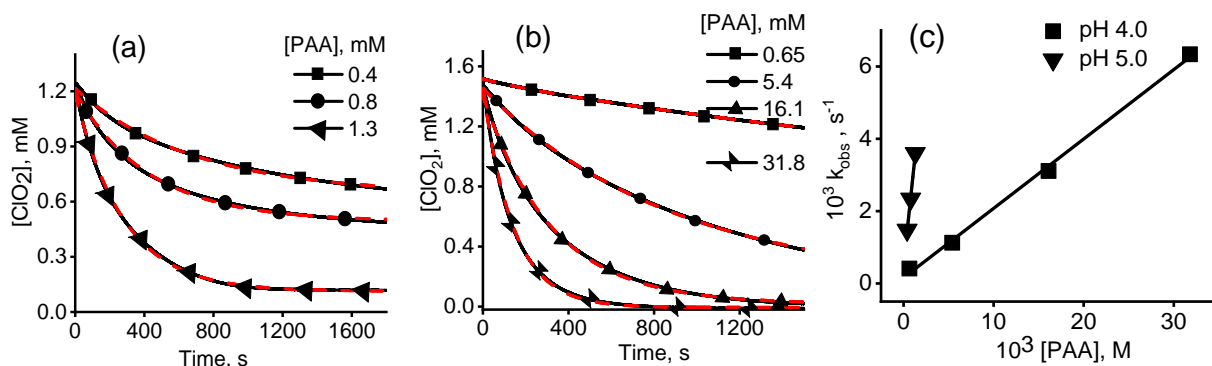


Figure 2.24 (a) Time profile of chlorine dioxide (1.2 mM) decomposition with Mn-DHEG (0.036 mM) and various concentration of PAA at pH 5.0 (black solid lines) and their first order kinetic fits (red dashed lines); (b) Time profile chlorine dioxide (1.5 mM) decomposition with Mn-DHEG (0.036 mM) and various concentration of PAA at pH 4.0 (solid lines) and their first order kinetic fits (dashed lines); (c) Plot of pseudo-first order rate constant (k_{obs}) of the ClO_2 decay versus $[\text{PAA}]$ at pH 4.0 and pH 5.0.

2.16.2 ClO_2 decay by catalyst **2**, Fe-DHEG

In similar investigations, the kinetics for the catalytic decomposition of ClO_2 by **2** (Fe-DHEG) were also investigated under steady-state conditions in 50.0 mM acetate buffer at pH 4.0 leading to the same experimental rate-law observed for catalyst **3**. The second-order rate constant for the iron complex **2** $k_{2,\text{ClO}_2} = 7.6 \text{ M}^{-1} \text{ s}^{-1}$, which is significantly higher than the rate constant for ClO_2 decay with catalyst **3** (Figure 2.25).

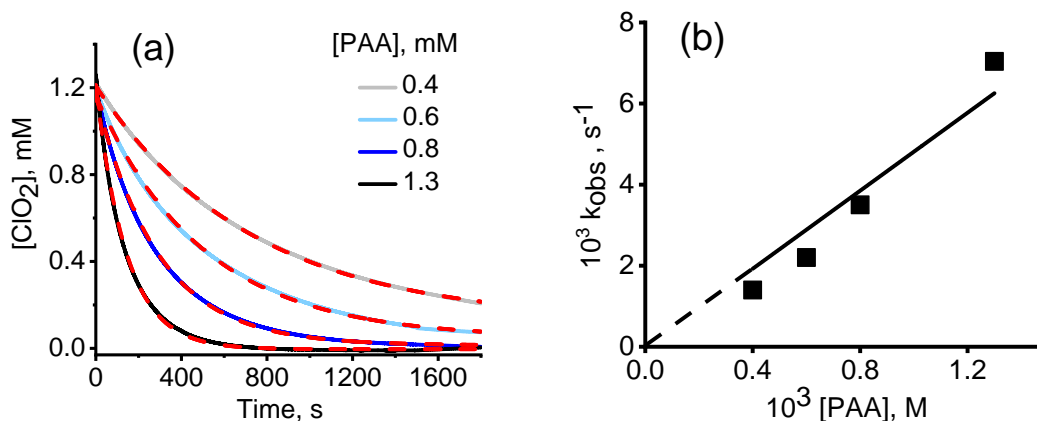


Figure 2.25 (a) Time profile of chlorine dioxide (1.2 mM) decomposition with Fe-DHEG (0.070 mM) and various concentration of PAA at pH 4.0; (b) Plot of pseudo-first order rate constant (k_{obs}) of the ClO_2 decay versus $[\text{PAA}]$ at pH 4.0 ($k_{2,\text{PAA}} = 7.6 \pm 0.2$).

2.17 Iodometric method to determine the concentration of chlorite and chlorate ions

During the catalytic decomposition of chlorine dioxide, the band at 260 nm increases, which is indicative of chlorite ion formation. 1:3 equivalence of chlorite to the initial concentration of chlorine dioxide is produced. Furthermore, chlorate ion is identified via iodometric titration (Table 2.4) and produced in 2:3 ratio of the initial concentration of ClO_2 .

The iodometric method has been reported as a reliable analytical technique to measure the concentration of chlorine dioxide, chlorite and chlorate ions at milligram per liter level with high precision and accuracy.^{39,40}

Under mildly basic conditions (pH 7-8.5) chlorine dioxide reacts with iodide ion to form iodine and chlorite ion:



CHAPTER 2

Under rather acidic conditions ($\leq \text{pH } 2$) chlorite ion reacts with iodide ion to form iodine and the chlorite ion is reduced to chloride ion:



The reaction of chlorate and iodide ions under these conditions is very slow³⁹, and requires severely acidic conditions (6M HCl) for the reaction to be of use analytically.



The selective determination of each species, chlorite and chlorate ions can be achieved by controlling the pH of the solution as described above for the iodometric chemistry.

In the presence of excess amount of KI, I_2 reacts with iodide I^- producing triiodide, I_3^- a red-yellow solution which can be titrated with sodium thiosulfate ($\text{Na}_2\text{S}_2\text{O}_3$) reducing I_3^- to iodide (clear solution). Thyodene (starch) can be used as an indicator for a reliable method of end point detection taking advantage of deep blue color of the starch complex with triiodide.

The chlorite and chlorate ion concentration were determined sequentially by using the procedure described here. The catalytic decomposition of chlorine dioxide (10ml, 1.6 mM) in the presence of PAA (1.3 mM) by **3**, Mn-DHEG (0.036 mM) was repeated in acetic buffer at pH 5.0 in order to measure the concentration of chlorite and chlorate ions at 3000 s. The reaction was undergone to completion according to the time profile UV-vis absorption spectral changes of chlorine dioxide decomposition. The reaction mixture was also purged with N_2 gas to remove the trace amount of the remaining chlorine dioxide from the solution. 2ml of this solution is transferred to a 20 ml vial with

CHAPTER 2

potassium iodide (2 ml, 0.3 M, excess). Concentrated hydrochloric acid was added to the sample solution to adjust the pH 2. After the reaction is complete (about 20 minutes), the triiodide ion was titrated with standard sodium thiosulfate solution (3.0×10^{-4} M). Close to the end point, Thyodene (2-3 drops) is added which will form a deep blue solution. The iodometric end point can be easily detected visually turning the blue solution to colorless.

To the 2ml of this solution, concentrated HCl was added to the sample solution to adjust it to 6M in acid where chlorate ions get reduced by excess amount of KI turning the solution into red. The triiodide ion solution is titrated using standard sodium thiosulfate (3.0×10^{-4} M) and Thyodene as an indicator. The above procedure is repeated three times. The results agree with the anticipated amount of chlorite and chlorate ions as shown in Table below.

Table 2.4 Iodometric method to determine the concentration of chlorite and chlorate ions for the catalytic decomposition of ClO_2 by Mn-DHEG **3** at pH 5.0.^a

$[\text{ClO}_2]$, mM	$[\text{ClO}_2^-]$, mM theoretical ^b	$[\text{ClO}_2^-]$, mM experimental	$[\text{ClO}_3^-]$, mM theoretical	$[\text{ClO}_3^-]$, mM experimental
1.6	0.53	0.65 ± 0.02	0.8	0.79 ± 0.04
1.6	0.53	0.64 ± 0.02	0.8	0.85 ± 0.04
1.6	0.53	0.62 ± 0.02	0.8	0.86 ± 0.04

^aChlorine dioxide (1.6 mM) was undergone disproportionation in the presence of PAA (1.3 mM) by **3**, Mn-DHEG (0.036 mM) in acetic buffer at pH 5.0. ^bTheoretical amount of chlorite and chlorate ions were calculated according to the proposed stoichiometric equation for the catalytic decomposition of ClO_2 .

2.18 Results and discussion

A new ligand motif denoted as **1** (**DHEG**) was prepared in good yield from a lignin derived precursor, 2-methoxy-4-propylphenol (dihydroeugenol, DHE), glycine and formaldehyde under mild conditions. Synthesis of a similar ligand has been reported using various bases (NEt_3 ⁴¹ or NaOH ⁴²) or without the use of a base.²⁰ Initial attempts to prepare **1** using NaOH resulted in numerous products and lower yields with complicated purification steps. In an optimized procedure, the reactions were performed in methanol without added base. A clean product **1** was obtained by addition of water into the reaction mixture followed by filtration of the white precipitate. Various temperatures were investigated, and the best yield was achieved at 50 °C. Ligand **1** was characterized by ¹H-NMR, ¹³C-NMR, and elemental analysis.

Addition of **1** to a methanol slurry of Fe(III) or Mn(III) salts in the presence of an amine base led to the formation of **2** [$\text{Fe}^{\text{III}}(\text{DHEG-3H})(\text{H}_2\text{O})_2$] or **3** [$\text{Mn}^{\text{III}}(\text{DHEG-3H})(\text{H}_2\text{O})_2$] using a slight variation of literature protocols (Section 1.5).²⁰ Methanolic solutions of ligand **1** were treated with Fe or Mn salts and Et_3N in equimolar amounts and the solutions were heated to reflux in air for 2 hours to yield complexes **2** and **3** in good isolated yields (Scheme 2.1). ESI-MS in the positive ionization mode of these complexes are indicative of mononuclear compounds. The elemental analysis data of **2** and **3** are consistent with the calculated results from the empirical formula of each compound.

Structure of Fe/Mn-DHEG complexes. Single crystals of **2** suitable for X-ray diffraction were obtained in acetone/water (1:1 ratio) by slow evaporation at ambient temperature.

CHAPTER 2

An ORTEP diagram of **2** is shown in Figure 2.2. The X-ray single-crystal structure of **2** indicates a mononuclear Fe^{III}-DHEG complex where Fe is coordinated by three oxygens of ligand **1**, one N atom as well as two solvent (water) molecules to complete the octahedral geometry. This structure agrees with elemental analysis data and the mass spectrum. The conformation of the n-propyl substituents on the phenol rings is captured in two various crystalline packings. Rotation about the carbon-carbon sigma bonds in the n-propyl group results in two configurations.

Electron paramagnetic resonance (EPR) spectroscopy of **2**, in perpendicular mode at 10 K, shows peaks with g values at 8.4 and 4.3 that are consistent with a rhombic mononuclear high spin Fe(III) ($S = 5/2$). This oxidation state (3+) for **2** was further supported by magnetic susceptibility measurements determined in CD₃OD solution (Evan's method) at ambient temperature, $\mu_{\text{eff}} = 5.7 \mu_{\text{B}}$. The calculated magnetic moment for 5 unpaired electrons is $5.92 \mu_{\text{B}}$. The Mössbauer spectrum of **2** (Figure 2.6) showed a well resolved doublet with isomer shift of 0.32 mm/s and quadrupole splitting of 0.44 mm/s indicative of a high spin Fe³⁺ ($S = 5/2$).

Attempts to obtain a molecular structure of **3** (Mn-DHEG) were unsuccessful even though crystalline solids were obtained several times. Crystal structures of similar complexes indicate a wide diversity of conformations due to the flexibility of the tetradentate ligand. In this study, the n-propyl groups on the ligand may also increase the number of degrees of freedom and the number of possible crystal packing alternatives. However, magnetic susceptibility of **3** was determined in CD₃OD solution (Evan's

CHAPTER 2

method) at ambient temperature giving $\mu_{\text{eff}} = 4.2 \mu_{\text{B}}$, which is consistent with Mn(III) high spin $S = 2$. The calculated magnetic moment for 4 unpaired electrons is $4.9 \mu_{\text{B}}$.

Several manganese (III) porphyrin complexes have been previously examined for the catalytic formation of chlorine dioxide independently by our group and the Groves group.^{5,31} High valent Mn (IV and V) has been identified as the reactive species in catalytic oxidation of chlorite with Mn porphyrin.^{5,31} Mn(IV)=O has been proposed as the active species in catalysis with non-heme Mn(N₄Py) (where N₄Py is N,N-bis(2-pyridylmethyl)bis(2-pyridyl)methylamine).³¹ The initial step for the heme complexes is oxygen atom transfer from chlorite to [Mn^{III}] via either heterolytic or homolytic Cl–O bond cleavage of chlorite. Homolytic Cl–O bond cleavage results in a Mn^{IV}(O) complex. In contrast to the previously described manganese systems, the catalysts studied here showed that neither Fe nor Mn gets oxidized by chlorite. The catalytic oxidation of chlorite with catalysts **2** and **3** requires an oxidant such as PAA. These observations are consistent with the activation of catalyst, **3** Mn-DHEG, with PAA. ClO₂ production is proportional to the concentration of PAA and consistent with the stoichiometry of equation 1. The yield of ClO₂ production is reduced at higher pH 5.0. This lowered yield at pH 5.0 corresponds to faster decomposition of the ClO₂ product at higher pH per the rate law in equation 3.

For the formation of chlorine dioxide the kinetics show no dependence on [ClO₂⁻]. The reaction of PAA with **3** to make the proposed Mn(IV) is the rate-determining step.

Steady-state kinetics provide a rate constant that agrees with what we measure independently by stopped-flow for the reaction of **3** with PAA. The situation is a little

CHAPTER 2

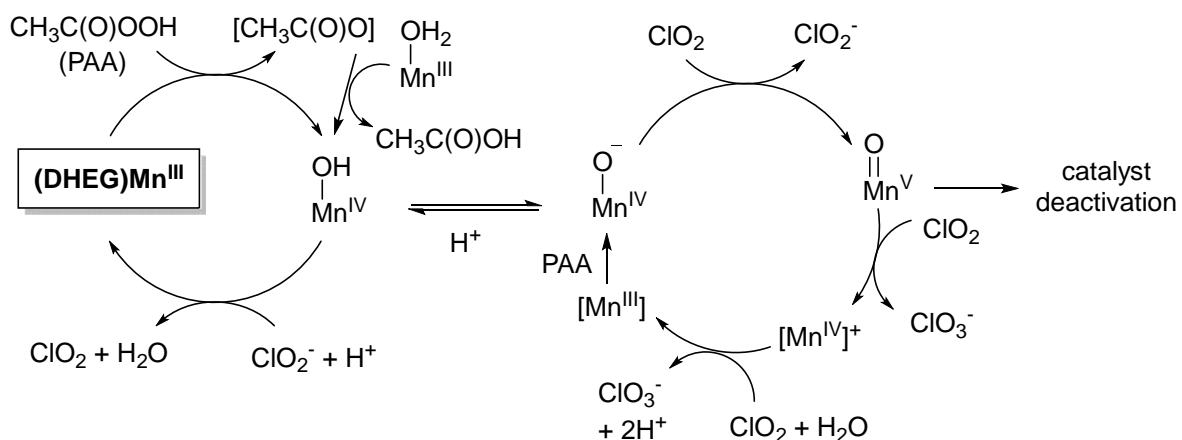
different for iron complex **2**. While the rate law for ClO_2 production is first-order in [**2**] and [PAA], the rate constant from steady-state kinetics ($k_2 = 32 \text{ M}^{-1} \text{ s}^{-1}$) is markedly lower than the rate constant measured directly by stopped-flow for the stoichiometric reaction of **2** and PAA ($k_{2,\text{PAA}} = 306 \text{ M}^{-1} \text{ s}^{-1}$). This discrepancy is attributed to higher rate of ClO_2 degradation for catalyst **2** resulting in lower observed rate constant. In this regard the Mn catalyst **3** shows longevity more than iron, complex **2**.

The reaction between **3** and PAA is postulated to produce a Mn(IV)-OH intermediate. The UV-vis spectrum from stopped-flow experiments and the EPR spectrum of frozen aliquots support Mn(IV) formation. Reaction of PAA with Mn(III) can proceed via oxygen atom transfer to give a Mn(V)=O, which reacts readily with Mn(III) to afford Mn(IV). Alternatively, PAA is known to undergo homolytic cleavage which would provide Mn(IV) directly.^{43,44} While these two mechanisms are not kinetically distinguishable, the reaction with PAA initiates via a manganese peroxo [Mn-OOR] intermediate followed by O-O bond cleavage. The resulting Mn(IV)-OH oxidizes ClO_2^- via electron transfer to produce ClO_2 (Scheme 2.4). A similar mechanism can be envisaged for the iron catalyst complex **2**, although detection of Fe(IV) in this system has been difficult (EPR and Mössbauer show only Fe(III)). The catalyst activation **3** by PAA did not show pH dependence in the range pH 3.7-4.3. Whereas the observed rate constant value for the catalytic oxidation of chlorite increased by 20% in the same pH range. As a result, the pH influences subsequent reactions rather than the reaction of **3** with PAA.

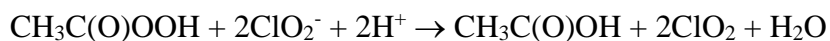
CHAPTER 2

As the ClO_2 product accumulates it reacts further with the catalyst system **3**/PAA. According to the kinetics rate law (equation 3), we suggest reaction of $[\text{Mn(IV)-O}]^-$, resulting from the deprotonation of Mn(IV)-OH , with ClO_2 giving a Mn(V)=O , a highly oxidizing transient species. This Mn(V)=O oxidizes ClO_2 to chlorate³¹ or undergoes the catalyst decomposition. In the case of the iron complex **2** this degradation pathway is more significant than manganese leading to lower yields and rates under steady-state conditions. Since the further reactions with ClO_2 are pH dependent, the yields of ClO_2 are lower at higher pH. Scheme 2.4 summarizes the catalytic cycles for ClO_2 production and its subsequent decomposition. Table 2.5 provides rate constants measured in this study. It should be noted that in addition to the reactions shown in Scheme 2, catalytic decomposition of ClO_2 by **3**/PAA produces molecular oxygen (4%, PAA as a limiting reagent) through side reactions. These may include oxidation of PAA by ClO_2 analogous to dioxygen formation from the reaction of ClO_2 and hydrogen peroxide in basic solution.^{3, 45} Molecular oxygen and chloride may also form from the reaction of $[\text{Mn(IV)-O}]^-$ and ClO_2 via a peroxyhypochlorite adduct $[\text{Mn-OOCIO}]$ analogous to that postulated for porphyrin systems and the heme enzyme chlorite dismutase.^{5, 10, 46}

CHAPTER 2



Stoichiometric reaction for ClO_2 production:



Stoichiometric reaction for ClO_2 decomposition:



Scheme 2.4 proposed mechanism for chlorite oxidation catalyzed by 3 Mn-DHEG in the presence of PAA (left cycle), and decomposition of chlorine dioxide (right cycle). The overall stoichiometric reactions are provided below the proposed catalytic cycles.

Table 2.5 Rate constants for reactions of Fe-DHEG 2 and Mn-DHEG 3.^a

Reaction	Rate constant/ $M^{-1} s^{-1}$	
	Fe-DHEG (2)	Mn-DHEG (3)
$2(DHEG)Mn^{III} + PAA \rightarrow 2[(DHEG)Mn^{IV}]^-$	$k_{2,PAA} = 306 \pm 20^c$	$k_{3,PAA} = 175 \pm 8$
$PAA + 2ClO_2^- + 2H^+ \rightarrow AA + 2ClO_2 + H_2O^b$	$k_2 = 32 \pm 3$	$k_3 = 144 \pm 2$
$PAA + 6ClO_2 + 3H_2O \rightarrow AA + 2ClO_2^- +$	$k_{a,ClO_2} = 7.6 \pm 0.2$	$k_{a,ClO_2} = 0.56 \pm 0.02$

^a T = 25 °C. ^b PAA = $CH_3C(O)OOH$, AA = $CH_3C(O)OH$, rate constants determined at pH 4.0. ^c Fe(IV)-OH complexes are difficult to ascertain and this instant the product of iron(III) activation is not characterized.

CHAPTER 2

2.19 Conclusion

Two non-heme complexes Fe-DHEG **2** [$\text{Fe}^{\text{III}}(\text{DHEG-3H})(\text{H}_2\text{O})_2$] and Mn-DHEG **3** [$\text{Mn}^{\text{III}}(\text{DHEG-3H})(\text{H}_2\text{O})_2$] featuring a lignin-derived tetradentate ligand were synthesized and fully characterized. Both complexes are active catalysts for the production of chlorine dioxide from chlorite in aqueous solution with the use of PAA (peroxyacetic acid) as an oxidant. ClO_2 production proceeds with the reaction between the metal complexes and PAA being rate determining. For complex **3** this reaction affords manganese (IV) with a second order rate constant $k_{3,\text{PAA}} = 175 \text{ M}^{-1} \text{ s}^{-1}$. Under steady-state catalysis the same rate constant was obtained corresponding to a turnover frequency $\text{TOF} = 17 \text{ h}^{-1}$ at pH 4.0. Subsequent decomposition of ClO_2 was found to require both catalyst and PAA; also, the ClO_2 decomposition was faster at higher pH. Similar observations were made for iron suggesting analogous mechanism to manganese. However, iron(IV) was not detected. Yields of ClO_2 were lower under iron catalysis, which was attributed to faster ClO_2 decomposition with iron. Lastly, catalyst deactivation was more prominent for the iron complex **2**. These complexes, most particularly the manganese complex **3**, offer a clean and robust synthesis of ClO_2 on-demand in water under ambient conditions and moderate pH. The simple design of the ligand and its scalability at a reasonable cost (estimated cost of 1 mole of catalyst **3** = \$12) make this system of interest for further development of techno-economics analysis (TEA) for practical environmental applications such as treating produced water from shale gas production or as a disinfectant for bacteria and viruses on contaminated surfaces.

2.20 References

1. Coonrod, C. L.; Ben Yin, Y.; Hanna, T.; Atkinson, A. J.; Alvarez, P. J. J.; Tekavec, T. N.; Reynolds, M. A.; Wong, M. S., Fit-for-purpose treatment goals for produced waters in shale oil and gas fields. *Water Res.* **2020**, *173*, 115467. DOI: 10.1016/j.watres.2020.115467
2. Erkenbrecher, C. W.; Nurnberg, S.; Breyla, A. D., A Comparison of Three Nonoxidizing Biocides and Chlorine Dioxide in Treating Marcellus Shale Production Waters. *Spe Production & Operations* **2015**, *30* (4), 368-374. DOI: 10.2118/174560-Pa
3. Odeh, I. N.; Francisco, J. S.; Margerum, D. W., New pathways for chlorine dioxide decomposition in basic solution. *Inorg. Chem.* **2002**, *41* (24), 6500-6. DOI: 10.1021/ic0204676
4. Umile, T. P.; Groves, J. T., Catalytic generation of chlorine dioxide from chlorite using a water-soluble manganese porphyrin. *Angew. Chem. Int. Ed. Engl.* **2011**, *50* (3), 695-8. DOI: 10.1002/anie.201004482
5. Umile, T. P.; Wang, D.; Groves, J. T., Dissection of the mechanism of manganese porphyrin-catalyzed chlorine dioxide generation. *Inorg. Chem.* **2011**, *50* (20), 10353-62. DOI: 10.1021/ic201430v
6. Tratnyek, P. G.; Hoigné, J., Kinetics of reactions of chlorine dioxide (OCIO) in water—II. Quantitative structure-activity relationships for phenolic compounds. *Water Res.* **1994**, *28* (1), 57-66. DOI: 10.1016/0043-1354(94)90119-8
7. Stewart, D. J.; Napolitano, M. J.; Bakmutova-Albert, E. V.; Margerum, D. W., Kinetics and mechanisms of chlorine dioxide oxidation of tryptophan. *Inorg. Chem.* **2008**, *47* (5), 1639-47. DOI: 10.1021/ic701761p
8. Rook, J. J.; Gras, A. A.; van der Heijden, B. G.; de Wee, J., Bromide oxidation and organic substitution in water treatment. *Journal of Environmental Science and Health . Part A: Environmental Science and Engineering* **1978**, *13* (2), 91-116. DOI: 10.1080/10934527809374796
9. Hicks, S. D.; Petersen, J. L.; Bougher, C. J.; Abu-Omar, M. M., Chlorite dismutation to chlorine dioxide catalyzed by a water-soluble manganese porphyrin. *Angew. Chem. Int. Ed. Engl.* **2011**, *50* (3), 699-702. DOI: 10.1002/anie.201005128
10. Zdilla, M. J.; Lee, A. Q.; Abu-Omar, M. M., Bioinspired dismutation of chlorite to dioxygen and chloride catalyzed by a water-soluble iron porphyrin. *Angew. Chem. Int. Ed. Engl.* **2008**, *47* (40), 7697-700. DOI: 10.1002/anie.200801521
11. Ruiz-Duenas, F. J.; Martinez, A. T., Microbial degradation of lignin: how a bulky recalcitrant polymer is efficiently recycled in nature and how we can take advantage of this. *Microb Biotechnol* **2009**, *2* (2), 164-77. DOI: 10.1111/j.1751-7915.2008.00078.x
12. Luo, H.; Klein, I. M.; Jiang, Y.; Zhu, H. Y.; Liu, B. Y.; Kenttamaa, H. I.; Abu-Omar, M. M., Total Utilization of Miscanthus Biomass, Lignin and Carbohydrates, Using Earth Abundant Nickel Catalyst. *Acs Sustainable Chemistry & Engineering* **2016**, *4* (4), 2316-2322. DOI: 10.1021/acssuschemeng.5b01776
13. Parsell, T.; Yohe, S.; Degenstein, J.; Jarrell, T.; Klein, I.; Gencer, E.; Hewetson, B.; Hurt, M.; Kim, J. I.; Choudhari, H.; Saha, B.; Meilan, R.; Mosier, N.;

CHAPTER 2

- Ribeiro, F.; Delgass, W. N.; Chapple, C.; Kenttamaa, H. I.; Agrawal, R.; Abu-Omar, M. M., A synergistic biorefinery based on catalytic conversion of lignin prior to cellulose starting from lignocellulosic biomass. *Green Chemistry* **2015**, *17* (3), 1492-1499. DOI: 10.1039/c4gc01911c
14. Song, S.; Zhang, X.; Ma, H.; Yang, Y., Zinc complexes supported by claw-type aminophenolate ligands: synthesis, characterization and catalysis in the ring-opening polymerization of rac-lactide. *Dalton Trans* **2012**, *41* (11), 3266-77. DOI: 10.1039/c2dt11767c
15. Matos, C. P.; Valente, A.; Marques, F.; Adão, P.; Paula Robalo, M.; de Almeida, R. F. M.; Pessoa, J. C.; Santos, I.; Helena Garcia, M.; Tomaz, A. I., New polydentate Ru(III)-Salan complexes: Synthesis, characterization, anti-tumour activity and interaction with human serum proteins. *Inorg. Chim. Acta* **2013**, *394*, 616-626. DOI: 10.1016/j.ica.2012.09.026
16. Whiteoak, C. J.; Torres Martin de Rosales, R.; White, A. J.; Britovsek, G. J., Iron(II) complexes with tetradentate bis(aminophenolate) ligands: synthesis and characterization, solution behavior, and reactivity with O(2). *Inorg. Chem.* **2010**, *49* (23), 11106-17. DOI: 10.1021/ic1016998
17. Do an, A.; akıyan, .; Kılıç, E., Potentiometric Studies on Some -Amino Acid-Schiff Bases and Their Manganese (III) Complexes in Dimethyl Sulfoxide–Water Mixtures at 25° C. *J. Solution Chem.* **2004**, *33* (12), 1539-1547. DOI: 10.1007/s10953-004-1406-8
18. Kripli, B.; Garda, Z.; Solyom, B.; Tircso, G.; Kaizer, J., Formation, stability and catalase-like activity of mononuclear manganese(ii) and oxomanganese(iv) complexes in protic and aprotic solvents. *New J. Chem.* **2020**, *44* (14), 5545-5555. DOI: 10.1039/c9nj06004a
19. Szabó, O.; Farkas, E., Characterization of Mn (II) and Mn (III) binding capability of natural siderophores desferrioxamine B and desferricoprogen as well as model hydroxamic acids. *Inorg. Chim. Acta* **2011**, *376* (1), 500-508. DOI: 10.1016/j.ica.2011.07.010
20. Weyhermuller, T.; Wagner, R.; Chaudhuri, P., Asymmetrically Dibridged Diiron(III) Complexes with Aminebis(phenoxide)-Based Ligands for a Magnetostructural Study. *Eur. J. Inorg. Chem.* **2011**, 10.1002/ejic.201001340 (16), 2547-2557. DOI: 10.1002/ejic.201001340
21. Benesi, H. A.; Hildebrand, J. H., A Spectrophotometric Investigation of the Interaction of Iodine with Aromatic Hydrocarbons. *J. Am. Chem. Soc.* **1949**, *71* (8), 2703-2707. DOI: 10.1021/ja01176a030
22. Goswami, S.; Sen, D.; Das, N. K.; Fun, H. K.; Quah, C. K., A new rhodamine based colorimetric 'off-on' fluorescence sensor selective for Pd²⁺ along with the first bound X-ray crystal structure. *Chem Commun (Camb)* **2011**, *47* (32), 9101-3. DOI: 10.1039/c1cc12845k
23. Huang, X.; Zhao, S.; Abu-Omar, M.; Whelton, A. J., In-situ cleaning of heavy metal contaminated plastic water pipes using a biomass derived ligand. *Journal of Environmental Chemical Engineering* **2017**, *5* (4), 3622-3631. DOI: 10.1016/j.jece.2017.07.003

CHAPTER 2

24. Forshaw, A. P.; Smith, J. M.; Ozarowski, A.; Krzystek, J.; Smirnov, D.; Zvyagin, S. A.; Harris, T. D.; Karunadasa, H. I.; Zadrozny, J. M.; Schnegg, A.; Holldack, K.; Jackson, T. A.; Alamiri, A.; Barnes, D. M.; Telser, J., Low-spin hexacoordinate Mn(III): synthesis and spectroscopic investigation of homoleptic tris(pyrazolyl)borate and tris(carbene)borate complexes. *Inorg. Chem.* **2013**, *52* (1), 144-59. DOI: 10.1021/ic301630d
25. Stein, J.; Fackler, J. P.; McClune, G. J.; Fee, J. A.; Chan, L. T., Superoxide and manganese(III). Reactions of manganese-EDTA and manganese-CyDTA complexes with molecular oxygen. X-ray structure of potassium manganese-EDTA.2 water. *Inorg. Chem.* **1979**, *18* (12), 3511-3519. DOI: 10.1021/ic50202a044
26. Fackler, J. P.; Chawla, I. D., Spectra of Manganese(III) Complexes. I. Aquomanganese(III) Ion and Hydroxide, Fluoride, and Chloride Complexes. *Inorg. Chem.* **1964**, *3* (8), 1130-1134. DOI: 10.1021/ic50018a013
27. van Gorkum, R.; Berding, J.; Mills, A. M.; Kooijman, H.; Tooke, D. M.; Spek, A. L.; Mutikainen, I.; Turpeinen, U.; Reedijk, J.; Bouwman, E., The Synthesis, Structures and Characterisation of New Mixed-Ligand Manganese and Iron Complexes with Tripodal, Tetradentate Ligands. *Eur. J. Inorg. Chem.* **2008**, *2008* (9), 1487-1496. DOI: 10.1002/ejic.200701280
28. Conradie, J., Jahn-Teller effect in high spin d4 and d9 octahedral metal-complexes. *Inorg. Chim. Acta* **2019**, *486*, 193-199. DOI: 10.1016/j.ica.2018.10.040
29. Daneshmand, P.; Schaper, F., Exploring the reactivity of manganese(III) complexes with diphenolate-diamino ligands in rac-lactide polymerization. *Dalton Trans* **2015**, *44* (47), 20449-58. DOI: 10.1039/c5dt03756e
30. Kass, M.; Hohenberger, J.; Adelhardt, M.; Zolnhofer, E. M.; Mossin, S.; Heinemann, F. W.; Sutter, J.; Meyer, K., Synthesis and characterization of divalent manganese, iron, and cobalt complexes in tripodal phenolate/N-heterocyclic carbene ligand environments. *Inorg. Chem.* **2014**, *53* (5), 2460-70. DOI: 10.1021/ic4024053
31. Hicks, S. D.; Kim, D.; Xiong, S.; Medvedev, G. A.; Caruthers, J.; Hong, S.; Nam, W.; Abu-Omar, M. M., Non-heme manganese catalysts for on-demand production of chlorine dioxide in water and under mild conditions. *J. Am. Chem. Soc.* **2014**, *136* (9), 3680-6. DOI: 10.1021/ja5001642
32. Limburg, J.; Vrettos, J. S.; Liable-Sands, L. M.; Rheingold, A. L.; Crabtree, R. H.; Brudvig, G. W., A functional model for O-O bond formation by the O₂-evolving complex in photosystem II. *Science* **1999**, *283* (5407), 1524-7. DOI: 10.1126/science.283.5407.1524
33. Zaragoza, J. P. T.; Siegler, M. A.; Goldberg, D. P., A Reactive Manganese(IV)-Hydroxide Complex: A Missing Intermediate in Hydrogen Atom Transfer by High-Valent Metal-Oxo Porphyrinoid Compounds. *J. Am. Chem. Soc.* **2018**, *140* (12), 4380-4390. DOI: 10.1021/jacs.8b00350
34. Richens, D. T.; Sawyer, D. T., Bis(Tetramethylammonium)Tris(Sorbitolato)Manganate (Iv), an EPR-Active Monomeric Complex of Manganese(Iv). *J. Am. Chem. Soc.* **1979**, *101* (13), 3681-3683. DOI: 10.1021/ja00507a055
35. Bryliakov, K. P.; Kholdeeva, O. A.; Vanina, M. P.; Talsi, E. P., Role of MnIV species in Mn(salen) catalyzed enantioselective aerobic epoxidations of alkenes: an EPR

CHAPTER 2

- study. *J. Mol. Catal. A: Chem.* **2002**, *178* (1-2), 47-53. DOI: 10.1016/s1381-1169(01)00296-5
36. Chin Quee-Smith, V.; DelPizzo, L.; Jureller, S. H.; Kerschner, J. L.; Hage, R., Synthesis, Structure, and Characterization of a Novel Manganese(IV) Monomer, [Mn(IV)(Me(3)TACN)(OMe)(3)](PF(6)) (Me(3)TACN = N,N',N''-Trimethyl-1,4,7-triazacyclononane), and Its Activity toward Olefin Oxidation with Hydrogen Peroxide. *Inorg. Chem.* **1996**, *35* (22), 6461-6465. DOI: 10.1021/ic951522w
37. Kern, D. M.; Kim, C.-H., Iodine Catalysis in the Chlorite-Iodide Reaction1. *J. Am. Chem. Soc.* **1965**, *87* (23), 5309-5313. DOI: 10.1021/ja00951a008
38. Thøgersen, J.; Jepsen, P. U.; Thomsen, C. L.; Poulsen, J. A.; Byberg, J. R.; Keiding, S. R., Femtosecond Photolysis of ClO₂ in Aqueous Solution. *The Journal of Physical Chemistry A* **1997**, *101* (18), 3317-3323. DOI: 10.1021/jp9632302
39. Gordon, G.; Yoshino, K.; Themelis, D. G.; Wood, D.; Pacey, G. E., Utilization of Kinetic-Based Flow-Injection Methods for the Determination of Chlorine and Oxychlorine Species. *Anal. Chim. Acta* **1989**, *224* (2), 383-391. DOI: Doi 10.1016/S0003-2670(00)86574-5
40. Ikeda, Y.; Tang, T. F.; Gordon, G., Iodometric Method for Determination of Trace Chlorate Ion. *Anal. Chem.* **1984**, *56* (1), 71-73. DOI: DOI 10.1021/ac00265a019
41. Li, Y.; Yu, D.; Dai, Z.; Zhang, J.; Shao, Y.; Tang, N.; Wu, J., Bulky metallocavitands with a chiral cavity constructed by aluminum and magnesium atrane-like: enantioselective recognition and separation of racemic alcohols. *Dalton Trans* **2015**, *44* (12), 5692-702. DOI: 10.1039/c4dt03848g
42. Barroso, S.; Adao, P.; Coelho, A. M.; Pessoa, J. C.; Martins, A. M., Pinacol coupling of benzaldehydes mediated by titanium complexes displaying amine bis(phenolate) ligands. *J Mol Catal a-Chem* **2016**, *412*, 107-116. DOI: 10.1016/j.molcata.2015.11.021
43. Rokhina, E. V.; Makarova, K.; Lahtinen, M.; Golovina, E. A.; Van As, H.; Virkutyte, J., Ultrasound-assisted MnO₂ catalyzed homolysis of peracetic acid for phenol degradation: The assessment of process chemistry and kinetics. *Chem. Eng. J.* **2013**, *221*, 476-486. DOI: 10.1016/j.cej.2013.02.018
44. Ottenbacher, R. V.; Bryliakov, K. P.; Talsi, E. P., Nonheme manganese-catalyzed asymmetric oxidation. A Lewis acid activation versus oxygen rebound mechanism: evidence for the "third oxidant". *Inorg. Chem.* **2010**, *49* (18), 8620-8. DOI: 10.1021/ic101297x
45. Ni, Y.; Wang, X., Mechanism and kinetics of chlorine dioxide reaction with hydrogen peroxide under acidic conditions. *The Canadian Journal of Chemical Engineering* **1997**, *75* (1), 31-36. DOI: 10.1002/cjce.5450750107
46. Zdilla, M. J.; Lee, A. Q.; Abu-Omar, M. M., Concerted Dismutation of Chlorite Ion: Water-Soluble Iron-Porphyrins As First Generation Model Complexes for Chlorite Dismutase. *Inorg. Chem.* **2009**, *48* (5), 2260-2268. DOI: 10.1021/ic801681n

CHAPTER 3. PREPARATION OF SUSTAINABLE POLAR APROTIC
SOLVENTS FROM BIOMASS

3.1 Introduction

Solvent selection is a major decision in the synthesis of many industrial chemicals. For example, solvents account for 80% or more of the material used in a typical active pharmaceutical ingredient synthesis.¹ Of additional concern is the fact that a large portion of the environmental impact stems from the solvent life cycle (manufacture, distribution, use, and disposal).² Due to these facts, many companies and groups have devised solvent selection guides in which more favorable solvents are recommended and alternatives suggested for less favorable ones, balancing concerns over safety, performance, cost and toxicity towards human and the environment.^{3,4} Furthermore, in recent years, certain journals have made editorial policies to discourage use of highly undesirable solvents while encouraging the inclusion of green chemistry considerations in solvent selection.⁵

The use of petrochemical solvents is the key to the majority of chemical processes but not without severe implications on the environment. Green solvents were developed as a more environmentally friendly alternative to petrochemical solvents which are derived from the processing of agricultural crops. Ethyl lactate,^{6,7} 2-methyltetrahydrofuran (2-MeTHF),^{8,9} limonene,¹⁰ ethanol,¹¹ and glycerol¹² are examples of green solvents with numerous attractive advantages including being biodegradable, easy to recycle, noncorrosive, noncarcinogenic, and nonozone-depleting.^{6,7}

CHAPTER 3

Certain polar aprotic solvents (PAS) such as dimethylformamide (DMF), dimethylacetamide (DMAc), and *N*-methylpyrrolidinone (NMP) do not have good replacements, despite their critical roles at facilitating nucleophilic substitution reactions. While these are good solvents for a number of reactions, and sometimes the only ones which will dissolve polar materials or salts, they face growing scrutiny and regulations as more concerns over their environmental toxicity emerge.³ Newer PAS solvents, represented as cyclic urea *N,N'*-dimethylpropyleneurea (DMPU) and *N,N'*-dimethylimidazolidinone (DMI) have been used in place of these amide compounds, with preliminary data indicating them to be less endocrine disruptive. However, preparation of these new solvents by traditional means remains environmentally burdensome and the high cost of these new solvents is detrimental to their application.

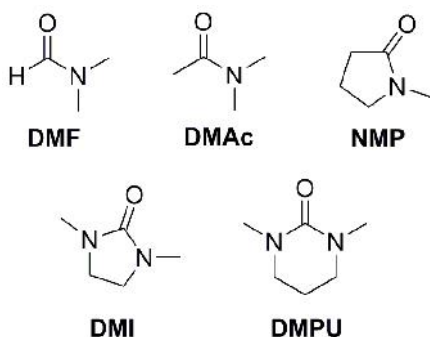
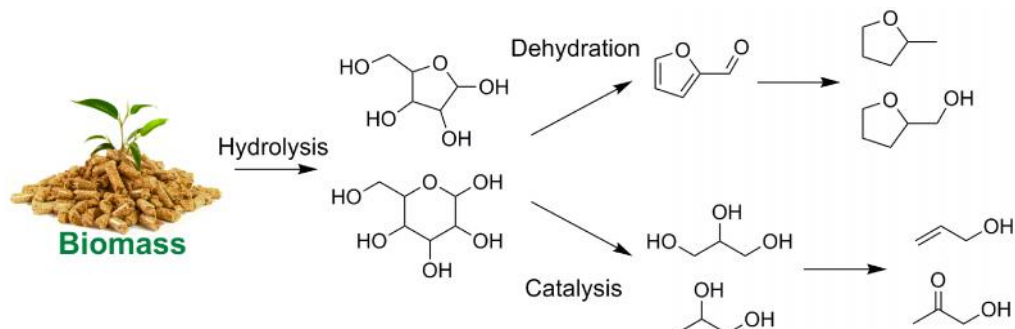


Figure 3.1 Industrially Important Polar Aprotic Solvents (PAS). DMF and DMAc have reprotoxicity issues and are strongly regulated particularly in European Union.¹³ NMP, DMI and DMPU are considered more eco-friendly substitutes of DMF and DMAc.

Considering the lack of PAS made from renewable sources, we seek to identify and develop environmentally friendly methods to produce sustainable PAS from biomass. As biomass depolymerization and conversion to simple chemical building blocks is becoming

CHAPTER 3

ever more viable,^{14, 15} we chose to focus on known derivatives with the ultimate goal of having a continuous process directly from biomass (Scheme 3.1).



Scheme 3.1 . Biomass conversion to chemicals useful for solvent synthesis.

Catalytic conversion of cellulose into polyols including ethylene glycol (EG) and 1,2-propylene glycol (1,2-PG), and furfural represents an important route for the effective utilization of renewable resources to produce PAS.

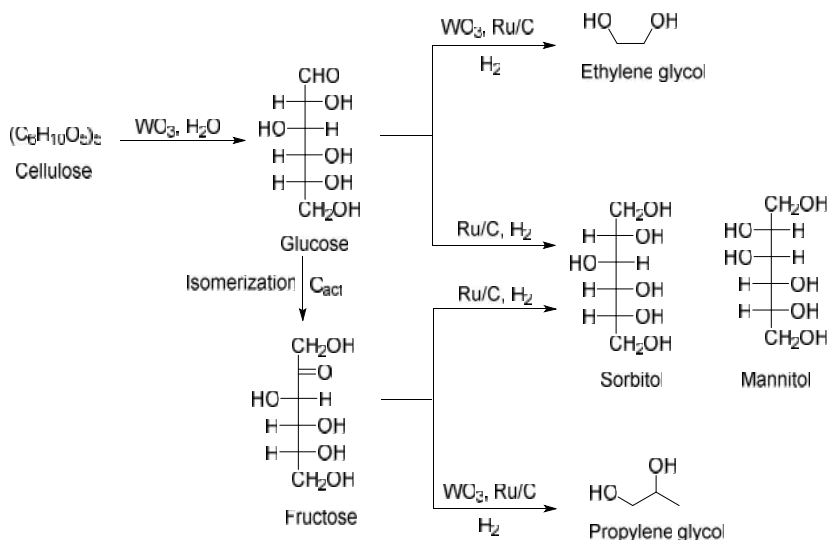
3.2 Cellulose conversion to polyols

The major components of biomass are cellulose (40-60%), hemicellulose (20-40%) and lignin (10-25%).^{16, 17} Cellulose is the most abundant source of biomass and has attracted much attention as vitally renewable alternative to fossil fuels.¹⁸ As such, catalytic conversion of cellulose to polyols is particularly noteworthy because of the versatile uses of polyols as chemicals directly and as precursors in the synthesis of fuels and value-added compounds (Scheme 3.1).^{18, 19} Conversion of cellulose to polyols involves hydrolysis of cellulose by inorganic acids to glucose, and subsequent hydrogenation of glucose to sorbitol and other polyols.¹⁸⁻²⁰ For example, recent studies showed that combination of

CHAPTER 3

water-soluble heteropoly acids and ruthenium on carbon (Ru/C) catalysts is efficient for cellulose conversion to hexitols (sorbitol and mannitol).¹⁸

Solid catalysts such as Ru/C promoted the hydrolytic hydrogenation of cellulose, which includes acid hydrolysis of cellulose to produce glucose, and the following hydrogenation of glucose to yield hexitols.^{18, 21} If the glucose produced from the hydrolysis process was not involved in the hydrogenation reaction immediately, glucose will undergo degradation, resulting in an increase in the yield of small polyol molecules (Scheme 3.2).



Scheme 3.2 Catalytic conversion of cellulose into polyols

Liu et al.¹⁸ found that tungsten trioxide promoted ruthenium catalysts showed outstanding performance in the hydrogenolysis of cellulose to yield glycols at 478 K, and 6 MPa of H_2 . Tungsten trioxide was found to promote the hydrolysis of cellulose as well as C–C bond cleavage in sugars efficiently. Ethylene glycol (EG) was found to be derived from the C–C cleavage of glucose, while 1,2-propylene glycol (1,2-PG) was produced by the degradation of fructose, which was formed by glucose isomerization (Scheme 3.2). The loss of catalyst

CHAPTER 3

during the recycling stage is not unusual, but it is surprising that no leaching of Ru could be detected by ICP in the reaction solution after the first run. The TEM images of the Ru/C catalyst after the first reaction showed that the average size of Ru particles had increased from 1.2 to 1.7 nm, and remained around 1.7 nm in subsequent runs this increase could therefore be one of the reasons for the decrease in activity.^{18, 22}

The commercial heteropoly acids (HPAs) $\text{H}_3\text{PW}_{12}\text{O}_{40}$ and $\text{H}_4\text{SiW}_{12}\text{O}_{40}$ were demonstrated to be very effective acid catalysts in combination with Ru/C to directly produce hexitols from cellulose. Notably, the HPAs performed much better than an equinormal aq. H_2SO_4 solution, an industrial standard for cellulose hydrolysis. Immediate hydrogenation of glucose at elevated H_2 pressure with Ru/C provides quantitative amounts of hexitols from cellulose.²¹

One of the low cost catalysts that can effectively convert cellulose to small molecules were the Ni based catalysts supported on various supports, including hydrothermally stable oxides with varying surface properties (Al_2O_3 , kieselguhr, TiO_2 , SiO_2 , ZnO , ZrO_2 and MgO) in previous investigations.^{19, 23} Ni/ZnO (20% Ni) catalyst could convert cellulose completely and give a 70.4% yield of 1,2-alkanediols composed of 1,2-propylene glycol (1,2-PG), ethylene glycol (EG), 1,2-butanediol (1,2-BDO) and 1,2-hexaindiol (1,2-HDO).¹⁹ The main drawback of this catalyst lay in its poor hydrothermal stability, which resulted in the decrease of catalytic activity after repeated reaction runs, which was partially ascribed to the leaching of Ni.¹⁹

Fukuoka and Dhepe²⁴ pioneered the conversion of cellulose over solid acid supported noble metal catalysts. Cellulose could be directly hydrolytically hydrogenated into sugar

CHAPTER 3

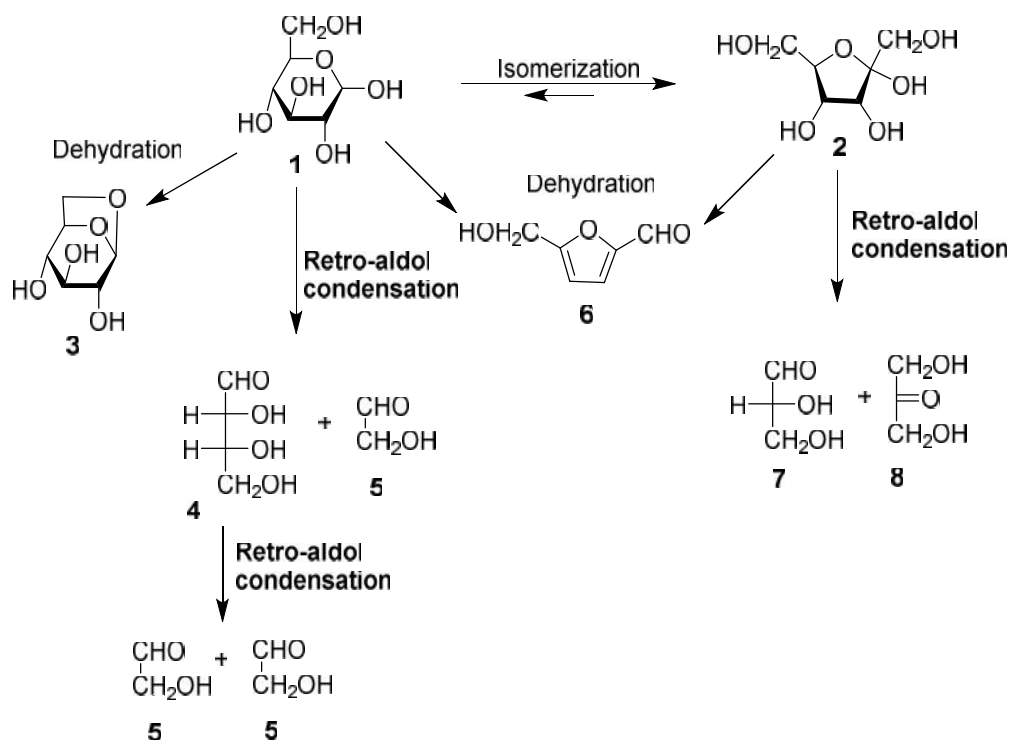
alcohols over a bifunctional Pt/Al₂O₃ catalyst at 463 K in around 30% yield of hexitols after 24 h and sorbitol was the dominating product. When promoted by SnO_x, as demonstrated by Liu et al.,²⁵ the product composition could be tuned by varying the Sn/Pt atomic ratios in the catalyst; sorbitol and mannitol were produced in 70% yield under the reaction.

3.3 Retro-aldol condensation of cellulose

According to the literature, conversion of cellulose into EG requires a multifunctional catalyst, and involves the hydrolysis of cellulose, C–C bond cleavage of cellulose-derived sugars, and hydrogenation of glycolaldehyde to EG.^{26, 27} The C-C bond cleavage of sugars or celooligosaccharides in supercritical water follows the retro-aldol condensation pathway.^{26, 27} In the presence of tungsten species but absence of a hydrogenation catalyst, glycolaldehyde was produced as a major product from cellulose in a yield of 5-7 wt % at 518 K, 6 MPa H₂, and 30 min. Although this yield is rather low due to the instability of glycolaldehyde, it is 4-6 times higher than that without the catalyst. Glycolaldehyde is the precursor to EG, and its presence as an intermediate strongly suggests that the H_xWO₃-catalyzed C-C cleavage of cellulose or sugars follows the retro-aldol pathway. Moreover, a comparative study using glucose and fructose as the feedstock showed that the former sugar produced primarily EG while the latter produced 1,2-PG under the catalysis of Ni-W₂C. The difference in the product results from the different positions of the C=O bond in the two sugar isomers, which follows well the rule of cleavage of C-C bonds via a retro-aldol reaction pathway.

CHAPTER 3

Retro-aldol condensation of glucose occurred preferentially relative to dehydration and isomerization under low water density conditions in supercritical water, and glycolaldehyde was successfully produced in a rapid and selective manner without any catalyst.²⁸ The proposed reaction pathways of glucose decomposition, glucose can primarily be converted to erythrose plus glycolaldehyde, to fructose, and to 1,6-anhydro- β -D-glucose (1,6-AHG) or 5-hydroxymethyl-2-furfural (5-HMF) via retro-aldol condensation, isomerization and dehydration, respectively (Scheme 3.3).²⁸



Scheme 3.3 Reaction pathways for the production of glycolaldehyde and dihydroxyacetone from glucose decomposition under low water density conditions in supercritical water: **1** glucose, **2** fructose, **3** 1,6-AHG, **4** erythrose, **5** glycolaldehyde, **6** 5-HMF, **7** glyceraldehyde, **8** dihydroxyacetone.

CHAPTER 3

3.4 Cellulose solubility

Pure cellulose is generally regarded as being insoluble in water and common organic solvents due to the existence of extensive intra- and inter-molecular hydrogen bonding.²⁹ Cellulose dissolves in water to the extent of 1.4 to 2.1 parts per 100,000 at room temperature.³⁰ Over the last decade, there has been increased interest in developing organic solvent systems for cellulose.³¹⁻³⁴ Such interest is not only academic but also has significant commercial potentials, one of which is the development of a new process for the manufacture of rayon.³⁵ However, due to increasing economic and environmental pressures, alternative processes for dissolving cellulose have been sought for developing new, efficient and green solvent system for biomass in general and for cellulose in particular.^{33, 34}

3.4.1 Non-aqueous cellulose solvent

Among the non-aqueous cellulose solvents, the LiCl/*N,N*-dimethylacetamide (DMAc), LiCl/*N*-methyl-2-pyrrolidinone (NMP), ammonium fluorides/dimethylsulfoxide (DMSO), and also *N*-methyl-morpholine-*N*-oxide (NMMO)³⁶ are some of the representative non-aqueous solvent systems suitable for the homogeneous reaction of cellulose.^{29, 35-38} Among these cellulose solvents, only NMMO are used along the industrial scale as a solvent for cellulose processing.³⁹ Moreover it also exhibits a low toxicity, biodegradable, and the recovery rate in large scale industrial process is achieved up to > 99%. It also was reported to dissolve 0.3 mass fraction of cellulose regarding to water content.³⁶ Nevertheless, NMMO also has some disadvantages, such as the occurrence of oxidative side reactions,

CHAPTER 3

thermal instability, or rather high temperatures required for the dissolution process. The characteristics of LiCl and DMAc or NMP solvent system are aprotic and the solution of cellulose in these solvent systems are very stable.^{35, 37, 38} These have been used to demonstrate the utility of this solvent system for synthesizing various cellulose derivatives. However, DMAc is prone to be saponified when heated in the presence of a strong base.³⁸ It was found that cellulose solutions of high concentrations, up to 16% cellulose, can be prepared by the dissolution of activated cellulose pulp in these solvent systems.³⁵ It was also observed that reconstituted, undegraded cellulose is recovered upon coagulation of these solutions in various nonsolvents. Furthermore, investigations of a large number of salt/aprotic solvents revealed that LiCl/DMAc and LiCl/NMP are unique solvent systems for cellulose.

Cellulose is also soluble in an aprotic and nontoxic solvent, 1,3-dimethyl-2-imidazolidinone (DMI) in the presence of LiCl.^{38, 40} DMI is now commercially available. The physical properties of 1,3-dimethyl-2-imidazolidinone (DMI) are similar to DMPU (1,3-dimethyl-2-oxo-hexahydropyrimidine), but the potential toxicological risk of DMI is less than DMPU. When used in the alkylation of terminal acetylenes, DMI is comparable with hexamethylphosphoric triamide (HMPA), thus it is a good alternative solvent to the carcinogen HMPA in the alkylation and it provides a safer working environment than DMPU and HMPA.

Ionic liquid as ecofriendly agents have the ability to dissolve cellulose in high concentration (up to 15 -20 %) due to their ionic structure. Ionic liquids are composed of an organic cation and an inorganic anion. It consists of pyridinium, imidazolium cations

CHAPTER 3

and OAc^- , HCOO^- , Cl^- anions which have the ability to dissolve cellulose.⁴¹ At high temperature, ion pairs in 1-allyl-3-methylimidazolium chloride (AMIMCl) can be dissociated to individual Cl^- and AMIM^+ ions, and then free Cl^- ions associated with the cellulose hydroxyl proton and the free cations disrupt the hydrogen bonding in cellulose, leading to its dissolution.^{41, 42} While these ionic liquids have been generally accepted as green solvents, some researchers have argued that with some evidence on being non-biodegradable, non-volatile, and potentially toxic.

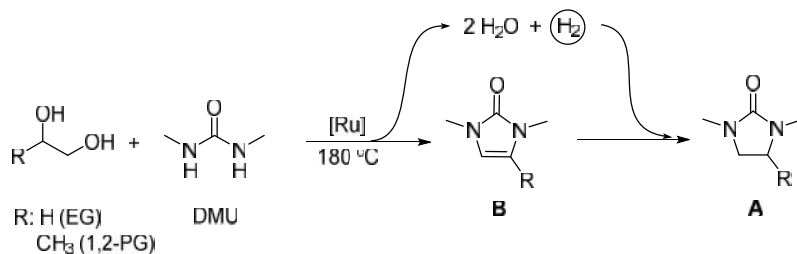
3.5 Synthesis of polar aprotic solvents (PAS)

3.5.1 Coupling of diols with dimethylurea

The synthesis of *N,N'*-dimethylimidazolidinone (**DMI**) and 1,3,4-trimethylimidazolidin-2-one (**TMI**) from small chain of polyols have been explored. The physical and chemical properties of **DMI** and **TMI** including high boiling point, remarkable chemical stability, and being more eco-friendly than DMF make them appealing for use in the pharmaceutical industry.^{38, 43} The coupling of diols, ethylene glycol (EG) and 1,2-propylene glycol (1,2-PG), with dimethylurea (DMU) was first described in 1992 to yield unsaturated 2-imidazolone compounds (**B**) using tris(triphenylphosphine)ruthenium(II) chloride $\text{RuCl}_2(\text{PPh}_3)_3$ as a homogeneous catalyst.⁴⁴ However, no further study or development of this reaction has been reported. This reaction was carried out in refluxing diglyme for 12 hours, giving a modest and good yield of 40% and 79% for EG and 1,2-PG, respectively. One appealing aspect of this reaction is that its only byproducts are hydrogen gas and water. Ideally, the hydrogen gas would be used to hydrogenate **B** to **A** (Scheme 3.4).

CHAPTER 3

Chemical stability and physical properties of **A** are suitable to serve as a PAS. We seek to further develop this reaction methodology as well as obtain the saturated product **A** directly as chemical stability and physical properties of **B** are not suitable to serve as a solvent. Of particular interest for our work is the direct conversion of cellulose to short chain polyols, especially ethylene glycol (EG) and 1,2-propylene glycol (1,2-PG)⁴⁵⁻⁴⁷, and then the coupling of these diols with dimethylurea (DMU) to yield **B** which upon hydrogenation creating **A** as a high boiling PAS.



Scheme 3.4 Synthesis of **A** and **B** from coupling of biomass derived diols with DMU through atom economically tandem reactions.

3.5.2 Coupling of furfural derivatives with amines

The formation of amide from alcohol and amine is well documented through the use of various ruthenium catalysts.⁴⁸⁻⁵² We chose to utilize a well studied Ru(PNN) complex, developed by the Milstein group (Figure 2). Through activation with base to form the dearomatized complex, an active acceptorless dehydrogenation catalyst is obtained. This catalyst first dehydrogenates the alcohol to form ketone, releasing hydrogen gas. The ketone reacts with amine to form a hemiaminal, which then undergoes catalytic dehydrogenation to make the amide and another equivalent of hydrogen.

CHAPTER 3

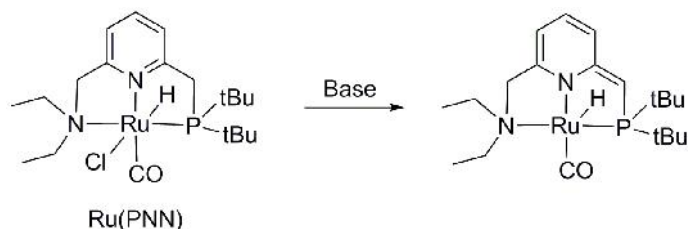


Figure 3.2 Ru(PNN) complex and dearomatization by base.

Taking advantage of this catalytic system, the coupling of furfural derivatives with secondary amines to give aprotic compounds (Figure 3.2). Using 0.1 mol% Ru(PNN) catalyst, activated with potassium hydroxide, THFA was successfully coupled with several secondary amines by refluxing in mesitylene (B.P.=165°C) with a five-fold excess of amine. Reactions with secondary amines usually require higher temperature and excess amount (especially for dimethylamine) for high yield, compared to primary amines. Using this approach, furfuryl alcohol can also be coupled with secondary amine in high yield, however; lower selectivity was achieved due to the higher reactivity of furfural leading to many byproducts.

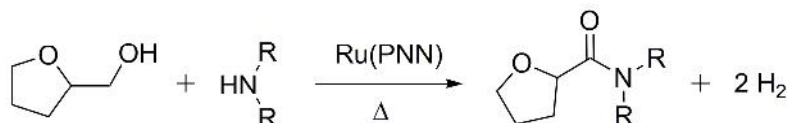


Figure 3.3 Dehydrogenative coupling of THFA with secondary amine to synthesize aprotic amides with Ru(PNN) catalyst.

3.6 Conclusions

Catalytic conversion of cellulose into polyols including ethylene glycol (EG) and 1,2-propylene glycol (1,2-PG), and furfural represents an important route for the effective utilization of cellulose. Of particular interest for this work is the catalytic conversion of

CHAPTER 3

cellulose to short chain polyols and the coupling of these polyols with N,N-dimethylurea (DMU) to produce cyclic PAS such as *N,N'*-dimethylimidazolidinone (DMI) and 1,3,4-trimethylimidazolidin-2-one (TMI). Chemical stability and physical properties of DMI and TMI are suitable to serve as a high boiling point PAS.^{38, 43} An appealing aspect of the reaction of diols with DMU is that the only byproducts will be hydrogen and water.

The coupling of furfural derivatives with secondary amines using Ru(PNN) catalyst can be investigated to yield aprotic amides in high yields. The only byproduct of this process is hydrogen.

3.7 References

1. Constable, D. J. C.; Jimenez-Gonzalez, C.; Henderson, R. K., Perspective on Solvent Use in the Pharmaceutical Industry. *Organic Process Research & Development* **2007**, *11* (1), 133-137. DOI: 10.1021/op060170h
2. Jiménez-González, C.; Curzons, A.; Constable, D. C.; Cunningham, V., Expanding GSK's Solvent Selection Guide—application of life cycle assessment to enhance solvent selections. *Clean Techn Environ Policy* **2004**, *7* (1), 42-50. DOI: 10.1007/s10098-004-0245-z
3. Dunn, P. J., The importance of Green Chemistry in Process Research and Development. *Chemical Society Reviews* **2012**, *41* (4), 1452-1461. DOI: 10.1039/c1cs15041c
4. Alfonsi, K.; Colberg, J.; Dunn, P. J.; Fevig, T.; Jennings, S.; Johnson, T. A.; Kleine, H. P.; Knight, C.; Nagy, M. A.; Perry, D. A.; Stefaniak, M., Green chemistry tools to influence a medicinal chemistry and research chemistry based organisation. *Green Chemistry* **2008**, *10* (1), 31-36. DOI: 10.1039/b711717e
5. Laird, T., Green Chemistry is Good Process Chemistry. *Organic Process Research & Development* **2012**, *16* (1), 1-2. DOI: 10.1021/op200366y
6. Kua, Y. L.; Gan, S. Y.; Morris, A.; Ng, H. K., Ethyl lactate as a potential green solvent to extract hydrophilic (polar) and lipophilic (non-polar) phytonutrients simultaneously from fruit and vegetable by-products. *Sustainable Chemistry and Pharmacy* **2016**, *4*, 21-31. DOI: 10.1016/j.scp.2016.07.003

CHAPTER 3

7. Paul, S.; Pradhan, K.; Das, A. R., Ethyl Lactate As a Green Solvent: A Promising Bio-compatible Media for Organic Synthesis. *Current Green Chemistry* **2016**, *3* (1), 111-118. DOI: 10.2174/2213346103666151203203139
8. Pace, V.; Hoyos, P.; Castoldi, L.; Dominguez de Maria, P.; Alcantara, A. R., 2 Methyltetrahydrofuran (2 MeTHF): a biomass derived solvent with broad application in organic chemistry. *ChemSusChem* **2012**, *5* (8), 1369-1379. DOI: 10.1002/cssc.201100780
9. Al-Shaal, M. G.; Dzierbinski, A.; Palkovits, R., Solvent-free γ -valerolactone hydrogenation to 2-methyltetrahydrofuran catalysed by Ru/C: a reaction network analysis. *Green Chemistry* **2014**, *16* (3), 1358-1364. DOI: 10.1039/c3gc41803k
10. Lopresto, C. G.; Petrillo, F.; Casazza, A. A.; Aliakbarian, B.; Perego, P.; Calabrò, V., A non-conventional method to extract D-limonene from waste lemon peels and comparison with traditional Soxhlet extraction. *Sep. Purif. Technol.* **2014**, *137*, 13-20. DOI: 10.1016/j.seppur.2014.09.015
11. Jalbert, J.; Duchesne, S.; Rodriguez-Celis, E.; Tétreault, P.; Collin, P., Robust and sensitive analysis of methanol and ethanol from cellulose degradation in mineral oils. *J. Chromatogr. A* **2012**, *1256*, 240-245. DOI: 10.1016/j.chroma.2012.07.069
12. Luo, C.; Wang, S.; Liu, H., Cellulose Conversion into Polyols Catalyzed by Reversibly Formed Acids and Supported Ruthenium Clusters in Hot Water. *Angew. Chem.* **2007**, *119* (40), 7780-7783. DOI: 10.1002/ange.200702661
13. Dunn, P. J., The importance of green chemistry in process research and development. *Chem. Soc. Rev.* **2012**, *41* (4), 1452-61. DOI: 10.1039/c1cs15041c
14. Corma, A.; Iborra, S.; Velty, A., Chemical Routes for the Transformation of Biomass into Chemicals. *Chemical Reviews* **2007**, *107* (6), 2411-2502. DOI: 10.1021/cr050989d
15. Parsell, T.; Yohe, S.; Degenstein, J.; Jarrell, T.; Klein, I.; Gencer, E.; Hewetson, B.; Hurt, M.; Kim, J. I.; Choudhari, H.; Saha, B.; Meilan, R.; Mosier, N.; Ribeiro, F.; Delgass, W. N.; Chapple, C.; Kenttamaa, H. I.; Agrawal, R.; Abu-Omar, M. M., A synergistic biorefinery based on catalytic conversion of lignin prior to cellulose starting from lignocellulosic biomass. *Green Chemistry* **2015**, *17* (3), 1492-1499. DOI: 10.1039/c4gc01911c
16. Luo, H.; Klein, I. M.; Jiang, Y.; Zhu, H. Y.; Liu, B. Y.; Kenttamaa, H. I.; Abu-Omar, M. M., Total Utilization of Miscanthus Biomass, Lignin and Carbohydrates, Using Earth Abundant Nickel Catalyst. *Acs Sustainable Chemistry & Engineering* **2016**, *4* (4), 2316-2322. DOI: 10.1021/acssuschemeng.5b01776
17. Chen, D. Y.; Gao, A. J.; Cen, K. H.; Zhang, J.; Cao, X. B.; Ma, Z. Q., Investigation of biomass torrefaction based on three major components: Hemicellulose, cellulose, and lignin. *Energy Convers. Manage.* **2018**, *169*, 228-237. DOI: 10.1016/j.enconman.2018.05.063
18. Liu, Y.; Luo, C.; Liu, H., Tungsten trioxide promoted selective conversion of cellulose into propylene glycol and ethylene glycol on a ruthenium catalyst. *Angew. Chem. Int. Ed. Engl.* **2012**, *51* (13), 3249-53. DOI: 10.1002/anie.201200351
19. Liu, X.; Wang, X.; Yao, S.; Jiang, Y.; Guan, J.; Mu, X., Recent advances in the production of polyols from lignocellulosic biomass and biomass-derived compounds. *RSC Adv.* **2014**, *4* (90), 49501-49520. DOI: 10.1039/c4ra06466f

20. Rinaldi, R.; Schuth, F., Acid Hydrolysis of Cellulose as the Entry Point into Biorefinery Schemes. *Chemsuschem* **2009**, *2* (12), 1096-1107. DOI: 10.1002/cssc.200900188
21. Geboers, J.; Van de Vyver, S.; Carpentier, K.; de Blochouse, K.; Jacobs, P.; Sels, B., Efficient catalytic conversion of concentrated cellulose feeds to hexitols with heteropoly acids and Ru on carbon. *Chem Commun (Camb)* **2010**, *46* (20), 3577-9. DOI: 10.1039/c001096k
22. Liang, G. F.; Wu, C. Y.; He, L. M.; Ming, J.; Cheng, H. Y.; Zhuo, L. H.; Zhao, F. Y., Selective conversion of concentrated microcrystalline cellulose to isosorbide over Ru/C catalyst. *Green Chemistry* **2011**, *13* (4), 839-842. DOI: 10.1039/c1gc15098g
23. Wang, X. C.; Meng, L. Q.; Wu, F.; Jiang, Y. J.; Wang, L.; Mu, X. D., Efficient conversion of microcrystalline cellulose to 1,2-alkanediols over supported Ni catalysts. *Green Chemistry* **2012**, *14* (3), 758-765. DOI: 10.1039/c2gc15946e
24. Fukuoka, A.; Dhepe, P. L., Catalytic conversion of cellulose into sugar alcohols. *Angew. Chem. Int. Ed. Engl.* **2006**, *45* (31), 5161-3. DOI: 10.1002/anie.200601921
25. Deng, T.; Liu, H., Promoting effect of SnOx selective conversion of cellulose to polyols over bimetallic Pt-SnOx/Al₂O₃ catalysts. *Green Chem.* **2013**, *15* (1), 116-124. DOI: 10.1039/c2gc36088h
26. Wang, S.; Chen, J.; Chen, L., Selective Conversion of Cellulose into Ethylene Glycol over Metal-Organic Framework-Derived Multifunctional Catalysts. *Catal. Lett.* **2014**, *144* (10), 1728-1734. DOI: 10.1007/s10562-014-1334-1
27. Wang, A.; Zhang, T., One-pot conversion of cellulose to ethylene glycol with multifunctional tungsten-based catalysts. *Acc. Chem. Res.* **2013**, *46* (7), 1377-86. DOI: 10.1021/ar3002156
28. Sasaki, M.; Goto, K.; Tajima, K.; Adschiri, T.; Arai, K., Rapid and selective retro-aldol condensation of glucose to glycolaldehyde in supercritical water. *Green Chemistry* **2002**, *4* (3), 285-287. DOI: 10.1039/b203968k
29. Chen, X.; Chen, J.; You, T.; Wang, K.; Xu, F., Effects of polymorphs on dissolution of cellulose in NaOH/urea aqueous solution. *Carbohydr. Polym.* **2015**, *125*, 85-91. DOI: 10.1016/j.carbpol.2015.02.054
30. Strachan, J., Solubility of Cellulose in Water. *Nature* **1938**, *141* (3564), 332-333. DOI: 10.1038/141332b0
31. Philipp, B., Organic-Solvents for Cellulose as a Biodegradable Polymer and Their Applicability for Cellulose Spinning and Derivatization. *J Macromol Sci Pure* **1993**, *A30* (9-10), 703-714. DOI: 10.1080/10601329308021256
32. Dawsey, T. R.; McCormick, C. L., The Lithium Chloride/Dimethylacetamide Solvent for Cellulose - a Literature-Review. *J Macromol Sci R M C* **1990**, *C30* (3-4), 405-440. DOI: 10.1080/07366579008050914
33. Heinze, T.; Koschella, A., Solvents applied in the field of cellulose chemistry: a mini review. *Polímeros* **2005**, *15* (2), 84-90. DOI: 10.1590/S0104-14282005000200005
34. Sathitsuksanoh, N.; George, A.; Zhang, Y. H. P., New lignocellulose pretreatments using cellulose solvents: a review. *J. Chem. Technol. Biotechnol.* **2013**, *88* (2), 169-180. DOI: 10.1002/jctb.3959

35. El Kafrawy, A., Investigation of the cellulose/LiCl/dimethylacetamide and cellulose/LiCl/N methyl 2 pyrrolidinone solutions by ^{13}C NMR spectroscopy. *J. Appl. Polym. Sci.* **1982**, 27 (7), 2435-2443. DOI: 10.1002/app.1982.070270714
36. Rosenau, T.; Potthast, A.; Sixta, H.; Kosma, P., The chemistry of side reactions and byproduct formation in the system NMMO/cellulose (Lyocell process). *Prog. Polym. Sci.* **2001**, 26 (9), 1763-1837. DOI: 10.1016/S0079-6700(01)00023-5
37. Takahashi, S.-I.; Fujimoto, T.; Miyamoto, T.; Inagaki, H., Relationship between distribution of substituents and water solubility of O-methyl cellulose. *J. Polym. Sci., Part A: Polym. Chem.* **1987**, 25 (4), 987-994. DOI: 10.1002/pola.1987.080250405
38. Takaragi, A.; Minoda, M.; Miyamoto, T.; Liu, H. Q.; Zhang, L. N., Reaction characteristics of cellulose in the LiCl/1, 3 dimethyl 2 imidazolidinone solvent system. *Cellulose* **1999**, 6 (2), 93-102. DOI: 10.1023/a:1009208417954
39. Nishino, T.; Matsuda, I.; Hirao, K., All-cellulose composite. *Macromolecules* **2004**, 37 (20), 7683-7687. DOI: 10.1021/ma049300h
40. Liu, H. Q.; Zhang, L. N.; Takaragi, A.; Miyamoto, T., Effect of substituent distribution on water solubility of O-methylcellulose. *Cellulose* **1997**, 4 (4), 321-327. DOI: 10.1023/A:1018404426960
41. Qi, H. S.; Chang, C. Y.; Zhang, L. N., Effects of temperature and molecular weight on dissolution of cellulose in NaOH/urea aqueous solution. *Cellulose* **2008**, 15 (6), 779-787. DOI: 10.1007/s10570-008-9230-8
42. Zhang, H.; Wu, J.; Zhang, J.; He, J. S., 1-Allyl-3-methylimidazolium chloride room temperature ionic liquid: A new and powerful nonderivatizing solvent for cellulose. *Macromolecules* **2005**, 38 (20), 8272-8277. DOI: 10.1021/ma0505676
43. Lo, C. C.; Chao, P. M., Replacement of carcinogenic solvent HMPA by DMI in insect sex pheromone synthesis. *J. Chem. Ecol.* **1990**, 16 (12), 3245-53. DOI: 10.1007/BF00982095
44. Kondo, T.; Kotachi, S.; Watanabe, Y., Ruthenium Complex-Catalyzed Synthesis of 1,3-Disubstituted 2,3-Dihydroimidazol-2-Ones from N,N'-Disubstituted Ureas and Vicinal Diols. *J Chem Soc Chem Comm* **1992**, 10.1039/c39920001318 (18), 1318-1319. DOI: 10.1039/c39920001318
45. Liu, X.; Wang, X.; Yao, S.; Jiang, Y.; Guan, J.; Mu, X., Recent advances in the production of polyols from lignocellulosic biomass and biomass-derived compounds. *RSC Advances* **2014**, 4 (90), 49501-49520. DOI: 10.1039/c4ra06466f
46. Liu, Y.; Luo, C.; Liu, H., Tungsten trioxide promoted selective conversion of cellulose into propylene glycol and ethylene glycol on a ruthenium catalyst. *Angew. Chem. Int. Ed.* **2012**, 51 (13), 3249-53. DOI: 10.1002/anie.201200351
47. Liu, X. R.; Wang, X. C.; Yao, S. X.; Jiang, Y. J.; Guan, J.; Mu, X. D., Recent advances in the production of polyols from lignocellulosic biomass and biomass-derived compounds. *Rsc Advances* **2014**, 4 (90), 49501-49520. DOI: 10.1039/c4ra06466f
48. Gnanaprakasam, B.; Milstein, D., Synthesis of Amides from Esters and Amines with Liberation of H₂ under Neutral Conditions. *Journal of the American Chemical Society* **2011**, 133 (6), 1682-1685. DOI: 10.1021/ja109944n
49. Chen, C.; Zhang, Y.; Hong, S. H., N-Heterocyclic Carbene Based Ruthenium-Catalyzed Direct Amide Synthesis from Alcohols and Secondary Amines: Involvement of

CHAPTER 3

Esters. *The Journal of Organic Chemistry* **2011**, 76 (24), 10005-10010. DOI: 10.1021/jo201756z

50. Muthaiah, S.; Ghosh, S. C.; Jee, J.-E.; Chen, C.; Zhang, J.; Hong, S. H., Direct Amide Synthesis from Either Alcohols or Aldehydes with Amines: Activity of Ru(II) Hydride and Ru(0) Complexes. *The Journal of Organic Chemistry* **2010**, 75 (9), 3002-3006. DOI: 10.1021/jo100254g

51. Gunanathan, C.; Ben-David, Y.; Milstein, D., Direct Synthesis of Amides from Alcohols and Amines with Liberation of H₂. *Science* **2007**, 317 (5839), 790-792. DOI: 10.1126/science.1145295

52. Srimani, D.; Balaraman, E.; Hu, P.; Ben-David, Y.; Milstein, D., Formation of Tertiary Amides and Dihydrogen by Dehydrogenative Coupling of Primary Alcohols with Secondary Amines Catalyzed by Ruthenium Bipyridine-Based Pincer Complexes. *Advanced Synthesis & Catalysis* **2013**, 355 (13), 2525-2530. DOI: 10.1002/adsc.201300620

CHAPTER 4. ONE-POT TWO-STEP CATALYTIC REACTION OF CELLULOSE
AND *N,N*-DIMETHYLUREA OVER RU/C

4.1 Introduction

Recently, significant effort has been directed to the development of green and sustainable procedures for the chemical conversion of non-edible biomass to high value-added compounds.¹⁻⁶ Environmentally benign solvents constitute an interesting target for bio-based products.^{7, 8} Examples of solvents from renewable sources include 2-methyltetrahydrofuran (2-MeTHF),^{9, 10} limonene,¹¹ ethanol,¹² and glycerol.¹³ Although certain polar aprotic solvents (PAS) such as dimethylformamide (DMF) and dimethylacetamide (DMAc) are widely used in nucleophilic substitution reactions (nearly 50% of the PAS usage)^{7, 14, 15} and in the pharmaceutical industry,⁷ these solvents do not have good replacements from renewable sources (Figure 4.1). While these are good solvents for a number of reactions, and sometimes the only ones which dissolve polar materials and salts, they face growing scrutiny and regulations as more concerns over their environmental impact and toxicity emerge.^{8, 16} Newer PAS represented by cyclic urea *N,N'*-dimethylimidazolidinone (DMI) and *N,N'*-dimethylpropyleneurea (DMPU) have been used in place of DMF and DMAc with preliminary data indicating that they are safer for the endocrine system (Figure 4.1).¹⁷ Considering the lack of PAS made from biomass, we sought to identify and develop environmentally friendly methods to produce sustainable PAS from renewable and non-edible bio-based resources.

CHAPTER 4

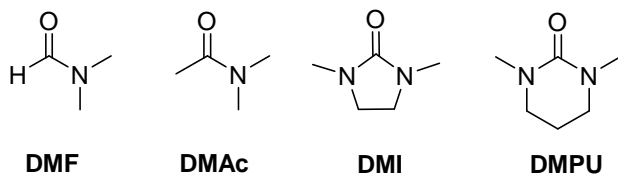
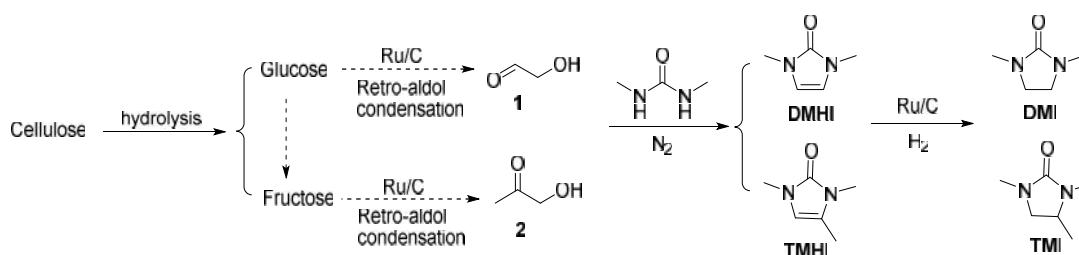


Figure 4.1. Industrially Important Polar Aprotic Solvents (PAS). DMF and DMAc have reprotoxicity issues and are strongly regulated particularly in European Union.¹⁶ DMI and DMPU are considered more eco-friendly substitutes of DMF and DMAc.

Cellulose is one of the world's largest renewable, non-edible resources available with production of nearly 40 billion ton residues per year.¹⁸ It is being considered as a promising alternative to petroleum and a sustainable resource to produce fuels and chemicals.^{18,19} Catalytic conversion of cellulose into polyols including sorbitol, glycerol, ethylene glycol (EG) and 1,2-propylene glycol (1,2-PG) represents an important route for the effective utilization of cellulose.^{4, 5, 13, 18, 19} Of particular interest for this work is the catalytic conversion of cellulose to short chain polyols and the coupling of these polyols with *N,N*-dimethylurea (DMU) to produce cyclic PAS such as *N,N'*-dimethylimidazolidinone (DMI) and 1,3,4-trimethylimidazolidin-2-one (TMI) (Scheme 4.1). Chemical stability and physical properties of DMI and TMI are suitable to serve as a high boiling point PAS.^{8, 20} For cellulose conversion to EG, there are three consecutive reactions: (1) hydrolysis of cellulose to glucose; (2) retro-aldol condensation of glucose to glycolaldehyde **1**; and (3) hydrogenation of glycolaldehyde to EG.²¹⁻²⁶ Cellulose hydrolysis into fructose or isomerization of glucose into fructose undergoes C-C bond cleavage via the retro-aldol reaction to form hydroxyacetone **2** over heterogenous Ru/C catalyst as shown in Scheme 4.1.^{18, 22, 26} Water was recognized as the best solvent for cellulose conversion to short chain polyols. On the other hand, coupling of hydroxy ketones with urea has been investigated.²⁷⁻²⁹ The synthesis of imidazolidinone derivatives from urea was

CHAPTER 4

achieved in high boiling organic solvents²⁸ or under microwave irradiation.²⁷ The coupling of diols, EG and 1,2-PG with DMU was first described in 1992 using tris(triphenylphosphine)ruthenium(II) chloride as catalyst;³⁰ however, no further study or development of this reaction has been reported. These reactions were conducted in refluxing diglyme for 12 hours, giving a modest to good yield of EG and 1,2-PG, 40% and 79%, respectively. Coupling of these diols with DMU to produce PAS proceeds through the catalytic oxidation of hydroxyl group to ketone and the subsequent condensation of ketone with DMU as previously reported by Watanabe.³⁰ Scheme 4.1 shows the reaction pathway for the production of PAS from cellulose, conversion to acyloins and subsequent condensation with DMU. Hydrogen gas can be used in the final step to hydrogenate unsaturated PAS (Scheme 4.1).



Scheme 4.1 Catalytic conversion of cellulose into polar aprotic solvent (PAS) via tandem catalysis.

The traditional approach of biomass valorization via platform molecules requires additional steps for the separation, purification, and drying of intermediates resulting in lower yield of the final products with a large amount of waste. A one-pot reaction is more promising for large-scale cellulose conversion to PAS. In this process, hydrolysis of cellulose, C-C bond cleavage of the sugars, coupling of hydroxy ketones **1** and **2** with DMU, and hydrogenation of the unsaturated products 1,3-dimethyl-1,3-dihydro-2H-

CHAPTER 4

imidazol-2-one (DMHI) and 1,3,4-trimethyl-1,3-dihydro-2H-imidazol-2-one (TMHI) occur in sequence to reach the maximum selectivity of the target products DMI and TMI (Scheme 4.1). The success of these tandem catalytic reactions in one-pot requires a multifunctional catalyst and a good solvent system. Ruthenium supported on activated carbon (Ru/C) is known for its high efficiency of cellulose conversion to EG and 1,2-PG²² as well as its excellent reusability.²⁴ Solvent selection is challenging in this tandem reaction because of low cellulose conversion into hydroxy ketones **1** and **2** in organic solvents, whereas the highest yield for the reaction of hydroxy ketones with DMU are obtained in organic solvents.^{27, 28} An elevated temperature 200 °C and as a result a higher pressure are required for cellulose and sugar conversion to PAS. To the best of our knowledge, there have been no attempts so far to produce PAS from renewable resources. Herein, one-pot reactions of cellulose with DMU have been investigated in various solvents over Ru/C. The reaction proceeds efficiently in one-pot, two-step process. Reactions under N₂ atmosphere result in unsaturated intermediates glycolaldehyde **1** and hydroxyacetone **2** which upon coupling with DMU generate DMHI and TMHI. PAS is produced by hydrogenation of DMHI and TMHI in a second step in the same pot without a need for separation and purification of the intermediates. The overall 85% selectivity for PAS was achieved for cellulose and sugar conversion. A mechanism that agrees with all experimental observations is also presented.

CHAPTER 4

4.2 Experimental section

4.2.1 Material

1,2-Propylene glycol and D-(-)-Fructose were purchased from Acros-Organics. D-(+)-Glucose was purchased from Alfa-Aesar. Ruthenium (5wt%) supported on activated carbon (Ru/C), sigmacell cellulose, and all other chemicals were purchased from Sigma Aldrich. Naphthalene, benzyl alcohol, and cis-1,5-cyclooctane diol from Sigma-Aldrich was used as an internal standard for $^1\text{H-NMR}$, and HPLC/UV, and HPLC/RID respectively. All chemicals were used as received without further purification.

4.2.2 General procedure

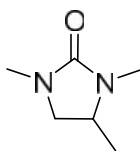
A 75 mL stainless steel autoclave reactor from Parr Instruments is being charged with the substrates, Ru/C, and a glass magnetic stir bar. Prior to the reaction, the autoclaves were flushed three times with nitrogen before applying 35 bars of nitrogen pressure and heating to 200 °C. After termination of the reaction periods, the autoclaves were cooled down, released the nitrogen pressure, and charged with 35 bars of hydrogen gas conducting the hydrogenation step at 200 °C. The reaction conditions are described under the table footnote. Following the one-pot catalytic conversion, the reaction mixture is fractioned into two forms, PAS derivatives that are analyzed by High-Performance Liquid Chromatography equipped with a UV detector (HPLC/UV) and the polyol molecules analyzed by HPLC- Reflective Index Detector (HPLC/RID). Details on characterization methods are provided in the Supporting Information. Cellulose conversion was determined

CHAPTER 4

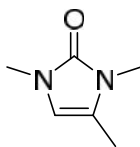
by the weight difference of cellulose before and after the reaction; product selectivities were calculated on the DMU basis for one-pot, two-step experiments.

In homogeneous catalytic reactions, catalyst $\text{RuCl}_3 \cdot 3\text{H}_2\text{O}$ and the respective phosphine ligands were added to the reaction vessel along with DMU, 1,2-PG, and 2-MeTHF solvent. After briefly sparging with inert N_2 gas, the reaction vessel was sealed and heated at 180 °C. Microwave reactions were performed using a CEM Discover SP System and a standard heating method with a set point of 180 °C (reaction temperature determined by a vertically focused IR temperature sensor).

4.2.3 Product Characterization for Compounds TMI and TMHI



1,3,4-trimethylimidazolidin-2-one (TMI); colorless liquid, $^1\text{H-NMR}$ (400 MHz, CDCl_3) 3.40 (d, 2H, $J=8$ Hz), 2.76 (m, 1H), 2.74 (s, 3H), 2.71 (s, 3H), 1.20 (d, 3H, $J=8$ Hz); $^{13}\text{C-NMR}$ (100 MHz, CDCl_3) 161.3, 52.6, 50.9, 30.9, 28.5, 17.8; MS (EI) m/z (rel. intensity): 128 (M^+ , 39), 113 (100), 98 (5), 85 (20), 72 (22), 58 (29), 42 (40)



1,3,4-trimethyl-2,3-dihydroimidazol-2-one (TMHI); Pale yellow solid, $^1\text{H-NMR}$ (400 MHz, CDCl_3) 5.9(q, 1H, $J=1.3$ Hz), 3.18 (s, 3H), 3.16 (s, 3H), 2.00 (d, 3H, $J=1.3$ Hz); $^{13}\text{C-NMR}$ (100 MHz, CDCl_3) 153.6, 118.4, 106.9, 29.9, 27.1, 10.1; MS (EI) m/z (rel. intensity): 126 (M^+ , 100), 125 (26), 111 (16), 97 (18), 70 (6), 56 (92), 42 (40)

CHAPTER 4

4.2.4 Instrumentation and Analysis

4.2.5 HPLC analysis

The selectivity and the yield of the target molecules in DMI, ethanol, Methanol, and water and the remaining amount of DMU were analyzed with Agilent 1260 Infinity Quaternary High-Performance Liquid Chromatography (HPLC) system, using Zorbax Eclipse XDB-C18 Column (250 x74.6mm) set at 25 °C. The chromatography apparatus is equipped with G1315D Diode Array Detector (DAD). All analysis was done at the wavenumber of 210 nm. A mixture of H₂O (A) and acetonitrile (B) were used as the mobile phase at a flow rate of 0.5 mL/min. Nonlinear gradient was used (95% A and 5% B from beginning to 80% A and 20 % B at 30.0 minute and then back to the starting point over 10 minutes). A fixed amount (500µL) of internal standard benzyl alcohol (5.0 mM) was added into each sample for the quantification purposes. Standard curves for all the target products were made by comparison of the products to internal standard. All results were analyzed and quantified according to standard curves. Before analyzing by HPLC, the liquid samples were filtered through a 0.22µm cutoff syringe filter (2 5mm diameter).

All sugar and cellulose samples as well as the polyol products from their C-C bond cleavage were analyzed with Agilent 1260 Infinity Quaternary High-Performance Liquid Chromatography (HPLC) system, using Aminex HPX-87H column (300 x 7.8 mm) set at 70 °C. The chromatography apparatus is equipped with G1362A Refractive Index Detector (RID) calibrated with external standards. A 0.005 M sulfuric acid solution was employed as the mobile phase with flow of 0.6 mL/min. A fixed amount (500µL) of internal standard cis-1,5-cyclooctane diol (10 mM) was added into each sample for quantification purposes.

CHAPTER 4

Before analyzing by HPLC, the aqueous solutions were filtered through a 0.22 μ m cutoff syringe filter (25 mm diameter).

$$\text{Cellulose conversion} = [m(i) - m(\text{dried, after rxn}) - m(\text{Ru/C})] * 100 / m(i)$$

$m(i)$ = Initial mass of cellulose before the reaction

$m(\text{dried, after rxn})$ = mass of dried cellulose at 60 °C overnight after the reaction

$m(\text{Ru/C})$ = Initial mass of Ru/C before the reaction

$$\text{Polyol selectivity} = \# \text{ moles of C in each compound} * 100 / \# \text{ moles of C converted}$$

$$\text{PAS selectivity \%} = \# \text{ moles of C in each compound} * 100 / \# \text{ moles of DMU converted}$$

4.2.6 NMR Analysis

NMR analysis was performed on either a Varian Mercury-300 instrument equipped with a 5mm 4-nucleus/BB probe or a Bruker DRX-500 instrument equipped with a 5mm TXI Z-gradient cryoprobe.

NMR yields were determined by integration of the produce versus a known quantity of internal standard (naphthalene). The amount of product was calculated by the following equation:

$$\text{Mol}_{\text{prod}} = \text{mol}_{\text{std}} * (\text{Integral}_{\text{pro}} / \text{Integral}_{\text{std}}) * (N_{\text{std}} / N_{\text{prod}})$$

CHAPTER 4

Where N is the number of nuclei for the corresponding signal. The yield is then determined by the following formula:

$$\text{Yield}_{\text{prod}} (\%) = (\text{mol}_{\text{prod}} / \text{mol}_{\text{l.r.}}) * 100$$

Where $\text{mol}_{\text{l.r.}}$ is the moles of limiting reactant in the reaction. The selectivity is then defined as:

$$\text{Selectivity} (\%) = (\text{mol}_{\text{prod}} / \text{mol}_{\text{i(reactant)}} - \text{mol}_{\text{f(reactant)}}) * 100$$

4.3 Results

4.3.1 PAS from cellulose

A one-pot, two-step catalytic conversion of cellulose in the presence of DMU to PAS has been studied in various solvents at elevated temperature. Water is known to be an efficient medium for cellulose and sugar conversion to produce polyols using Ru/C catalyst under H_2 atmosphere.^{4, 13, 18, 22} In our initial investigations, the reactions were performed in water under H_2 atmosphere resulting in little or no yield of PAS. Ironically, switching the gasses from H_2 to N_2 showed remarkably higher selectivity towards formation of unsaturated PAS, 1,3-dimethyl-1,3-dihydro-2H-imidazol-2-one (DMHI) and 1,3,4-trimethyl-1,3-dihydro-2H-imidazol-2-one (TMHI), leading us to design this process as a one-pot, two-step cellulose conversion to PAS. The reaction was conducted under N_2 (35 bar) gas for 6 hours at 200 °C generating unsaturated PAS. After cooling down to room temperature and

CHAPTER 4

purging the N₂ gas, the reaction vessel was pressurized with H₂ gas to hydrogenate the unsaturated products in the same vessel in a second step.

Figure 4.2A provides an experimental schematic of the isolation and characterization of the products. Following the one-pot catalytic conversion and filtration of solid residues, the bio-oil-PAS mixture is fractionated into two forms for characterization and quantification of PAS and polyol derivatives. The PAS products are separated using High-Performance Liquid Chromatography (C18 preparative column), extracted with chloroform, and analyzed by various techniques as shown in Figure 4.2A. Product distribution of the reaction of diols with DMU were quantified by HPLC equipped with UV detector (HPLC/UV) at 210 nm. The HPLC chromatogram and the retention time associated with saturated and unsaturated PAS products are shown in Figure 4.2C. The polyol molecules including sorbitol, glycerol, 1,2-PG, and EG are analyzed by HPLC- Refractive Index Detector (HPLC/RID) at 70 °C.

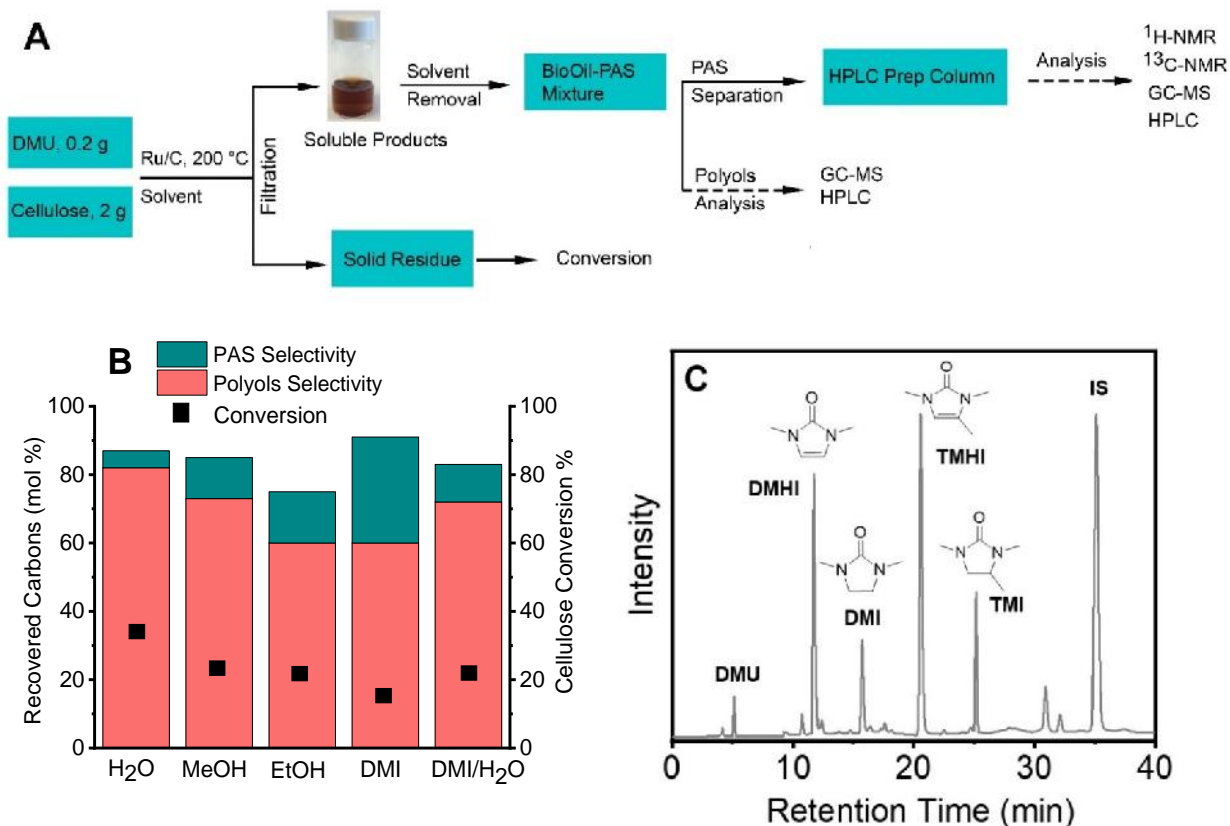


Figure 4.2. Cellulose conversion to PAS and polyols, the experimental schematic and mass balance. (A) Diagram showing the overall experimental procedure and analysis. (B) Cellulose conversions (■) in various solvents and mass balance accompanying the diagram shown in Figure 4.2A. Condition: Sigmacell cellulose (2.0 g), DMU (0.2 g, 2.23 mmol), Ru/C (0.2 g) with the corresponding solvent (20 mL) were heated in a 75 mL stainless steel autoclave at 200 °C in two steps: first, under N₂ inert atmosphere (35 bar) for 6 hours, then H₂ (30 bar) for 6 hours. DMI/H₂O (1:1 ratio) was used as solvent. (C) Exemplary HPLC chromatogram and retention time of the PAS product distributions, the reaction of hydroxy ketones from cellulose conversion with DMU at 200 °C.

Cellulose conversions were determined by the change of cellulose weight before the reaction and after the solid residue (Figure 4.2A) is dried at 60 °C overnight (See Supporting Information II for more details on calculation). Compositional analysis of the solid residue revealed that cellulose hydrolysis and its conversion to polyols and PAS compounds were less than 40%, in various solvents (Figure 4.2B). In our optimized procedure, large excess amount of cellulose (2.0 g) relative to DMU (0.2 g) is required to

CHAPTER 4

compensate the low cellulose conversion. The role of the catalyst loading in cellulose depolymerization has been investigated in water, methanol, and DMI where the stainless-steel autoclave reactor was loaded with high (0.4 g) or low (0.1 g) amount of Ru/C with 5 wt% Ru content. Higher cellulose conversions were achieved at high catalyst loading without significant improvement on the yield of PAS derivatives (Table 4.1). However, as catalyst loading was decreased, cellulose conversions, the remaining polyols, and PAS yields declined significantly indicating that the catalyst is necessary and responsible for cellulose cleavage. The effect of the reaction temperature was studied in water at 240, 180, and 150 °C. A slightly better yield of PAS was obtained at 200 °C relative to 180 °C, whereas it was significantly lower at 150 °C (less than 8%). The reactions at higher temperature 240 °C did not improve the yield of PAS.

Table 4.1 The effect of catalyst loading on the cellulose conversion and PAS selectivities.^a

Mass (g)	% Cellulose conversion (% PAS selectivity)		
	H ₂ O	MeOH	DMI
0.4	46 (7)	37 (15)	23 (35)
0.2	32 (5)	21 (12)	13 (31)
0.1	19 (1)	14 (5)	8 (11)

^aSigmacell cellulose (2.0 g), DMU (0.2 g, 2.23 mmol), Ru/C (0.4, 0.2, 0.1 g), and solvent (20 ml) were heated in a 75 ml stainless steel autoclave at 200 °C in two steps: first, under N₂ inert atmosphere (35 bar) for 6 hours, then H₂ (30 bar) for 6 hours. Ru/C has 5 wt% Ru content.

As seen in Figure 4.2B under optimized conditions (0.2 g of Ru/C (5 wt%) at 200 °C), cellulose conversion steadily decreases from 32% in water as a protic solvent to 13% in DMI as an aprotic polar solvent. However, the amount of PAS generated from the reaction of small molecules with DMU is the lowest in water (5%) relative to protic or aprotic organic solvents, such as methanol (12 %), ethanol (15%) and DMI (31%). DMI is a viable

CHAPTER 4

solvent to improve PAS selectivity. The mass balance shows that above 80% moles of carbons from cellulose conversion was recovered in various forms of PAS and polyol products (Figure 4.2B). On molar basis, only two carbons in DMI and three carbons in TMI are accounted from cellulose. The missing mass, 9% in DMI up to 16% in DMI/water is presumably mostly volatile hydrocarbons, which were not analyzed in this study.

Product distribution of PAS derivatives and polyols selectivity are shown in Figure 4.3A-B. The remaining DMU was measured by HPLC/UV at 210 nm to calculate DMU conversion and the selectivity for PAS derivatives (Figure 4.3A). At 200 °C, most of DMU (~ 60%) is converted in two steps with DMI and TMI as the major products. They are likely due to the hydrogenation of unsaturated compounds DMHI and TMHI. Formation of DMHI and TMHI was verified by ¹HNMR and HPLC analysis from the reaction in ethanol under N₂ at 200 °C. Overall, PAS selectivity is higher in the aprotic polar solvent DMI, than the protic solvents MeOH and EtOH, with the lowest amount in water. The missing mass of DMU is partly associated with a product, 1,3,4,5-tetramethylimidazolidin-2-one from the reaction of 2,3-butandiol with DMU (Figure 4.2C, retention time = 32 min); however, this byproduct was not quantified.

Sorbitol (~ 20 %) is the major component of the polyol fraction along with ethylene glycol, 1,2-propylene glycol, and glycerol as shown in Figure 4.3B. Cellulose depolymerization to glucose and fructose, their subsequent hydrogenation in the second step under H₂ account for the production of sorbitol.^{18, 19} EG and 1,2-PG is produced by hydrogenation of intermediates 1 and 2, respectively. Analysis on the remaining amount of EG (1.3 mmoles) and 1,2-PG (1.1 mmoles) after the second step in DMI revealed that significant amount of

CHAPTER 4

1 and 2 are converted to the corresponding PAS products, 0.91 mmoles of DMI and 1.63 mmoles of TMI. Therefore, improving the cellulose conversion to 1 and 2 would result in higher PAS yields.

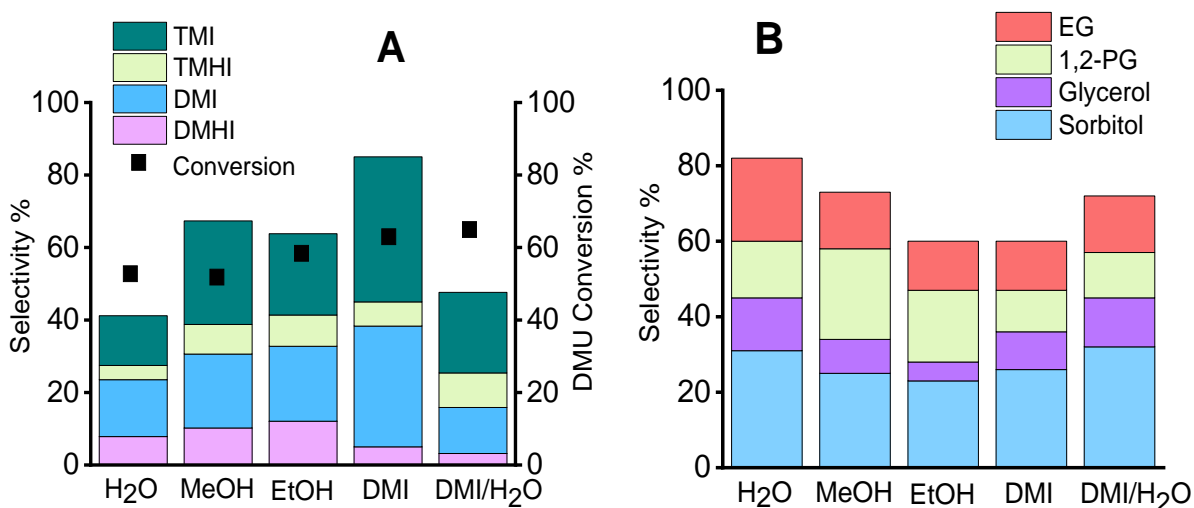


Figure 4.3. Analysis of PAS and polyol fractions from the catalytic conversion of cellulose in various solvents. A) PAS fraction composition analyzed by HPLC-UV detection at 210 nm with benzyl alcohol solution (5.0 mM) as an internal standard. B) Polyol fraction composition. Reaction conditions are identical to Figure 4.2B.

When various tungsten species such as tungsten trioxide (WO_3) or ammonium metatungstate (AMT) was used with Ru/C, higher cellulose conversion was achieved: $\text{WO}_3 + \text{Ru/C}$ (65%), AMT + Ru/C (72%) in DMI. However, according to HPLC/UV analyses, PAS products were small. The unsaturated PAS intermediates DMHI and TMHI probably underwent C-C bond cleavage in the presence of acidic tungsten species. Tungsten bronze (H_xWO_3) is the active species in catalytic tungsten-based systems which is known to promote cleavage of C-C bonds.^{21, 22, 25} Acid catalyzes cellulose conversion as well as coupling of hydroxy ketones with DMU.²⁸ Addition of sulfuric acid in water (5mM solution) enhanced cellulose conversion to polyols in the presence of Ru/C; mainly

CHAPTER 4

ethylene glycol (33%) and sorbitol (45%) were obtained. However, it did not improve PAS yields, which is likely due to protonation of unsaturated intermediates 1 and 2 in acid. PAS yield strongly depends on cellulose depolymerization as well as the reaction medium. The reaction of glucose or fructose was investigated in various solvents to further understand the relationship between these intermediates with the production of PAS and elucidate the pertinent mechanism (Scheme 4.1).

4.3.2 Conversion of glucans directly to PAS

Sugar conversion was also studied in an autoclave under the optimized conditions in one pot, two steps process using Ru/C at 200 °C. After the second step under H₂ atmosphere, 100% of the sugar was converted to polyols and PAS products in both protic and aprotic solvents. The absence of glucose or fructose was confirmed by HPLC- reflective index detector (HPLC-RID) where excess amounts of polyols EG and 1,2-PG were detected (Figure 4.4). The polyol product distribution is consistent with previous results reported for sugar conversion.^{4, 22}

The amount of DMU left in the reaction mixture was measured by HPLC-UV detection at 210 nm. The majority of DMU (between 70-80 %) was converted to PAS (Figure 4.4A), which is higher than that of observed for cellulose (~ 55-60 %, *vide supra*). The overall PAS selectivity followed a similar trend as that observed for cellulose where it is the lowest in water (approximately 40%) and highest in DMI (~ 80%). DMI is a good solvent choice because it affords high PAS selectivity and it is the product. One of the interesting observations is that the higher selectivity of TMI achieved from fructose whereas a better selectivity of DMI was obtained from glucose conversion in both protic and aprotic

CHAPTER 4

solvents similar to what is predicted by retro-aldol condensation (Scheme 4.1). TMI was obtained in 61 % from fructose vs. 26% from glucose in DMI (Figure 4.4A). Reactions in water, methanol, and ethanol also verified this observation. Analysis of the polyol fractions revealed a higher selectivity of EG from glucose as well as a higher selectivity of 1,2-PG from fructose in both protic and aprotic solvents (Figure 4.4B). Catalytic conversion of fructose to 1,2-PG (32%) is significantly higher than EG (11%) over Ru/C catalyst in DMI. Glycolaldehyde 1 is likely the main intermediate of the glucose conversion to generate DMHI and the corresponding hydrogenated compound DMI (Scheme 4.1). 2 is the main intermediate of the fructose conversion leading to the production of TMHI and TMI. Reactions performed in one-step under hydrogen gas atmosphere suppressed PAS production, which is indicative of hydrogenation of hydroxy ketones 1 and 2, and as a result EG and 1,2-PG do not react with DMU.

In molar mass balance calculation, 80- 88% moles of carbon from sugar conversion was recovered PAS and polyol products (Figure 4.4B). Two carbons in DMI and three carbons in TMI were accounted for (originated) from the sugar molecule. The missing mass was due to 1,3,4,5-tetramethylimidazolidin-2-one and volatile hydrocarbons byproducts; however, these were not large enough to justify extensive effort to quantify in this study.

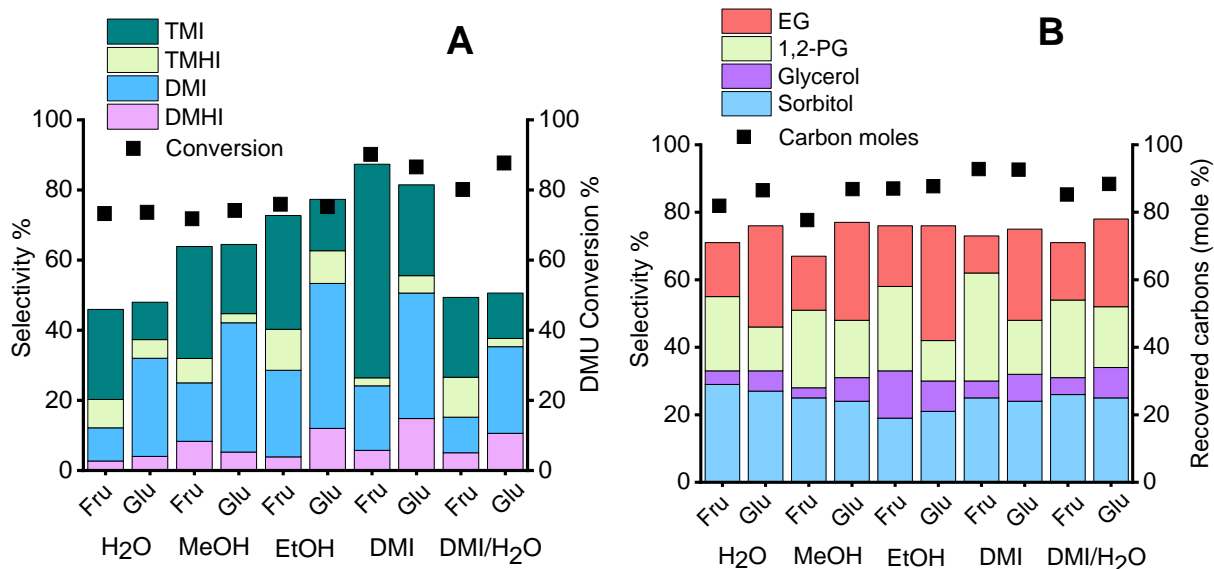


Figure 4.4. Analysis of PAS and polyol products obtained from the catalytic conversion of fructose (Fru) and glucose (Glu) in various solvents. A) PAS products in various solvents. Selectivity was calculated based on the DMU conversion using HPLC/UV at 210 nm with benzyl alcohol solution (5.0 mM) as an internal standard. B) Polyol selectivity and the molar mass balance of carbons from sugar conversion. Sugar conversion is 100% in all solvents. Conditions: sugars (1.0 g), DMU (0.2 g, 2.23 mmol), Ru/C (0.1 g) in various solvents (20 ml) were heated in a 75 ml stainless steel autoclave at 200 °C in two steps: first, under N₂ inert atmosphere (35 bar) for 6 hours, then H₂ (30 bar) for 6 hours. Ru/C catalyst contains 5 wt% Ru on activated carbon. DMI/H₂O (1:1 ratio) was used as a solvent.

Because of the different positions of the C=O group in glucose and fructose, glucose was primarily converted to glycolaldehyde 1 to form ethylene glycol while fructose produced primarily hydroxyacetone 2 under N₂ and ultimately hydrogenated to 1,2-PG under H₂ atmosphere.^{22, 23, 31-33} Due to the lack of stability of 1 and 2 at room temperature and the better overall yield of PAS from fructose, the coupling of 1,2-PG instead of hydroxyacetone with DMU was investigated.

4.3.3 Coupling of 1,2-PG with DMU and solvent effects

In a parallel study to further understand the catalytic conversion of polyols to PAS, reactions between 1,2-PG and DMU were performed under either N₂ or H₂ atmosphere at 200 °C. Coupling of 1,2-PG and DMU produces TMHI in high yield (> 80%) in organic solvents such as toluene, 2-MeTHF, and DMI under N₂ in one step (Table 4.1b), whereas lower yields were obtained in protic solvents such as MeOH (59%), Ethanol (65%), with the lowest in water (37%). These results are comparable to those previously obtained in two-phase reactions for cellulose and sugar conversion. Coupling of 1,2-PG and DMU gave low yields (< 14%) under H₂ atmosphere (Table 4.1c). Two hypotheses are put forward to rationalize this observation: either the catalyst is fully hydrogenated resulting in the loss of catalytic activity or hydrogenation of hydroxyacetone 2, the anticipated intermediate, shifts the reaction towards reactants.

Performing these reactions in one pot two-steps under identical conditions to reactions performed with cellulose and sugars verified formation of TMI (Table 4.1d). The results from various solvents were consistent with what were achieved from the cellulose and sugar conversions to PAS. Higher yields (> 81%) were obtained in organic solvents using toluene (86%), 2-MeTHF (81%), and DMI (85%) (Table 4.1d, entries 1-4). These yields are comparable to those previously reported using diglyme as a solvent.³⁰ Comparing the results from the reactions under N₂ atmosphere (Table 4.1b) and the two-step reaction (Table 4.1d), it is conceivable that hydrogenation of unsaturated PAS occurs in the second step under H₂ atmosphere. There are two main advantages of using DMI as a solvent in this reaction; first: the reaction can be conducted at atmospheric pressure because of the

CHAPTER 4

high boiling point of DMI (Table 4.2, entry 4); second, the product of the reaction can serve as a solvent dissolving the reactants as the reaction proceeds. TMI was obtained in high yield (78%) using minimal amount of DMI (5 mL) as a solvent under identical conditions to entry 4, Table 4.2. The reaction yield is lower in protic solvents MeOH (63 %), EtOH (70%), and water (47%). In previous scanning tunneling microscope (STM) studies, adsorption of water on Ru surfaces results in various surface species such as molecular H₂O, H₂O-C complexes, H, O, OH species where the related reaction can occur on Ru surface. It is likely that intermediate 2 is reduced to 1,2-PG in water or protic solvents preventing the coupling of 2 with DMU and hence PAS production.^{27, 34, 35}

Table 4.2 Coupling of 1,2-PG and DMU.^a

Entry	Solvent	^b TMHI	^c TMI %	^d TMI %
1	Toluene	88	14	86
2	2-MeTHF	86	11	81
3	DMI	84	12	85
4 ^e	DMI	83	15	83
5	MeOH	59	4	62
6	EtOH	65	5	70
7	water	37	2	48

^a1,2-PG (1.7 g, 22.8 mmol), DMU (0.5 g, 5.7 mmol), 0.2 g Ru/C (5 wt%), and 20 mL solvent were heated in a 75 mL stainless steel autoclave at 200 °C. ^bOne step reactions under N₂ (35 bar) for 12 hours. ^cReactions under H₂ (30 bar) for 12 hours. ^dTwo step reactions: first, under N₂ inert atmosphere (35 bar) for 6 hours, then H₂ (30 bar) for various times. Yields were analyzed by HPLC/UV with benzyl alcohol solution (5.0 mM) as an internal standard. TMHI Yields were also confirmed by ¹H-NMR with naphthalene as an internal standard (entries 1-4). ^eDMI under N₂ inert gas at 1 bar.

The product distribution was altered by varying the ratio of the starting materials under N₂ atmosphere (Table 4.3). Evidently, an increase of the 1,2-PG ratio leads to higher yields of TMHI, while the excess amount of DMU does not promote TMHI yields. Significant

CHAPTER 4

improvements on PAS yields were obtained when 1.5 ratio of 1,2-PG or higher were applied in this reaction (Table 4.3, entries 5-7). This effect is related to the higher rate of formation of hydroxyacetone during the reaction. The reaction time can be halved to 6 hours by increasing the ratio of 1,2-PG to 2 times that of DMU (Table 4.3, entry 7), a comparable outcome to DMU conversion in the sugar study above (>70%). This indicates that a longer reaction time on the first step (under N₂) for the cellulose/sugar conversion would promote the DMU conversion to PAS. To verify this observation, the reaction of cellulose with DMU was repeated under N₂ in EtOH for a longer time of 12 hours at 200 °C. Slightly higher DMU conversion (65% vs 58%) was achieved. It can be concluded that C-C bond cleavage and formation of 1 and 2 occurs faster than coupling of 1 and 2 with DMU in this catalytic cellulose or sugar conversion over the Ru/C catalyst. Decreasing the amount of catalyst (0.1 g Ru/C) resulted in lower yield of TMHI (54%) under identical conditions as entry 3, Table 4.3.

CHAPTER 4

Table 4.3 Results of reactions with varying ratios of 1,2-PG and DMU.^a

Entry	Diol/DMU	Time (hour)	TMHI %	Remaining Diol, %	Remaining DMU, %
1	1 : 1	12	27	65	71
2	1 : 2	12	32	42	81
3	1.5 : 1	12	79	28	9
4	2 : 1	12	85	47	4
5	4 : 1	12	88	57	5
6	1.5 : 1	6	45	51	50
7	2 : 1	6	66	65	31
8	4 : 1	6	78	66	9

^a1 Equivalent of 1,2-PG (7.0 mmol), DMU (7 or 14 mmol), 0.2 g Ru/C (5wt%), and 2-MeTHF (20 ml) were heated in a 75 ml stainless steel autoclave under N₂ inert atmosphere (35 bar) at 200 °C. Yields and the remaining amount of 1,2-PG were analyzed by ¹H-NMR with naphthalene as an internal standard. The remaining amount of DMU was characterized by both ¹H-NMR and HPLC/UV detection.

The effect of temperature on the reaction was examined for the coupling of 1,2-PG with DMU under N₂ (Table 4.4). TMHI was obtained in 80% yield at 180 and 200 °C (Table 4.4, entries 4-5). Significantly lower yields (< 32%) were obtained at 150 °C and below. Performing this reaction under H₂ atmosphere instead of a two-step reaction resulted in a significant decline in PAS formation.

Table 4.4 Results of coupling reactions of 1,2-PG and DMU at various temperature.^a

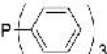
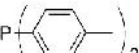
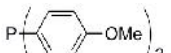
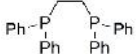
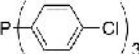
	Time	Temp (°C)	TMHI %
1	24	80	0
2	12	120	10
3	12	150	32
4	12	180	79
5	12	200	81

^a1,2-PG (0.15 g, 14 mmol), DMU (0.088 g, 7 mmol), 0.2 g Ru/C (5wt%), and 20 ml 2-MeTHF were heated in a 75 ml stainless steel autoclave under inert atmosphere (N₂, 35 bar) at 200 °C. Yields were analyzed by ¹H-NMR with naphthalene as an internal standard.

4.3.4 Electronic effect of Ruthenium on the reaction of 1,2-PG and DMU

In order to understand how electronic variation on the Ru catalyst affect the reaction 1,2-PG and DMU, experiments were conducted with a homogeneous ruthenium catalyst system generated *in situ*. These studies of a well-defined homogeneous system would elucidate electronic effects that can inform heterogeneous catalyst design. $\text{RuCl}_3 \cdot 3\text{H}_2\text{O}$ was combined with various phenyl phosphine ligands, in a 1:2 ratio, respectively. The catalyst mixtures were added in a microwave vial to 1,2-PG and DMU in 2-MeTHF as a solvent under nitrogen atmosphere (details provided in Table 4.5).

Table 4.5 Results of *in situ* formation of Ru catalysts with varying phosphine ligands.^a

Entry	Ligand	TMHI %	Diol Selectivity %	DMU Selectivity %
1		38	19	44
2		44	30	60
3		61	56	82
4		68	55	80
5		23	23	56

^a $\text{RuCl}_3 \cdot 3\text{H}_2\text{O}$ (0.02 mmol), phosphine ligands (0.04 mmol), 1,2-PG (0.15 g, 2 mmol), DMU (0.088 g, 1 mmol), and 2-MeTHF (1.5 ml) were heated in a 10 ml microwave vial under N_2 inert atmosphere at 200°C for 2 hours. Yields were analyzed by $^1\text{H-NMR}$ with naphthalene as an internal standard.

A linear pattern is drawn based on the TMHI yield vs. the Hammett constant of the para phenyl substituents (Figure 4.5).³⁶ Using triphenylphosphine, the yield of TMHI was only 38%. Adding an electron donating substituent to the phenyl ring increased the yield up to 61%. On the other hand, an electron withdrawing substituent dropped the yields to 20%.

CHAPTER 4

Therefore, higher electron density on Ru accelerates the rate of reaction. Although Hammett constant is not defined for bidentate 1,2-bis(diphenylphosphino)ethane (dppe), the best yield was obtained using dppe as a ligand indicating its positive electronic effect on the rate of the reaction.

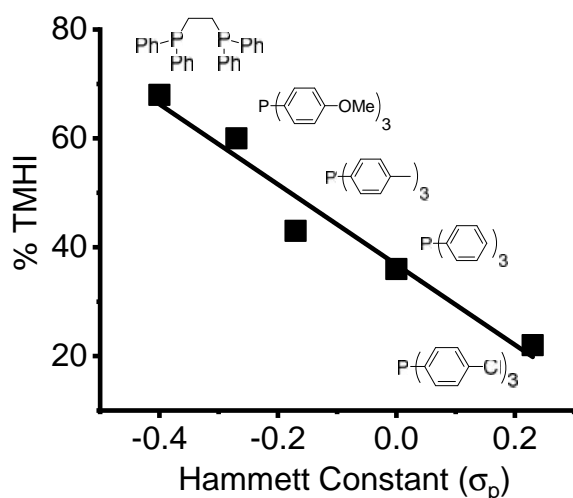


Figure 4.5 Plot of TMHI yields vs. Hammett constants of various para substituents on the phenyl phosphine ligands.

4.4 Discussion

A novel, direct, catalytic, and green process to obtain polar aprotic solvents (PAS) from renewable resources was described. PAS can be successfully produced in high selectivity in one-pot catalytic reactions of cellulose or sugars with N,N-dimethylurea (DMU) under Ru/C at 200 °C in two steps. The first step was conducted under N₂ atmosphere to yield the unsaturated PAS including 1,3-dimethyl-1,3-dihydro-2H-imidazol-2-one (DMHI) and 1,3,4-trimethyl-1,3-dihydro-2H-imidazol-2-one (TMHI). In the second step, hydrogenation of DMHI and TMHI was performed in the same pot over Ru/C under H₂ atmosphere. The initial hypothesis that the first step consists of two consecutive reactions, cellulose or sugar

CHAPTER 4

conversion to hydroxy ketones and their subsequent condensation reaction with DMU.

Formation of unsaturated PAS, DMHI and TMHI were verified in ethanol by ¹HNMR and HPLC-UV detector at 210 nm proceeding through the condensation of glycolaldehyde 1 and hydroxyacetone 2 intermediates with DMU, respectively. According to retro-aldol condensation, glucose and fructose are the precursors of 1 and 2, respectively.^{25, 26}

Experimentally, higher selectivity of DMI was obtained from the reactions of glucose with DMU in various solvents, while the selectivity of TMI was higher from analogous reactions with fructose. All supports the acyloins character of the species involved in the reaction pathway.

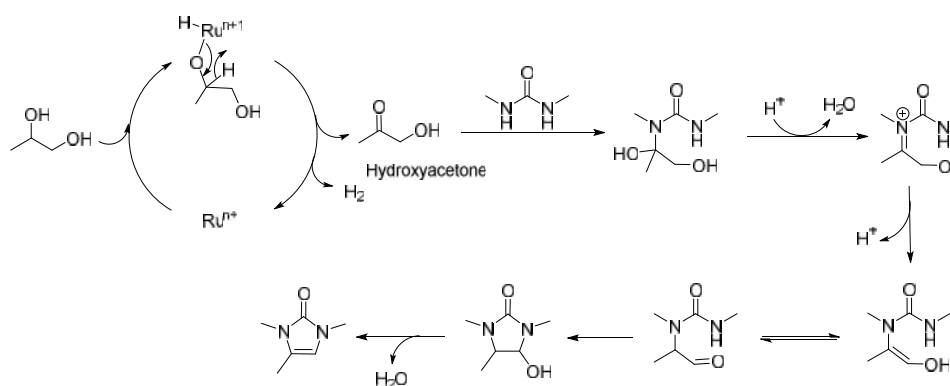
A simpler system composed of vicinal diols and DMU to produce PAS proceeds through the catalytic oxidation of vicinal diols to the corresponding acyloins over Ru/C as previously reported by Watanabe.³⁰ Hydroxyacetone 2 is identified by ¹HNMR as the product of the catalytic oxidation of 1,2-PG by homogeneous or heterogeneous ruthenium catalysts in 2-MeTHF in the absence of DMU (SI-III) which provides another evidence for formation of hydroxy ketone 2 in the reaction pathway. Upon coordination of diols to Ru, the corresponding adduct intermediate undergoes β -hydride elimination releasing acyloin product and an equivalent amount of hydrogen as shown in Scheme 4.2. The reaction of ethylene glycol with DMU under the same conditions produced DMI at a lower yield (22%) indicating that oxidation of the secondary alcohol proceeds faster than the primary alcohol over Ru/C.

Various studies have documented the condensation reactions between acyloins and urea for preparation of 4-imidazolin-2-one derivatives by refluxing the mixture in a solvent in the

CHAPTER 4

absence of a catalyst.^{27, 28} In some cases, an acid or a base was used as a catalyst.

Performing the reaction of 2 with DMU in the absence of a catalyst gives a yield of TMHI (69%) comparable to the catalytic reactions of 1,2-PG with DMU. Therefore, Ru/C is not required for the reaction of 2 with DMU. Once hydroxyacetone 2 is generated by catalytic oxidation of 1,2-PG over Ru/C, the condensation step proceeds thermally with an amine from DMU reacting with the carbonyl group of hydroxyacetone, forming enamine after dehydration and rearrangement. Upon tautomerization, enamine gives another carbonyl that can react with the second amine in a similar manner. The product TMHI is then obtained following a second dehydration (Scheme 4.2).



Scheme 4.2 Plausible mechanism for the production of unsaturated product TMHI

Finally, it should be noted that a two-step reaction allows the unsaturated intermediates glycolaldehyde 1 and hydroxyacetone 2 to react with DMU under N₂ in the first step when starting with cellulose or sugar. These intermediates (1 and 2) along with imine and enamine can easily undergo hydrogenation in the presence of Ru/C catalyst under H₂ atmosphere inhibiting production of the desired PAS, necessitating two-steps, first under N₂ to form unsaturated PAS followed by step two under H₂ to give the desired PAS products.

4.5 Conclusions

A green and catalytic approach for the conversion of cellulose and sugar to polar aprotic solvents (PAS) using Ru/C at 200 °C is presented. Cellulose and sugar conversion follows a pattern predicted by retro-aldol mechanism with glycolaldehyde 1 and hydroxyacetone 2 being the major intermediates en route to PAS.^{22, 23, 25, 26} Ru/C is an effective multifunctional catalyst where C-C bond cleavage of cellulose and sugars, coupling of 1 and 2 with N,N'-dimethylurea (DMU), and hydrogenation of the unsaturated products were achieved in one-pot two-step reactions without a need of separation and purification of intermediates. One of the appealing aspects of this reaction is that the product of the reaction can serve as the solvent. This gives an opportunity for designing a greener reaction using a minimal amount of solvent and improving sustainability and atom-economy of this process. PAS in general (DMI in this study) is the best solvent to generate PAS at atmospheric pressure because of its high polarity and boiling point. The overall high PAS selectivity of 85% was achieved in one-pot, two-step process for both cellulose and sugar conversion over Ru/C at 200 °C.

Coupling of 1,2-PG with DMU using Ru/C catalyst provide a novel synthetic design to yield the imidizolone TMHI which upon hydrogenation gives the imidizolidinone TMI, an appealing compound worthy of further study as a solvent. Oxidation of diol to the corresponding acyloins is the key step for this reaction catalyzed by Ru/C. TMI was obtained in 80% yield in two-step under heterogeneous catalysis in organic solvents with only hydrogen and water as the byproducts. Electronic effects from an *in situ* prepared homogeneous Ru phosphine catalysts revealed that electron-donating phosphine ligands

CHAPTER 4

(i.e. higher electron density on Ru) accelerated the reaction. Further studies on the design of Ru catalyst using different supports should provide more effective catalysts for C-C cleavage of carbohydrates and oxidation of vicinal diols to improve the productivity of PAS from renewable sources.

4.6 References

1. Dhepe, P. L.; Fukuoka, A., Cellulose conversion under heterogeneous catalysis. *ChemSusChem: Chemistry & Sustainability Energy & Materials* **2008**, *1* (12), 969-975. DOI: 10.1002/cssc.200800129
2. Climent, M. J.; Corma, A.; Iborra, S., Heterogeneous catalysts for the one-pot synthesis of chemicals and fine chemicals. *Chem. Rev.* **2011**, *111* (2), 1072-133. DOI: 10.1021/cr1002084
3. Mascal, M.; Nikitin, E. B., Direct, High yield conversion of cellulose into biofuel. *Angew. Chem.* **2008**, *120* (41), 8042-8044. DOI: 10.1002/ange.200801594
4. Ji, N.; Zhang, T.; Zheng, M.; Wang, A.; Wang, H.; Wang, X.; Chen, J. G., Direct catalytic conversion of cellulose into ethylene glycol using nickel-promoted tungsten carbide catalysts. *Angew. Chem. Int. Ed. Engl.* **2008**, *47* (44), 8510-3. DOI: 10.1002/anie.200803233
5. Corma, A.; Iborra, S.; Velty, A., Chemical routes for the transformation of biomass into chemicals. *Chem. Rev.* **2007**, *107* (6), 2411-2502. DOI: 10.1021/cr050989d
6. Satari, B.; Karimi, K.; Kumar, R., Cellulose solvent-based pretreatment for enhanced second-generation biofuel production: a review. *Sustainable energy & fuels* **2019**, *3* (1), 11-62. DOI: 10.1039/C8SE00287H
7. Ashcroft, C. P.; Dunn, P. J.; Hayler, J. D.; Wells, A. S., Survey of Solvent Usage in Papers Published in Organic Process Research & Development 1997–2012. *Organic Process Research & Development* **2015**, *19* (7), 740-747. DOI: 10.1021/op500276u
8. Lo, C. C.; Chao, P. M., Replacement of carcinogenic solvent HMPA by DMI in insect sex pheromone synthesis. *J. Chem. Ecol.* **1990**, *16* (12), 3245-53. DOI: 10.1007/BF00982095
9. Pace, V.; Hoyos, P.; Castoldi, L.; Dominguez de Maria, P.; Alcantara, A. R., 2 Methyltetrahydrofuran (2 MeTHF): a biomass derived solvent with broad application in organic chemistry. *ChemSusChem* **2012**, *5* (8), 1369-1379. DOI: 10.1002/cssc.201100780
10. Al-Shaal, M. G.; Dzierbinski, A.; Palkovits, R., Solvent-free γ -valerolactone hydrogenation to 2-methyltetrahydrofuran catalysed by Ru/C: a reaction network analysis. *Green Chemistry* **2014**, *16* (3), 1358-1364. DOI: 10.1039/c3gc41803k

11. Lopresto, C. G.; Petrillo, F.; Casazza, A. A.; Aliakbarian, B.; Perego, P.; Calabrò, V., A non-conventional method to extract D-limonene from waste lemon peels and comparison with traditional Soxhlet extraction. *Sep. Purif. Technol.* **2014**, *137*, 13-20. DOI: 10.1016/j.seppur.2014.09.015
12. Jalbert, J.; Duchesne, S.; Rodriguez-Celis, E.; Tétreault, P.; Collin, P., Robust and sensitive analysis of methanol and ethanol from cellulose degradation in mineral oils. *J. Chromatogr. A* **2012**, *1256*, 240-245. DOI: 10.1016/j.chroma.2012.07.069
13. Luo, C.; Wang, S.; Liu, H., Cellulose Conversion into Polyols Catalyzed by Reversibly Formed Acids and Supported Ruthenium Clusters in Hot Water. *Angew. Chem.* **2007**, *119* (40), 7780-7783. DOI: 10.1002/ange.200702661
14. Bhuvaneshwari, D. S.; Elango, K. P., Solvent hydrogen bonding and structural effects on nucleophilic substitution reactions: Part 4 — Reaction of 2-chloro-5-nitropyridine with para-substituted anilines in acetonitrile/dimethylformamide mixtures. *J. Mol. Liq.* **2008**, *143* (2-3), 147-153. DOI: 10.1016/j.molliq.2008.07.008
15. Mancini, P. M. E.; Terenzani, A.; Adam, C.; Pérez, A.; Vottero, L. R., Characterization of solvent mixtures. Part 8 — preferential solvation of chemical probes in binary solvent systems of a polar aprotic hydrogen-bond acceptor solvent with acetonitrile or nitromethane. Solvent effects on aromatic nucleophilic substitution reactions. *J. Phys. Org. Chem.* **1999**, *12* (3), 207-220. DOI: 10.1002/(sici)1099-1395(199903)12:3<207::Aid-poc113>3.0.Co;2-w
16. Dunn, P. J., The importance of green chemistry in process research and development. *Chem. Soc. Rev.* **2012**, *41* (4), 1452-61. DOI: 10.1039/c1cs15041c
17. Laird, T., Green Chemistry is Good Process Chemistry. *Organic Process Research & Development* **2012**, *16* (1), 1-2. DOI: 10.1021/op200366y
18. Liu, X.; Wang, X.; Yao, S.; Jiang, Y.; Guan, J.; Mu, X., Recent advances in the production of polyols from lignocellulosic biomass and biomass-derived compounds. *RSC Adv.* **2014**, *4* (90), 49501-49520. DOI: 10.1039/c4ra06466f
19. Fukuoka, A.; Dhepe, P. L., Catalytic conversion of cellulose into sugar alcohols. *Angew. Chem. Int. Ed. Engl.* **2006**, *45* (31), 5161-3. DOI: 10.1002/anie.200601921
20. Takaragi, A.; Minoda, M.; Miyamoto, T.; Liu, H. Q.; Zhang, L. N., Reaction characteristics of cellulose in the LiCl/1, 3 dimethyl 2 imidazolidinone solvent system. *Cellulose* **1999**, *6* (2), 93-102. DOI: 10.1023/a:1009208417954
21. Zhang, J. Y.; Hou, B. L.; Wang, A. Q.; Li, Z. L.; Wang, H.; Zhang, T., Kinetic Study of the Competitive Hydrogenation of Glycolaldehyde and Glucose on Ru/C with or Without AMT. *AlChE J.* **2015**, *61* (1), 224-238. DOI: 10.1002/aic.14639
22. Liu, Y.; Luo, C.; Liu, H., Tungsten trioxide promoted selective conversion of cellulose into propylene glycol and ethylene glycol on a ruthenium catalyst. *Angew. Chem. Int. Ed. Engl.* **2012**, *51* (13), 3249-53. DOI: 10.1002/anie.201200351
23. Sasaki, M.; Goto, K.; Tajima, K.; Adschiri, T.; Arai, K., Rapid and selective retro-aldol condensation of glucose to glycolaldehyde in supercritical water. *Green Chemistry* **2002**, *4* (3), 285-287. DOI: 10.1039/b203968k
24. Tai, Z.; Zhang, J.; Wang, A.; Zheng, M.; Zhang, T., Temperature-controlled phase-transfer catalysis for ethylene glycol production from cellulose. *Chem Commun (Camb)* **2012**, *48* (56), 7052-4. DOI: 10.1039/c2cc32305b

CHAPTER 4

25. Zhang, J.; Hou, B.; Wang, A.; Li, Z.; Wang, H.; Zhang, T., Kinetic study of retro aldol condensation of glucose to glycolaldehyde with ammonium metatungstate as the catalyst. *AIChE J.* **2014**, *60* (11), 3804-3813. DOI: 10.1002/aic.14554
26. Wang, A.; Zhang, T., One-pot conversion of cellulose to ethylene glycol with multifunctional tungsten-based catalysts. *Acc. Chem. Res.* **2013**, *46* (7), 1377-86. DOI: 10.1021/ar3002156
27. Feng, J.-C.; Meng, Q.-H.; Liu, Y.; Dai, L., Condensation Reaction of Acyloins with Urea without Solvent under Microwave Irradiation. *Org. Prep. Proced. Int.* **1997**, *29* (6), 687-689. DOI: 10.1080/00304949709355249
28. Kim, Y. B.; Kim, C. S.; Lee, C. K., Condensation-Reactions of Aryl Acyloins with Ureas in Ethylene-Glycol. *J. Heterocycl. Chem.* **1994**, *31* (6), 1653-1656. DOI: 10.1002/jhet.5570310663
29. Glasnov, T. N.; Kappe, C. O., Continuous-flow syntheses of heterocycles. *J. Heterocycl. Chem.* **2011**, *48* (1), 11-30. DOI: 10.1002/jhet.568
30. Kondo, T.; Kotachi, S.; Watanabe, Y., Ruthenium Complex-Catalyzed Synthesis of 1,3-Disubstituted 2,3-Dihydroimidazol-2-Ones from N,N'-Disubstituted Ureas and Vicinal Diols. *J Chem Soc Chem Comm* **1992**, 10.1039/c39920001318 (18), 1318-1319. DOI: 10.1039/c39920001318
31. Hayes, M. L.; Pennings, N. J.; Serianni, A. S.; Barker, R., Epimerization of Aldoses by Molybdate Involving a Novel Rearrangement of the Carbon Skeleton. *J. Am. Chem. Soc.* **1982**, *104* (24), 6764-6769. DOI: Doi 10.1021/Ja00388a047
32. Kabyemela, B. M.; Adschiri, T.; Malaluan, R. M.; Arai, K., Glucose and fructose decomposition in subcritical and supercritical water: Detailed reaction pathway, mechanisms, and kinetics. *Ind. Eng. Chem. Res.* **1999**, *38* (8), 2888-2895. DOI: Doi 10.1021/Ie9806390
33. Kabyemela, B. M.; Adschiri, T.; Malaluan, R. M.; Arai, K., Kinetics of glucose epimerization and decomposition in subcritical and supercritical water. *Ind. Eng. Chem. Res.* **1997**, *36* (5), 1552-1558. DOI: Doi 10.1021/Ie960250h
34. Shimizu, T. K.; Mugarza, A.; Cerdá, J. I.; Heyde, M.; Qi, Y.; Schwarz, U. D.; Ogletree, D. F.; Salmeron, M., Surface Species Formed by the Adsorption and Dissociation of Water Molecules on a Ru(0001) Surface Containing a Small Coverage of Carbon Atoms Studied by Scanning Tunneling Microscopy. *The Journal of Physical Chemistry C* **2008**, *112* (19), 7445-7454. DOI: 10.1021/jp711097j
35. Chang, C.-R.; Huang, Z.-Q.; Li, J., The promotional role of water in heterogeneous catalysis: mechanism insights from computational modeling. *Wiley Interdisciplinary Reviews: Computational Molecular Science* **2016**, *6* (6), 679-693. DOI: 10.1002/wcms.1272
36. Hansch, C.; Leo, A.; Taft, R. W., A Survey of Hammett Substituent Constants and Resonance and Field Parameters. *Chem. Rev.* **1991**, *91* (2), 165-195. DOI: 10.1021/cr00002a004